



Universität Potsdam



Alfred-Wegener-Institut für Polar- und
Meeresforschung

in der Helmholtz-Gemeinschaft

Late Quaternary environmental dynamics at the Duvanny Yar key section, Lower Kolyma, East Siberia

Diplomarbeit

zur Erlangung des akademischen Grades

Diplom-Geoökologe

vorgelegt von

Jens Strauß

aus Lünen

geboren am 08. Dezember 1984

Universität Potsdam

Institut für Erd- und Umweltwissenschaften

Potsdam, im Februar 2010

1. Gutachter

Dr. Lutz Schirrmeister

Alfred-Wegener-Institut für Polar- und Meeresforschung,
Telegrafenberg A43, 14473 Potsdam

2. Gutachter

Prof. Dr. Hans-Wolfgang Hubberten

Alfred-Wegener-Institut für Polar- und Meeresforschung,
Telegrafenberg A43, 14473 Potsdam;

Gemeinsam berufen mit dem Institut für Erd- und Umweltwissenschaften, Universität Potsdam, Lehrstuhl Terrestrische Geowissenschaften

Für Jan, Regina und Martin

„Die Neugier steht immer an erster Stelle eines Problems, das gelöst werden will.“

Galileo Galilei

Contents

Contents	I
List of figures	III
List of tables.....	V
Abbreviations and nomenclature.....	VI
Abstract.....	VII
Kurzfassung.....	VIII
1 Introduction.....	1
1.1 Scientific relevance and background	1
1.2 Aims	2
2 Geological and geographical background	4
2.1 The periglacial environment.....	4
2.1.1 Permafrost	4
2.1.2 Ground ice.....	5
2.1.3 Polygonal nets and lakes	7
2.1.4 Thermokarst and alas	7
2.1.5 Yedoma and Ice Complex.....	8
2.2 Regional setting.....	10
2.2.1 Geological and geographical setting.....	10
2.2.2 Climate, vegetation and soils.....	11
2.3 The Duvanny Yar section	12
3 Methods.....	15
3.1 General study scheme	15
3.2 Field work	15
3.2.1 Sediments studies and sampling.....	16
3.2.2 Studies and sampling of ground ice and recent waters.....	16
3.3 Sedimentological analysis.....	17
3.3.1 Mass specific magnetic susceptibility	17
3.3.2 Grain size analysis	17
3.3.3 Determination of TC, TOC and TN values.....	19
3.3.4 Bulk density and organic carbon ratio.....	20
3.4 Geochronology.....	21
3.5 Stable isotope geochemistry.....	22
3.5.1 Carbon isotopes ($\delta^{13}\text{C}$).....	22
3.5.2 Oxygen & hydrogen isotopes ($\delta^{18}\text{O}$, $\delta^2\text{H}$).....	24

3.6 Hydrochemistry.....	27
3.6.1 Alkalinity measurements.....	27
3.6.2 Determination of anion concentration.....	28
3.6.3 Determination of cation concentration.....	29
4 Results.....	30
4.1 General composition of the Duvanny Yar section.....	30
4.2 Lake deposits below/next to the Ice Complex sequence.....	30
4.2.1 Profile DY-02.....	30
4.2.2 Profile DY-03.....	34
4.2.3 Profile DY-06.....	37
4.3 Ice Complex.....	39
4.3.1 Profile DY-05.....	39
4.3.2 Profile DY-01.....	45
4.4 Alas deposits.....	51
4.5 Specific studies on Ice Complex and alas deposits.....	55
4.5.1 Peak fitting at the Ice Complex grain size distributions.....	55
4.5.2 Bulk density and organic carbon content for Ice Complex and alas deposits.....	57
4.6 Hydrochemistry.....	58
5 Discussion.....	61
5.1 General geomorphology.....	61
5.2 Geochronological and stratigraphical interpretation.....	61
5.3 Sediment facies discussion.....	63
5.3.1 Lake deposits.....	63
5.3.2 Ice Complex.....	66
5.3.3 Alas.....	72
5.4 Organic carbon content calculation.....	73
5.5 Climatic information from ground ice.....	74
5.5.1 Ice wedges.....	74
5.5.2 Fissure ice and texture ice.....	76
5.5.3 Summarised paleoclimate interpretation.....	79
5.5.4 Comparisons to other studies.....	80
5.6 Synthesis of the Late Quaternary environmental dynamics at Duvanny Yar.....	83
6 Conclusions and outlook.....	86
References.....	88
Appendix.....	96
Danksagung.....	107
Selbstständigkeitserklärung.....	108

List of figures

Fig. 1-1: Extent of Beringia	2
Fig. 2-1: Permafrost extent in the Northern Hemisphere	4
Fig. 2-2: Transect of the permafrost of East Siberia	4
Fig. 2-3: Vertical differentiation of the permafrost zone	5
Fig. 2-4: Scheme of the evolution of an ice wedge	6
Fig. 2-5: Schematic diagram showing the growth of epigenetic and syngenetic ice wedges	6
Fig. 2-6: Schematic view on modern polygonal nets.....	7
Fig. 2-7: Intrapolygonal ponds and polygonal tundra in the Lena Delta.....	7
Fig. 2-8: Sequence of alas relief development in Central Yakutia	8
Fig. 2-9: Schematic map of possible Ice Complex distribution in northern Siberia	9
Fig. 2-10: Main tectonic zones of the study area	11
Fig. 2-11: Climatic diagram of Kolymenskaya.....	12
Fig. 2-12: Location of Duvanny Yar site.....	13
Fig. 2-13: Generalised view of the Duvanny Yar section	13
Fig. 3-1: Organisation chart of methods and preparation for the majority of samples.....	15
Fig. 3-2: Example of the peak fitting for sample DY-05-H-48	19
Fig. 3-3: Rough estimation of carbon isotope composition of higher plants, algae and autotrophic prokaryotes	23
Fig. 3-4: CRAIG and GORDON (1965) model for isotopic fractionation in marine-atmosphere cycle.....	25
Fig. 4-1: Scheme of the Duvanny Yar section with positions of the studied profiles	30
Fig. 4-2: Scheme of the lake profile DY-02	31
Fig. 4-3: Summary of cryolithological and sedimentological parameters for the lake sediment profile DY-02...	32
Fig. 4-4: Grain size distribution and sediment triangle of the lake sediment profile DY-02	32
Fig. 4-5: Scheme and photo of the studied ice wedge at DY-02-A-100.....	33
Fig. 4-6: Stable isotope signature of ground ice in DY-02	34
Fig. 4-7: Scheme and photo of the lake sediment profiles DY-03 and DY-06.....	35
Fig. 4-8: Peat inclusions in silty matrix (sample DY-03-A-14).....	35
Fig. 4-9: Alternate bedding of silty fine sand and plant detritus layers close to the samples DY-03-10 to 13.....	35
Fig. 4-10: Summary of cryolithological and sedimentological parameters for the lake sediment profiles DY- 06 and DY-03	36
Fig. 4-11: Grain size distribution and sediment triangle of the lake sediment profile DY-03.....	37
Fig. 4-12: Alternate bedding of brown-grey laminated fine sand, laminated grey silt and dark brown plant detritus	38
Fig. 4-13: Grain size distribution and sediment triangle of the lake sediment profile DY-06.	39
Fig. 4-14: Thermocirque of the composite profile DY-05.	39
Fig. 4-15: Scheme of the composite Ice Complex profile DY-05	40
Fig. 4-16: Summary of cryolithological and sedimentological parameters for the Ice Complex profile DY-05 ..	41

Fig. 4-17: Grain size distribution and sediment triangle of the Ice Complex profile DY-05.....	42
Fig. 4-18: Ice wedges in the Ice Complex deposits of DY-05.....	43
Fig. 4-19: Stable isotope signature of ground ice in DY-05.....	44
Fig. 4-20: Overview of the thermocirque of the composite profile DY-01.....	45
Fig. 4-21: Scheme of the composite Ice Complex profile DY-01.....	46
Fig. 4-22: Irregular laminated cryostructures near sample point DY-01-F-35.....	46
Fig. 4-23: Laminated cryostructures in subprofile DY-01-C (DY-01-C-15).....	46
Fig. 4-24: Thermokarst mounds at the composite profile DY-01.....	47
Fig. 4-25: Topmost part of the Ice Complex profile.....	47
Fig. 4-26: Summary of cryolithological and sedimentological parameters for the Ice Complex profile DY-01..	47
Fig. 4-27: Grain size distribution and sediment triangle of the Ice Complex profile DY-01.....	49
Fig. 4-28: Fissure ice and ice wedges of the Ice Complex profile DY-01.....	50
Fig. 4-29: Stable isotope signature of ground ice in DY-01.....	51
Fig. 4-30: Overview of the alas into eastern direction.....	51
Fig. 4-31: Scheme of the alas profile DY-04.....	52
Fig. 4-32: Summary of cryolithological and sedimentological parameters for the alas profile DY-04.....	53
Fig. 4-33: Grain size distribution and sediment triangle of the alas profile DY-04.....	54
Fig. 4-34: Stable isotope signature of ground ice of DY-04.....	54
Fig. 4-35: Results of peak fitting at DY-05.....	55
Fig. 4-36: Results of peak fitting at DY-01.....	56
Fig. 4-37: Relevant parameters for the bulk density calculations and organic carbon content estimations.....	57
Fig. 4-38: Pie charts of the major ion of the mean for the ice wedges and fissure ice in the Ice Complex deposits and recent waters.....	59
Fig. 4-39: Piper plot of the major ions.....	59
Fig. 5-1: Summary of ¹⁴ C dates from different authors for different kind of organic material at Duvanny Yar	62
Fig. 5-2: Altitude-age relationship with a linear regression line of the Ice Complex profile DY-01.....	63
Fig. 5-3: Generalised cryostructures and lithostratigraphical schemes of the studied profiles.....	64
Fig. 5-4: Generalised stable carbon isotope ratios and TOC/TN- ratios of marine and lacustrine algae as well as C ₃ plant organic matter.....	65
Fig. 5-5: Compilation of the Ice Complex profiles DY-05 and DY-01.....	67
Fig. 5-6: Variations of gravimetric ice content, TOC and mean grain size of different Ice Complex studies.....	72
Fig. 5-7: Supposed moisture transport in Eurasia during the Late Glacial Maximum (LGM).....	75
Fig. 5-8: The <i>d</i> excess parameter as a function of humidity during kinetic evaporation from the ocean surface.....	77
Fig. 5-9: Evolution of melt water draining from base of snowpack.....	77
Fig. 5-10: Development of δ ¹⁸ O, δ ² H and <i>d</i> excess of all ground ice samples sorted in a stratigraphic order.....	80
Fig. 5-11: Comparison of the isotopic composition of different ice wedges at Duvanny Yar.....	81
Fig. 5-12: Comparison of the oxygen isotope composition of texture ice at Duvanny Yar.....	82

List of tables

Table 2-1: Concepts of Ice Complex development.....	9
Table 2-2: Comparison of the stratigraphic terminology used in Western Europe and Siberia	10
Table 3-1: Fine grain size fractions according to EN ISO 14688/ DIN 4022.....	18
Table 3-2: Equivalence of Φ and μm scales.....	18
Table 3-3: Approach of a classification of TOC/TN values	19
Table 3-4: Carbonate content in soil.....	20
Table 4-1: Radiocarbon accelerator mass spectrometer (AMS) dating results of DY-05.....	43
Table 4-2: Radiocarbon AMS dating results of DY-01.....	49
Table 5-1: Grain size parameters of sediments of chosen environments	70
Table 5-2: Synthesis of stratigraphy, facies interpretation and sedimentological, cryolithological and stable water isotope features.	85

Abbreviations and nomenclature

Notation	Meaning	Unit (if procurable related to SI units)
°C	degree Celsius	273.15 °K
°K	degree Kelvin	K
µl	microlitre	10 ⁻⁹ m ³
µm	micrometre	10 ⁻⁶ m
a	Latin: annus; year	3.1536 × 10 ⁷ s
AD	Latin: Anno Domini; in the year of the Lord	
AMS	accelerator mass spectrometry	
BC	before Christ	a
BP	before present [1950]	a
ca.	Latin: circa; approximately	
cm	centimetre	10 ⁻² m
DY	Duvanny Yar	
e.g.	Latin: exempli gratia; for example	
EC	electrical conductivity	S = Ω ⁻¹ ; m ⁻² · kg ⁻¹ · s ³ · A ²
Eq.	equation	
etc.	Latin: et cetera; and so on	
Fig.	figure	
g	gram	10 ⁻³ kg
i.e.	Latin: id est; that is	
IPF	interactive peak fitter	
ka	Latin: kilo annus; thousand years	3.1536 × 10 ¹⁰ s
km ²	square kilometre	1000000 m ²
KOS	Kolyma-Omolon Superterrane	
lab N ^o	number of a sample at an external laboratory	
LGM	Last Glacial Maximum	
m	metre	m
ml	millilitre	10 ⁻⁶ m ³
mm	millimetre	10 ⁻³ m
NICB	normalised inorganic charge balance	%
Ø	diameter	
PE	polyethylene	
pers. com.	personal communication	
pH	potential of Hydrogen	
pMC	per cent modern carbon	100 pMC = ¹⁴ C atmospheric concentration at 1950
RMS	root mean square error	
rpm	revolutions per minute	
s	second	s
SI	système international d'unités, here used as unit for the magnetic susceptibility	10 ⁻⁸ m ³ · kg ⁻¹
TC	total carbon	
TIC	total inorganic carbon	
TN	total nitrogen	
TOC	total organic carbon	
vol %	per cent by volume	
VPDB	Vienna PeeDee Belemnite	‰
VSMOW	Vienna Standard Mean Ocean Water	‰
wt %	per cent by weight	
Φ	logarithmic phi scale for grain size	-log ₂ (10 ⁻⁹ m)

Abstract

Duvanny Yar is a stratigraphic key site for the Late Quaternary in Beringia, the non-glaciated land-mass between the Taymyr Peninsula and Alaska. Moreover, Duvanny Yar is characteristic for ice-rich permafrost sequences, termed as “Ice Complex” or “Yedoma Suite” in Northeast Siberia and an important reference site for the Late Pleistocene history of Beringia. The investigated outcrop (68.6319°N, 159.1420°E) is exposed by the Kolyma River and is located in the Kolyma Lowland at the north-eastern edge of the Sakha (Yakutia) Republic.

The aim of this study was to reconstruct the paleoenvironmental dynamics at the Duvanny Yar site for the Late Quaternary using its terrestrial permafrost archive. A multidisciplinary approach of geocryological, geochronological, sedimentological, hydrochemical and isotope geochemical methods was applied to obtain multiproxy records. Sediment samples were analysed for ice contents, grain size parameters, biogeochemistry (total carbon, total organic carbon, total nitrogen and stable carbon isotopes), mineral density, mass specific magnetic susceptibility and for radiocarbon age. Stable isotopes of water were measured for ground ice (ice wedges, fissure ice, segregated ice and pore ice), modern surface waters and modern precipitation. Six profiles along the riverbank were sampled in August 2008. They contained Eemian lacustrine deposits, long sequences of Late Pleistocene Ice Complex deposits, Holocene lacustrine and boggy deposits in thermokarst depressions. All profiles showed very bad sorted sediment of fine to coarse silt. A remarkable homogeneity in the polymodal grain size distribution for the ice-rich Ice Complex (~30 to 60 wt % ice content) reveals different but proportionate stable processes of origin like alluvial, aeolian and *in-situ* frost weathering processes. Thus the pure “arctic loess” hypothesis for Ice Complex deposits of Duvanny Yar is disproved. Measurements of bulk density, ice content and total organic carbon content (TOC) enable relative carbon content calculations for Ice Complex and alas deposits of Duvanny Yar. The mean value of organic carbon at the ~43 m thick sampled Ice Complex is $14 \pm 9 \text{ kg TOC} \cdot \text{m}^{-3}$; for the short Holocene alas sequence it is $29 \pm 16 \text{ kg TOC} \cdot \text{m}^{-3}$. Geochronological results based on eight new AMS ages reveal that the Ice Complex was continuously formed from the Middle Weichselian (~40000 a BP) and at least until the Late Glacial period (~12000 a BP). Stable water isotopes measured in ice wedges, segregated ice and ice lenses were used to estimate paleotemperature changes. Isotopic signals reveal warm temperatures at Eemian times and stable cold and dry conditions for the whole period of Ice Complex formation. At the Pleistocene/Holocene transition the isotopes show a climate warming.

A better understanding of the paleoenvironmental dynamics at Duvanny Yar and further research may provide a basis for more reliable predictions of future reaction on global warming of organic-bearing ice-rich permafrost in Siberia, which is considered as potential greenhouse gas source permafrost.

Kurzfassung

Duvanny Yar gilt als ein Schlüsselaufschluss des spätquartären Beringialandes, welches sich als unvergletschter Bereich zwischen der Taimyrhalbinsel und Alaska erstreckte. Duvanny Yar ist ein charakteristischer Aufschluss für die in Nordost Sibirien vorkommenden eisreichen Permafrostablagerungen, welche auch als „Eiskomplex“ oder synonym als „Yedoma Suite“ bezeichnet werden. Des Weiteren dient dieser Aufschluss als Referenz für die spätpleistozäne Geschichte von Beringia. Duvanny Yar (68.6319°N, 159.1420°E), von dem Fluss Kolyma aufgeschlossen, liegt im Kolymatiefeld im nordöstlichen Randbereich der russischen Republik Sakha (Jakutien).

Das Ziel dieser Studie war die Rekonstruktion der Umweltveränderungen von Duvanny Yar während des Spätquartärs. Unter Verwendung des abgelagerten terrestrischen Archivs ist ein durch geokryologische, geochronologische, sedimentologische, hydrochemische und isotopengeochemische Methoden multidisziplinärer Ansatz umgesetzt worden, um ein möglichst umfassendes Indikatorenspektrum nutzen zu können. Die Sedimentproben wurden diesbezüglich auf Eisgehalt, Korngrößenparameter, biogeochemischen Kenngrößen (Gesamtkohlenstoffgehalt, organischer Kohlenstoffgehalt, Stickstoffgehalt und stabile Kohlenstoffisotope), mineralische Dichte, magnetische Suszeptibilität sowie Radiokohlenstoffdatierungen hin untersucht. Stabile Wasserisotope von Eiskeilen, Klufteis, Poreneis und Segregationseis sowie von rezenten Wässern wurden zwecks Temperaturrekonstruktion gemessen. Insgesamt sind während der Expedition im August 2008 sechs Profile innerhalb des Uferaufschlusses beprobt worden. Darunter waren Seeablagerungen aus der Eem-Warmzeit, zwei lange spätpleistozäne Eiskomplexprofile, holozäne Seeablagerungen und auch eine holozäne Thermodegradationsform des Eiskomplexes, ein sogenannter „Alas“. Alle Sedimentproben sind schlecht sortiert und bestehen aus feinem bis groben Silt. Eine bemerkenswerte Homogenität der polymodalen Korngrößenverteilung der eisreichen (~30 bis 60 Gewichtsprozent Eisgehalt) Eiskomplexablagerungen legen die Vermutung nahe, dass diese Art der Ablagerungen durch verschiedene, jedoch im Verhältnis zueinander konstante Ablagerungsprozesse bedingt wurden. Die vermuteten Hauptprozesse sind alluvialer und äolischer Art, verstärkt durch *in-situ* Frostverwitterung. Somit ist die Hypothese, dass Eiskomplexablagerungen reiner „arktischer Löss“ seien, für Duvanny Yar widerlegt. Messungen der Lagerungsdichte, des Eisgehalts und des organischen Kohlenstoffs machten die Berechnung des relativen organischen Kohlenstoffgehalts möglich. Der Mittelwert für den Eiskomplex ergibt 14 ± 9 Kilogramm organischen Kohlenstoff pro Kubikmeter. Der holozäne Alas beinhaltet 29 ± 16 kg TOC · m⁻³. Die acht Radiokohlenstoffdatierungen zeigen, dass der Eiskomplex von Duvanny Yar seit der mittleren Weichselvereisung (um 40000 Jahren vor heute) bis zum Übergang von Weichselzeit in das Holozän (ungefähr 12000 Jahre vor heute) kontinuierlich andauerte. Durch die Messungen der Wasserisotope konnten Aussagen über die Paläowintertemperatur getroffen werden. So sind die relativ schweren Isotope aus den Seeablagerungen des Eems als warme Temperaturen zu interpretieren, wobei die Isotopenzusam-

mensetzung des Eiskomplexes stabile kalte und trockene Klimate anzeigt. Am Pleistozän/Holozän-Übergang zeigen die Isotope eine Erwärmung.

Ein besseres Verständnis der Paläoumweltdynamik von Duvanny Yar und weitere Forschungsarbeiten könnte die Grundlage für verlässliche Voraussagen sein. Es wären genauere Prognosen zum Verhalten der sowohl eis- als auch kohlenstoffreichen Eiskomplexablagerungen, welche in Bezug auf eine globale Erwärmung klimarelevante Treibhausgase freisetzen könnten, möglich.

1 Introduction

1.1 Scientific relevance and background

The Arctic plays a key role in the Earth's climate system as it powers the oceanic and atmospheric circulation. Polar regions respond faster and more severely to climate change than the other regions on Earth. The Arctic is of global importance, because of an increasing risk for climatic feedback mechanisms, as e.g. the melting of arctic snow and (sea and terrestrial) ice:

- (1) increases the absorption of sun insolation (atmospheric circulation feedbacks),
- (2) increases river runoff and adds more fresh water to the ocean (sea level rise and potential disturbance of ocean circulations; ocean feedbacks) (SOMMERKORN and HASSOL 2009)
- (3) changes ecosystems from greenhouse gas sink to source (ecosystem feedbacks) (MCGUIRE et al. 2009).

These feedbacks could contribute to a faster global climate change than in predicted scenarios (ACIA 2004; IPCC 2007; SOMMERKORN and HAMILTON 2008). Already nowadays in arctic regions the annual mean air temperature raise two times faster compared to the global mean rise (ACIA 2004). At present, the warming trend in permafrost regions leads to an increase in ground temperatures with several environmental consequences. The permafrost is thawing especially at its margins and the seasonal unfrozen active layer gets thicker. Permafrost degrades and causes enhanced thermal erosion and surface subsidence. Wetland ecosystems change and cause a release of terrigenous stored carbon as additional greenhouse gases, particularly carbon dioxide and methane. These effects of global warming in permafrost regions threatens economy (e.g. pipelines and other infrastructure), ecology (e.g. arctic organisms) as well as indigenous people (ACIA 2004; IPCC 2007; OECHEL et al. 1993). By nature, there have been climatic changes in Earth's history but according to IPCC (2007) the current climate change is most likely man-made and occurs to be faster than natural climate cycles.

This study focuses on major natural caused climatic and environmental changes in Northeast Siberia during the Late Quaternary (from the Eemian interglacial, ~130000 a BP, to the beginning of the Holocene, ~10500 a BP; Table 2-2) in order to better understand its paleodynamics. The study is carried out in the framework of the joint Russian-German expedition "Beringia/Kolyma 2008" during the International Polar Year 2007/2008 and focuses on permafrost sequences at the Duvanny Yar section (Lower Kolyma River, East Siberia). During the expedition a multidisciplinary and multiproxy approach covering geocryology, sedimentology, hydrochemistry, isotope geochemistry, palynology and soil science was applied. So the data set for paleoenvironmental information, collected by the periglacial section of the Alfred-Wegener-Institute for Polar and Marine Research (Research Unit Potsdam) is expanded for another important section.

In particular, this study provides an extensive study of the terrestrial archive of the Duvanny Yar permafrost section using six profiles along the riverbank. Duvanny Yar is described in the literature as the characteristic

stratigraphic sequence for the Late Quaternary, especially for the ice-rich permafrost sequence of the also termed Ice Complex (in the study region called Yedoma Suite) in Northeast Siberia (GITERMAN et al. 1982; HOPKINS 1982; KAPLINA et al. 1978; SHER et al. 1979). In addition, this section is an important reference site for the Late Pleistocene history of Beringia, the unglaciated land mass between the Eurasian Barents-Kara ice sheet and the North American Laurentian ice sheet. That huge landmass extended between the Central Siberian Taymyr Peninsula and the Northeast Canadian MacKenzie River (Fig. 1-1).

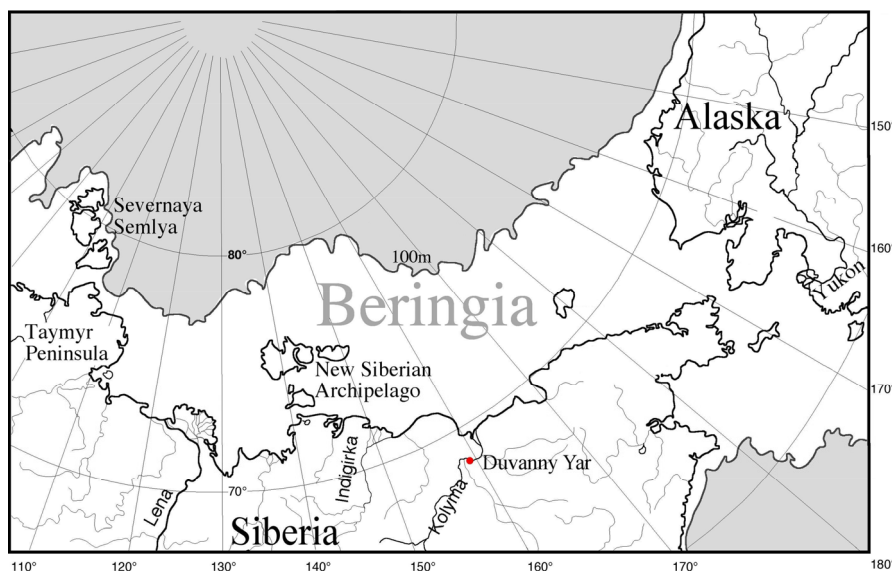


Fig. 1-1: Extent of Beringia with respect to the modern shoreline and to the 100 m isobaths, which indicates the approximately mean extent of Beringia at the Last Glacial Maximum (~18000 a BP); KIENAST et al. (2005), modified.

Such permafrost sections are well applicable to reconstruct paleoenvironmental conditions and variations, because numerous paleoproxies (e.g. sedimentological, geocryological and geochemical properties, pollen, organic matter and mammal fossils) are preserved (e.g. ANDREEV et al. 2009; MACKAY 1972; SCHIRRMESTER et al. 2002a; SHER et al. 1979; VASIL'CHUK and VASIL'CHUK 2008a, b). Furthermore, permafrost archives are the only more frequently available long-term paleoenvironmental records in Northeast Siberia.

1.2 Aims

The purpose of this study is to reconstruct the environmental dynamics at the Duvanny Yar section during the Late Quaternary. Sediments and ground ice which are both elements of permafrost are used as sources of information. The sediment data is employed to detect changes in the landscape dynamics, whereas data on ground ice samples serve as indicators of climatic changes. This approach leads to the following objectives and guiding questions:

Clarification of the history of sediment deposition in the Late Quaternary:

- Which different depositional milieus and sediment facies can be identified?
- What do these facies reveal about the paleogeography, i.e. landscape evolution, medium and energy of transportation, aggregation and degradation of permafrost at Duvanny Yar?

- How is the internal stratigraphy sequence of the studied profiles composed?
- Can profiles be correlated regarding to their stratigraphy and facies interpretation?
- What influence had the thermokarst development on permafrost?

Assessment of the climatic history since Late Quaternary times:

- Does the isotopic composition of ground ice differ and which climatic trends are noticeable?
- Do climatic trends preserved in ground ice correlate with changes in the sedimentation pattern?

Small- and large-scale comparisons:

- What is new about Duvanny Yar studies in comparison to previous studies?
- How does the local paleoclimate fit into the climatic context of the Northern Hemisphere?

2 Geological and geographical background

2.1 The periglacial environment

The term “periglacial” was introduced by the Polish geologist VON LOZINSKI (1909) to describe the climate and its features prevailing near the Pleistocene ice sheets (WASHBURN 1979). The modern usage of this term refers to a range of cold, non-glacial processes independent of their age or proximity to glaciers and ice sheets (FRENCH 2007; VAN EVERDINGEN 1998). According to this, the periglacial environment which is subject of this study is characterised (1) by the presence of perennally frozen ground (permafrost) and (2) by intense frost-action processes. The latter are the predominant landscape shaping processes, which involve freezing and thawing of the ground and lead to frost cracking, ice wedge growth, frost heaving and material sorting. The geomorphology of the study area is determined by ubiquitous periglacial features, such as permafrost (chapter 2.1.1), ice wedge polygonal nets (chapter 2.1.2 and 2.1.3), thermokarst depressions and lakes (chapter 2.1.4).

2.1.1 Permafrost

Permafrost is defined as “ground (soil or rock and included ice and organic material), that remains at or below 0 °C for at least two consecutive years” (HARRIS et al. 1988; VAN EVERDINGEN 1998). Permafrost regions make up ca. 24 % of the land area of the Northern Hemisphere (ZHANG 1999). During the Pleistocene up to ~50 % of it were affected by permafrost (FRENCH 2007). A total of 65 % of the Russian territory is underlain by permafrost, representing the world largest permafrost region (Fig. 2-1). However, it must be mentioned that the periglacial extent not only includes high latitude landscapes, but also vast areas of the continental shelves of the Arctic Ocean and mountainous areas in lower latitudes (ROMANOVSKY et al. 2007) (Fig. 2-1).



Fig. 2-1: Permafrost extent in the Northern Hemisphere; after AHLENIUS (2007) in ROMANOVSKY et al. (2007). The transect of Fig. 2-2 is illustrated as dashed black line.

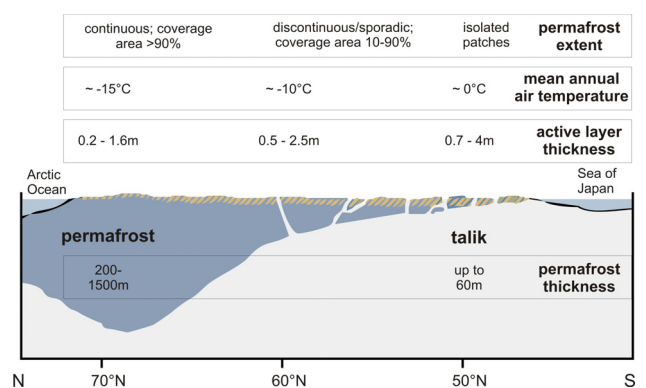


Fig. 2-2: Transect of the permafrost of East Siberia; after FRENCH (2007) and KOPPE (2003), modified.

The thickness and growth of permafrost reflects a negative heat balance at the surface between ground and surface temperatures, which is in turn regulated by air temperature and the geothermal gradient (FRENCH

2007). The most important environmental factors controlling permafrost conditions are topographic features (e.g. relief and aspect), snow cover, vegetation and the subsurface material as well as the moisture content of the ground (FRENCH 2007; WASHBURN 1979). Permafrost distribution is classified into three major regions (Fig. 2-1 and Fig. 2-2):

1. Continuous permafrost covers 90 to 100 % of the area. This type can be found in the high latitudes of the Northern Hemisphere, where climate conditions are favourable for active formation of frozen ground (ca. -15 °C Mean Annual Air Temperature; MAAT). Most continuous permafrost was formed during or before the last glacial period.
2. Discontinuous permafrost covers 50 to 90 % and is separated by taliks. Sporadic permafrost occupies an area of 10 to 50 %. It is often a relict, which is in the process of degradation, or it is much younger and formed within the last several thousand years.
3. Isolated permafrost represents single patches of frozen ground in an otherwise unfrozen area and covers <10 % of the total area. It is a result of advanced degradation (FRENCH 2007; ROMANOVSKY et al. 2007; WEISE 1983).

Permafrost is overlain by an active layer (Fig. 2-3), which is affected by seasonal freeze and thaw cycles. The active layer depth can vary significantly from year to year as well as between locations. It is depending on the permafrost controlling factors mentioned above. The boundary between the active layer and the upper limit of the permafrost is marked by the permafrost table (Fig. 2-3) (WASHBURN 1979). At the permafrost table a transient layer can be found, which lies between the active layer and the permafrost zone and is affected by freezing and thawing on decadal/century scales (FRENCH 2007; SHUR et al. 2005). In areas of perennially frozen ground layers or bodies of unfrozen ground occur. These elements are called taliks (Fig. 2-2 and Fig. 2-3). The differentiation of various types of taliks depends on their position to the permafrost (Fig. 2-3) or it can be distinguished by their interconnection to other unfrozen layers. A closed talik is completely surrounded by permafrost, whereas an open talik is open to the top or to the bottom.

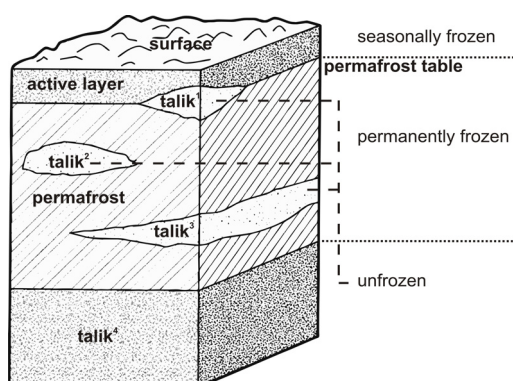


Fig. 2-3: Vertical differentiation of the permafrost zone; talik¹: suprapermafrost; talik²: closed; talik³: intrapermafrost; talik⁴: subpermafrost; after French (2007), modified.

2.1.2 Ground ice

The main feature that distinguishes permafrost from unfrozen ground is the presence of ground ice. The absolute ground ice content in permafrost can vary from a tenth of per cent up to 90 % or more of the total

volume. The mechanical strength of frozen soil with ice in it is close to the strength of bedrock. Due to this, the stability of ecosystems in permafrost regions strongly depends on the content of ground ice. A loss of permafrost would mean a loss in system stability (ROMANOVSKY et al. 2007). Ground ice is defined as all types of ice contained in frozen or freezing ground (HARRIS et al. 1988). According to MACKAY (1972) the ground ice can be classified in four types: (1) pore ice, (2) segregated ice, (3) vein ice and (4) intrusive ice. For this study the first 3 types are relevant. Pore ice is the bonding cement that holds soil grains together. It is ubiquitous wherever moisture is present within permafrost. Segregated ice occurs primarily in water-saturated sediments. Ice bands and lenses are a phenomenon of segregated ice and are defined as dominantly horizontal, lenticular bodies of ice, ranging in thickness from hairline to large ice bodies of ~10 m (VAN EVERDINGEN 1998). The distinction between pore and segregated ice is related to the water content of the soil. In this study texture ice is used as a descriptive term, which includes both pore ice and segregated ice. Moreover the term fissure ice is used in to describe vein ice of unclear origin. In this context, fissure ice is defined as a comprehensive term for ice of any origin occupying cracks caused e.g. by mass movements or shrinkage in permafrost. Another type of vein ice in the study area is present as ice wedges (Fig. 2-4 and Fig. 2-5). Syngenetic ice wedges form at approximately the same time as enclosing sediments accumulate, whereas epigenetic ice wedges form after the sediment deposition (FRENCH 2007, Fig. 2-5). Ice wedges originate through thermally induced cracking of the ground.

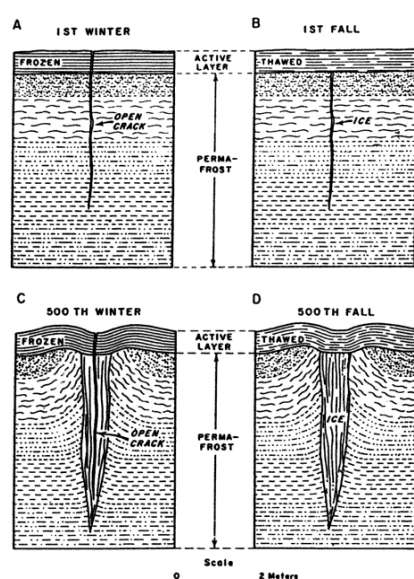


Fig. 2-4: Scheme of the evolution of an ice wedge according to the contraction cracks (LACHENBRUCH 1963).

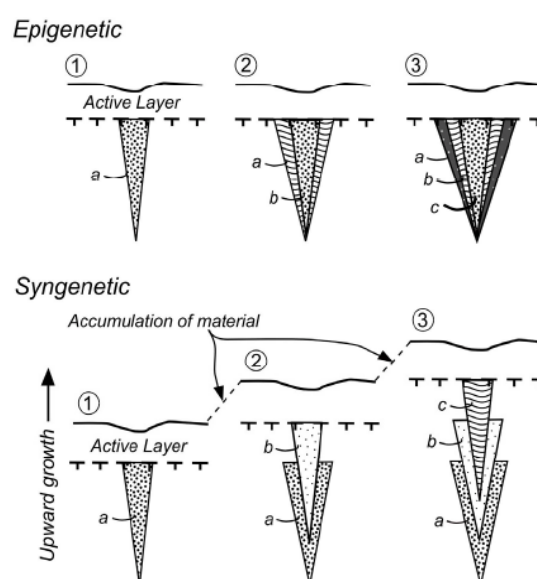


Fig. 2-5: Schematic diagram showing the growth of epigenetic and syngenetic ice wedges; point in time: (1) first, (2) second, (3) third; ice wedge at (a) first (b) second (c) third point in time (MACKAY 1990).

During the winter, following a rapid temperature drop, the ground may shrink and crack. In late May or early June, melt water from snow trickles down into the cracks and forms thin veinlets of ice. Through repeated cracking at the same place the ice wedge grows from year to year (LACHENBRUCH 1963; MACKAY 1972) (Fig. 2-4). Due to thawing of the active layer, the uppermost part of the ice vein is destroyed every summer (Fig. 2-4). The active layer expands above the ice wedge and prevents deeper thaw-

ing. Due to the contraction pressure associated with the frost crack opening and the expansion pressure related to the thawing of the polygon centre substrate, the adjacent sediments of an ice wedge develop a shoulder-like form (KARTE 1979; LACHENBRUCH 1963; MACKAY 2000) (Fig. 2-4). Ice wedges form under stable climatic conditions and therefore their existence already allows paleoclimatic interpretations (WASHBURN 1981).

2.1.3 Polygonal nets and lakes

Superficial expressed polygonal nets are formed by ice wedges (Fig. 2-6). This surface feature is characteristic for arctic tundra regions (e.g. FRENCH 2007) (Fig. 2-7).

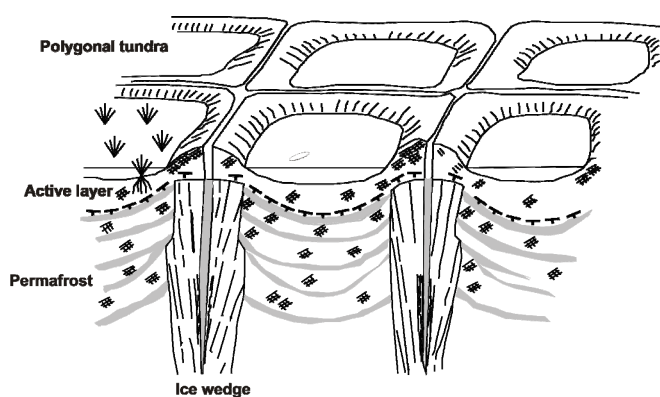


Fig. 2-6: Schematic view on modern polygonal nets (ROMANOVSKII 1977), modified.



Fig. 2-7: Intrapolygonal ponds and polygonal tundra in the Lena Delta, Siberian Arctic; Photo: K. PIEL, in BOIKE et al. (2009).

Two main types of ice wedge polygons occur: (1) low-centre polygons and (2) high-centre polygons. In low-centre polygons the rim is usually higher than the centre and therefore intrapolygon ponds (Fig. 2-7) are often developing inside. Later, the degradation of the polygon rims and changes in the hydrological regime may cause the formation of high-centre polygons, which are often accompanied by interpolygon ponds and thaw lakes.

The size of polygonal nets and the distance of ice wedges to each other can be used as an indicator for the harshness of the climate. Lower air temperatures and bigger amplitudes of the soil temperature initiate the formation of smaller polygonal nets. Furthermore, the substrate has a great influence on the distance between contraction cracks. In fine grained substrate the distance is shorter (YERSHOV and WILLIAMS 2004).

2.1.4 Thermokarst and alas

Thermokarst is the process, which forms characteristic landforms due to surface subsidence caused by the disturbance of the permafrost's thermal equilibrium. This can be induced for instance by climate change, disturbance of vegetation cover, fire, the shift of drainage channels or by human activities (FRENCH 2007; WASHBURN 1979). Thermokarst corresponds to an increase in the active layer depth and causes thawing of

permafrost beyond seasonal cycles. In addition, polygonal ponds can induce a positive feedback, because the high specific thermal conductivity of water promotes the development of thermokarst and the extension of an unfrozen body (talik, Fig. 2-3) underneath the water body (FRENCH 2007). Alas is a Yakutian word describing a grassy, treeless meadow occupying a flat-floored thermokarst depression with steep sides (TOMIRDIARO 1982). Alases are round to oval and many contain shallow lakes (WASHBURN 1979). Thermokarst causes both, a general and irreversible reorganisation of the old landscape and a 1100-1300 year polycyclic succession (Fig. 2-8) of lake and alas landscapes (TOMIRDIARO 1982). The vertical dimension of alases can be up to 40 m depth. Horizontally they can range from 100 m to a few kilometres in diameter when adjacent alases coalesce to thermokarst valleys (like Fig. 2-8, Stage 4a) (WASHBURN 1979).

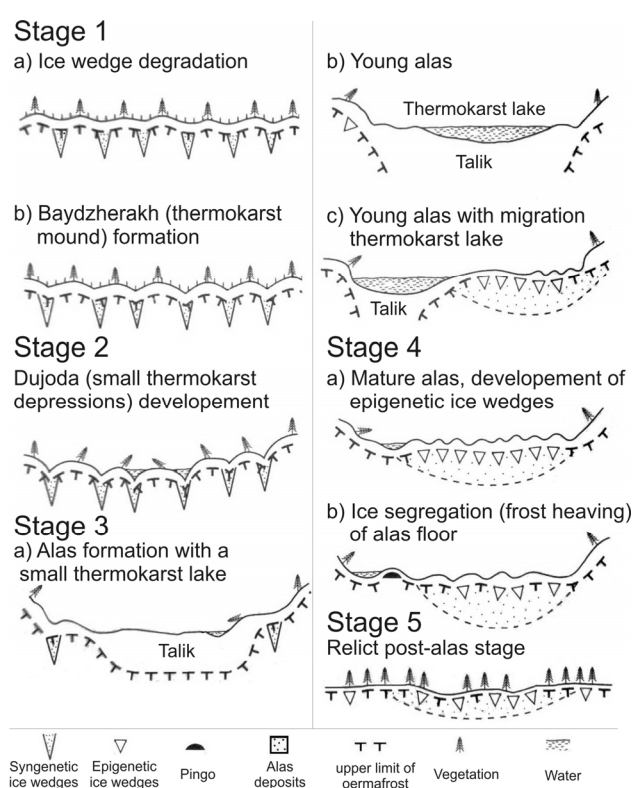


Fig. 2-8: Sequence of alas relief development in Central Yakutia; after SOLOVIEV (1973), in FRENCH (2007), modified.

2.1.5 Yedoma and Ice Complex

Originally, “Yedoma” defines relief features in East Siberian lowlands like for instance elevated areas dissected by thermokarst depressions. Due to this striking relief feature, the native Yakutian people called it “Yedoma”, which means “corroded earth” (KAPLINA and LOZHKIN 1979; TOMIRDIARO 1982). Nowadays Yedoma is regarded as a morphological unit consisting of hills that are dissected by alas depressions. “Yedoma Suite” is a regional stratigraphic term used for Late Pleistocene sediments in the Northeast Siberian lowlands. It was introduced by SHER (1979) on the basis of faunal studies at the Duvanny Yar site, the stratotype for these deposits (chapter 2.3). In this study the more general cryolithological term Ice Complex is used instead of Yedoma Suite. Ice Complex is exposed at shores and riverbanks by up to 50 m high out-

crops composed of more or less degraded ice wedge bodies and thermokarst mounds in between. These exposed outcrops are cutting vertically or diagonally the polygonal ice wedge systems. It is suggested that the Yedoma hills are remnants of former accumulation plains (e.g. GROSSWALD 1998; SCHIRRMEISTER et al. 2008b).

The possible spatial Ice Complex distribution is estimated to ~1 million km² (ROMANOVSKII 1993) (Fig. 2-9). SCHIRRMEISTER et al. (in review) suggested that the Ice Complex is chronologically and stratigraphically equivalent to Eurasian and Alaskan loess deposits, but not in a genetically context. There is still no generally accepted concept of the genesis of this up to 60 m thick and ice containing mostly silty deposits, but it seems to be clear that neither glacial, nor marine sedimentation was involved (Table 2-1) (FRADKINA et al. 2005; SCHIRRMEISTER et al. 2008b; SHER 1995).

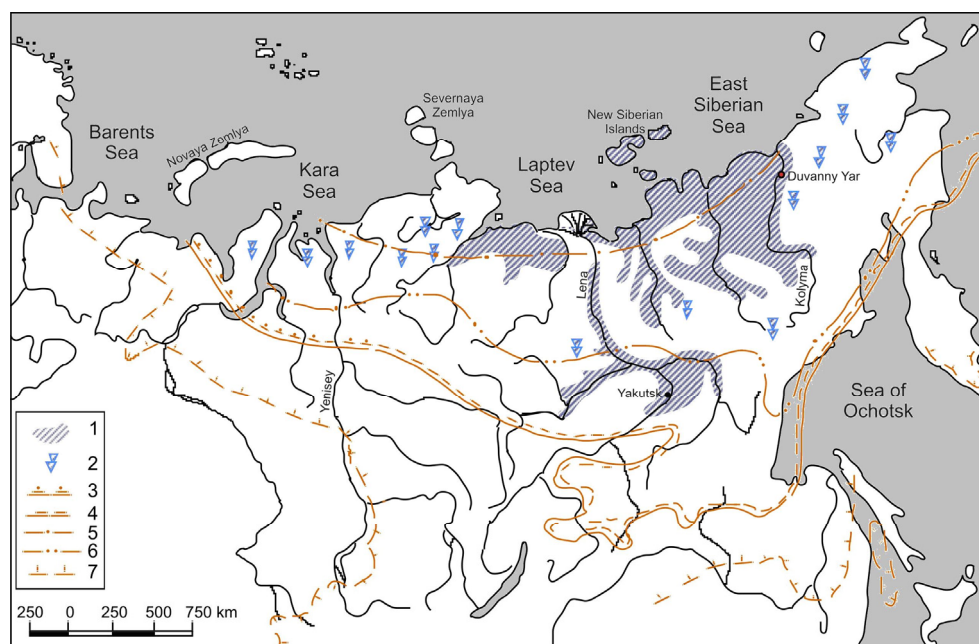


Fig. 2-9: Schematic map of possible Ice Complex distribution in northern Siberia; **1:** areas with a wide spreading of the Ice Complex at different relief elements; **2:** areas with Ice Complex spreading in river valleys and lake depressions; **3-5:** southern boundaries of areas with modern ice wedge formation in **(3)** peat soils, **(4)** clayed-silty deposits and **(5)** sandy pebble deposits; **6:** southern boundary of low-centred polygons; **7:** southern boundary of permafrost; according to ROMANOVSKII (1993), in SCHIRRMEISTER et al. (2002b), modified.

Table 2-1: Concepts of Ice Complex development.

Ice Complex development concepts	Author
Basin sediments dammed by a continuous ice-sheet in the Late Weichselian covering the entire Arctic margin of the continent	GROSSWALD (1998)
Formation in river deltas like the Lena delta	NAGAOKA (1994)
Proluvial and slope deposits, which are formed in foot-slope areas by periodic runoffs	GRAVIS (1969); KANEVSKIY (2003)
Fluvial and alluvial genesis	ROZENBAUM (1981)
Aeolian deposition, known as "artic loess"	TOMIRDIARO (1982); PEWE and JOURNAUX (1983)
Polygenetic origin (fluvial, lacustrine, aeolian, slope, redeposition etc.)	SHER (1995)
Nival lithogenesis, which is related to accumulation plains with a low topographic-gradient and perennial snow patches	KUNITSKY (2002), SCHIRRMEISTER et al. (2008b)

The first two concepts by GROSSWALD (1998) and NAGAOKA (1994) can be rejected, because paleo-environmental data is available, which excludes the involvement of an ice sheet (SHER 1995) or deltaic deposition (SCHIRRMEISTER et al. in review). However, it is accepted that Ice Complex was subaerially exposed most of the time and froze syngenetically during permafrost accumulation. For this reason, such sediments commonly contain Late Pleistocene mega-faunal remains like mammoth's bones and numerous plant fossils. Additionally, these deposits contain ice wedges making up to 50 % of the total volume (ZIMOV et al. 2006a). Sedimentological, geocryological and geochemical properties of Ice Complex deposits are used to characterise the environmental conditions during sediment deposition and ice wedge formation. Using these tracers, it is possible to characterise the environmental conditions during sediment deposition and ice wedge formation. With regard to climate change, it is predicted that the Ice Complex deposits will be transformed from a long-term carbon sink to a major carbon source as these organic-rich sediments thaw and greenhouse gases are subsequently released (WALTER et al. 2006; ZIMOV et al. 2006a).

2.2 Regional setting

2.2.1 Geological and geographical setting

The use of the Siberian Quaternary stratigraphy is associated with inconsistencies (ASTAKHOV 2001). For this reason as well as its notoriety in German geology the Western European terminology is used in this study. The correlation of different regional Pleistocene stratigraphic schemes is shown in Table 2-2 to avoid a discussion and confusion about the Late Quaternary stratigraphy terminology. This table is intended to support a comparison with other investigations, although there is no exact correlation between the different stratifications.

Table 2-2: Comparison of the stratigraphic terminology used in Western Europe and Siberia (ASTAKHOV 2001; 2HOPKINS 1982; 1KIND 1975; SHER et al. 2005; SVENDSEN et al. 2004; VELICHKO and NECHAEV 2005), in Andreev et al. (2009), modified.

Epoch	Western European	Siberian ¹	North American	Marine Isotope Stage	unglaci-ated regions of Beringia ²	Age [ka BP]	
Holo-cene				1	Birch interval	ca. 10.5 - present	
Late Pleistocene	Weichselian glaciation	Zyryanian glaciation	Wisconsinan glaciation	Late	2	Duvanny Yar interval	ca. 30 - 10.5
				Middle	3/4	Boutellier interval	ca. 50 - 30
				Early	4/5d-a	Happy interval	ca. 110 - 50
	Eemian interglacial	Kazantsevo interglacial	Sangamonian interglacial	5e		ca. 130 - 115	

The study area is a part of a Mesozoic continental collisional/accretionary zone of complex geology, which is summarised by HUH (1998) (Fig. 2-10).

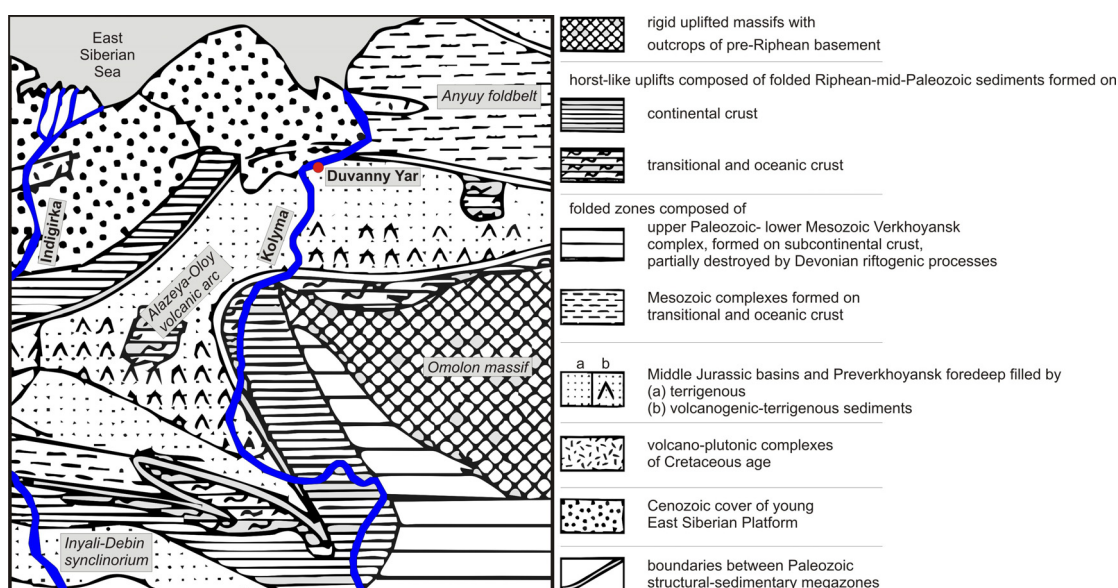


Fig. 2-10: Main tectonic zones of the study area; after PARFENOV (1991), in HUH (1998) and SOKOLOV (2002), modified.

The study area belongs to the Kolyma Lowland, which is restricted to the northern part of the Verkhoyansk-Chukot Mesozoic orogeny. The southern part of the lowland overlies the structure of the Alazeya-Oloy eugeosynclinal folded system. The southern margin of the lowland is supposed to be a continuation of the South Anyuy riftogenous trough (HUH et al. 1998). Moreover, the study site is situated at the northern border of the Kolyma-Omolon Superterrane (KOS), which contains several microcontinental fragments. To the north, near the study site, the KOS drifted into the North America-Chukotka plate forming the Anyuy foldbelt (Fig. 2-10) during the Cretaceous period. To the west, the KOS collided with the Siberian Platform and formed the Verkhoyansk foldbelt. As a result of neotectonic movements, individual patches of the Kolyma Lowland represent uplifted bedrock or outcrops of the Pliocene and Early Pleistocene deposits, but for most parts of the lowlands' area it consists of Late Pleistocene sediments of remarkable thickness like at the Duvanny Yar outcrop (SHER et al. 1979). Moreover VASIL'CHUK (2005) described local neotectonic movements during the formation of Duvanny Yar, visible by complicated river networks on air pictures. The previous mentioned Verkhoyansk foldbelt is a mountain range running from the Lena River Delta in the north to the Sea of Okhotsk in the south, comparable in size to the Ural Mountains. In the zone of westerly winds the north to south aligned Verkhoyansk mountain range is of climatic relevance, because it constrains wet air masses and consequently precipitation at their lee side (rain-shadow or lee effect). This supported the case that there is no evidence for vast ice sheets at Beringia during the Last Glacial Maximum (e.g. HUBBERTEN et al. 2004).

2.2.2 Climate, vegetation and soils

The Duvanny Yar section is located in an area of harsh subarctic climate with long and cold winters. Daily mean temperatures remain below the freezing point from October to May (Fig. 2-11); the mean temperature in January is -35°C . Summer spans four months with mean temperatures ranging up to 11°C during July. The mean annual air temperature (MAAT) is about -13°C . The climate is extremely continental as

shown by the annual temperature amplitude at Kolymskaya of about 45 °C (Fig. 2-11). The average annual precipitation is rather low with about 156 mm, of which ~40 % occur as rain and ~60 % as snow (DUTTA et al. 2006). Half of the precipitation occurs during June and October (Fig. 2-11). The snow cover becomes permanent in October and reaches its maximum thickness by the end of April. At Kolymskaya the average snow cover thickness is about 45 cm; in treeless areas it does not exceed 25 cm. The river gets usually frozen early in October and breaking and floating of ice usually starts late in May (SHER et al. 1979).

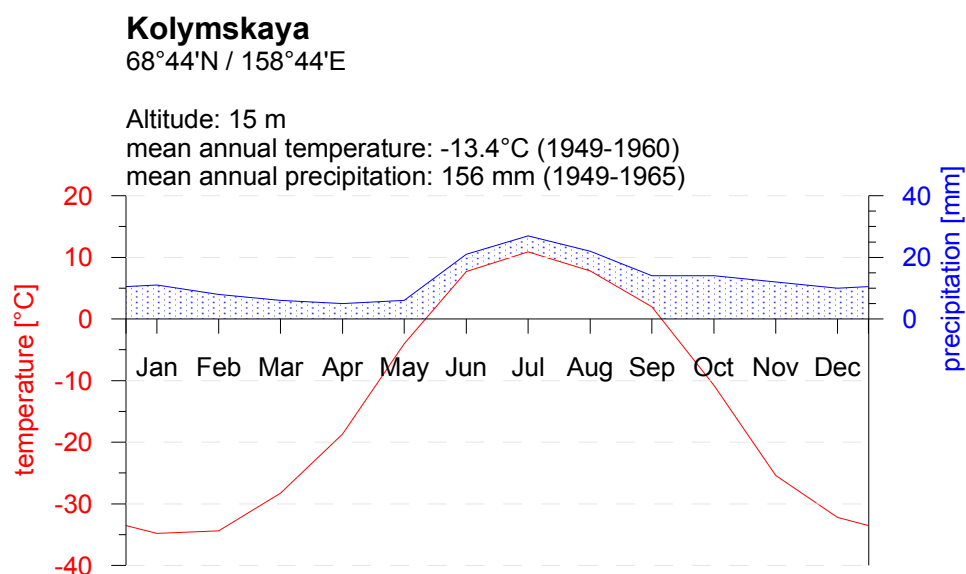


Fig. 2-11: Climatic diagram of Kolymskaya, ~20 km away from the study site (Fig. 2-12); after RIVAS-MARTÍNEZ (1996-2009) and SHER (1979), modified.

The harsh climate induces the development of “typical” forest tundra and boreal forest dominated by larch, which grows in sparsely spaced associations. In this manner lichen-larch forests with sparsely growing willow coppice, dwarf birch and tundra low shrubs, which constitute the ground layer, are formed (SHER et al. 1979). In the northern lowlands like at the Lower Kolyma, thermokarst lakes or bogs are prevalent. As drainage is poor due to the frozen ground, extensive wetlands, which are dominated by mosses and herbs are common (GITERMAN et al. 1982). In summary, the whole Yana-Indigirka-Kolyma Lowland region is characterised by a mosaic of open *Larix* forests, *Betula-Salix-Ericales* tundra and moist graminoid (i.e., *Cyperaceae* and *Poaceae*) tundra (ANDERSON and LOZHKIN 2001). The soils of this region are classified as loamy cryosols with partly appearing podzolisation processes (IUSS-WORKING-GROUP-WRB 2007; JAKOBSEN et al. 1996), which are derived from moderately weathered colluviums from acidic schist and diorite parent rocks (DUTTA et al. 2006; SHER et al. 1979).

2.3 The Duvanny Yar section

The study site Duvanny Yar (68° 37' N, 159° 06' E) is situated in the right hand Lower Kolyma river bank in the northeastern part of the Republic of Sakha (Yakutia), Russia. The site is located about 40 km upstream from Cherskii (Fig. 2-12). At the study site the Kolyma River meander incises into the surface. Thus the permafrost deposits became exposed in a ca. 12 km long section, which consists of Yedoma hills that are dissected by deep (up to 40m, Fig. 2-13) alluvial and thermo-erosional valleys (SHER et al. 1979).

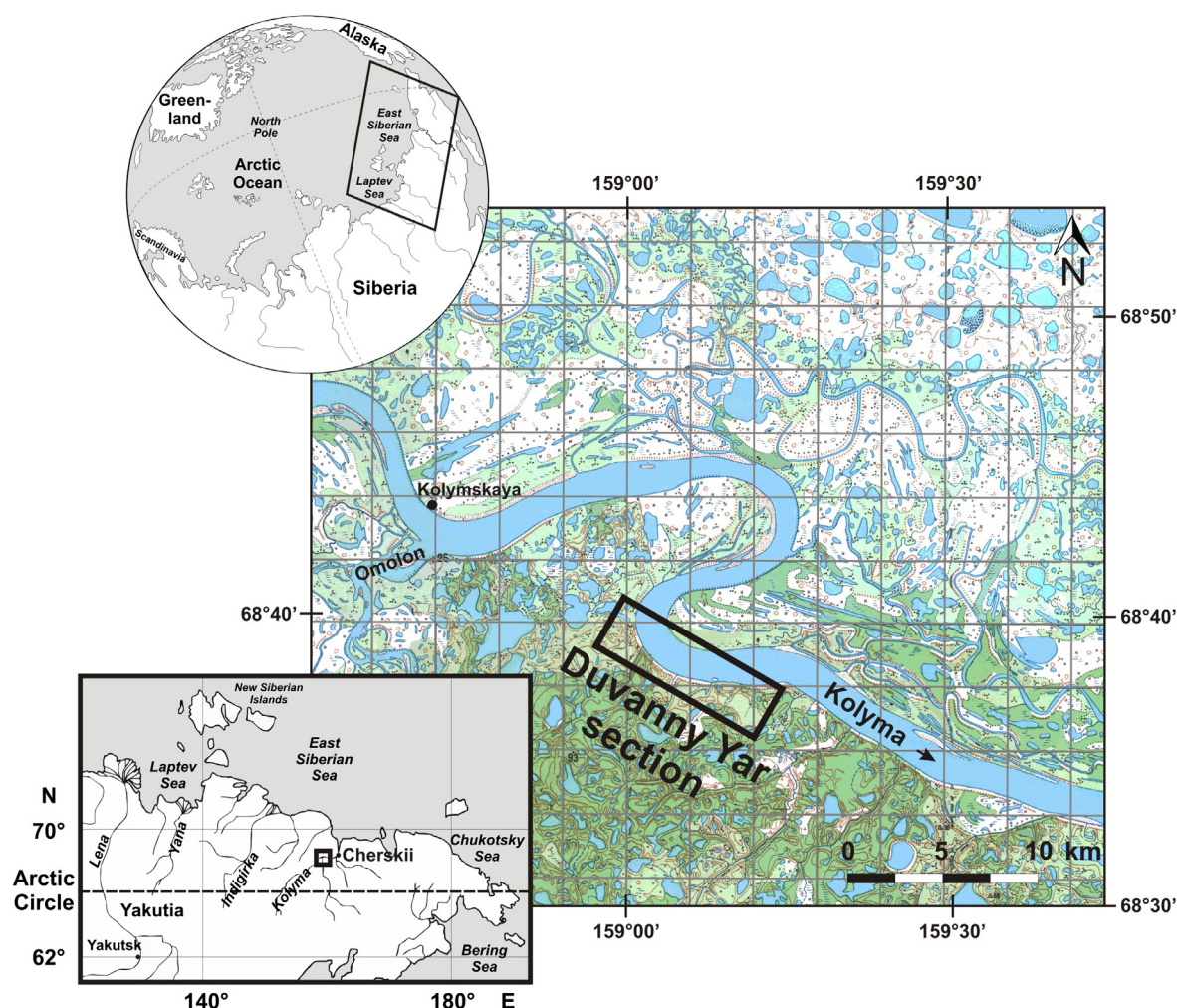


Fig. 2-12: Location of Duvanny Yar site; the frame at the globe is the extent of the overview map of Northeast Russia down right. The small black frame on the Northeast Russia overview map displays the extent of the map showing the Duvanny Yar site; topographic map sheets: (1) R-57-27-28 and (2) R-57-33-34; scale 1:200 000; actuality: (1) 1989 and (2) 1991, modified.

The Duvanny Yar section is considered to be the stratotype of the Ice Complex (KAPLINA et al. 1978; SHER et al. 1979). Furthermore, it is an important section for the paleoenvironmental history of the Late Pleistocene Beringia (Duvanny Yar interval in Table 2-2) (GITERMAN et al. 1982; HOPKINS 1982). Duvanny Yar was first described by BISKE (1957) and BARANOVA (1957). SHER (1971) carried out paleozoological studies with horse bones and differentiated the permafrost sequence in a late Middle Pleistocene and an upper Late Pleistocene segment (Fig. 2-13).

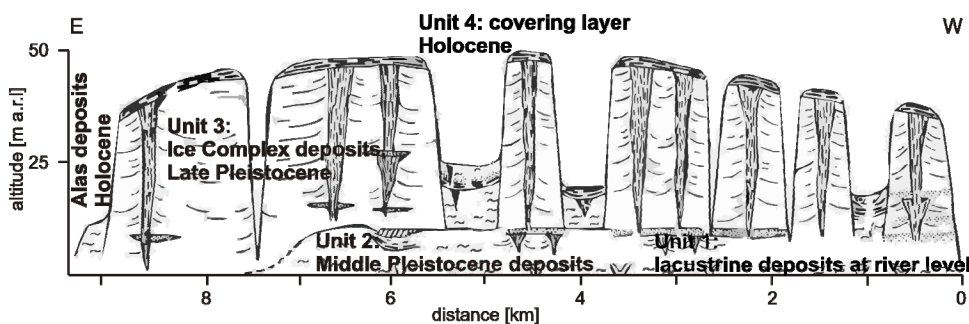


Fig. 2-13: Generalised view of the Duvanny Yar section; in GITERMAN et al. (1982), after SHER (1979), modified.

Cryolithological and sedimentological structures of Duvanny Yar were described in detail by KAPLINA et al. (1978), SHER et al. (1979), ARKHANGELOV et al. (1979) and KONISHCHEV (1983). VASIL'CHUK et al. (1988) published stable isotope data from ice wedges of Duvanny Yar and pollen data from these ice wedges (VASIL'CHUK et al. 2008a). Furthermore, Duvanny Yar was studied paleopedologically by GUBIN (1999). VASIL'CHUK et al. (2001) suggested that the Duvanny Yar Ice Complex was formed during ~40000 to 13000 a BP. Recent studies at this site investigate soil respiration and methane production making the carbon available which is stored in permafrost (DUTTA et al. 2006; ZIMOV et al. 2006a).

Continuous permafrost is a distinguishing feature of the Kolyma Lowland region and except some talik zones under the Kolyma River it is ubiquitous and impressively thick (about 500 m) (SHER et al. 1979). According to DUTTA et al. (2006), the permafrost active layer in the study area ranges from ~20 to 180 cm depth. Ice wedges at Duvanny Yar were formed under stable conditions over at least 30000 years (VASIL'CHUK et al. 2001). In the vertical dimension the ice wedges can reach 30 m or more (FRADKINA et al. 2005). Due to the high ice content and its massive ice wedges, the sediments of the Duvanny Yar erode rapidly by the Kolyma River. According to VASIL'CHUK (2001), the outcrop degrades several metres per year and Duvanny Yar has been displaced by ~100 m over the last 30 years.

3 Methods

3.1 General study scheme

A multidisciplinary approach using geocryological, sedimentological, geochronological, isotope geochemical and hydrochemical methods was applied to obtain multiproxy records. Sediment samples were analysed for ice contents, mass specific magnetic susceptibility, biogeochemistry (TC, TOC, TN, $\delta^{13}\text{C}$), grain size parameters, radiocarbon age (^{14}C AMS) and mineral density. Stable isotopes of water ($\delta^2\text{H}$, $\delta^{18}\text{O}$) were measured for ground ice (ice wedges, texture ice), modern surface waters and modern precipitation.

The study can be subdivided into two major tasks: (1) field studies of sediment and ground ice (Fig. 3-1, upper part) and (2) analysis of samples in the home laboratories (Fig. 3-1, lower part). During field work the ice content for most of the sediment samples was determined as well as the pH and electrical conductivity for few ice wedge and recent water samples. In the laboratory, the sediment samples are prepared and analysed for grain size, biogeochemistry, mineral density, magnetic susceptibility and radiocarbon age determinations of organic matter. Stable isotopes of water were measured for the recent water and ground ice samples. Hydrochemical analyses are performed on five ice wedge, seven fissure ice and twelve recent waters samples (ten periglacial lake and two river water samples). All in all within this study 143 sediment samples and 107 ground ice and recent water samples were analysed.

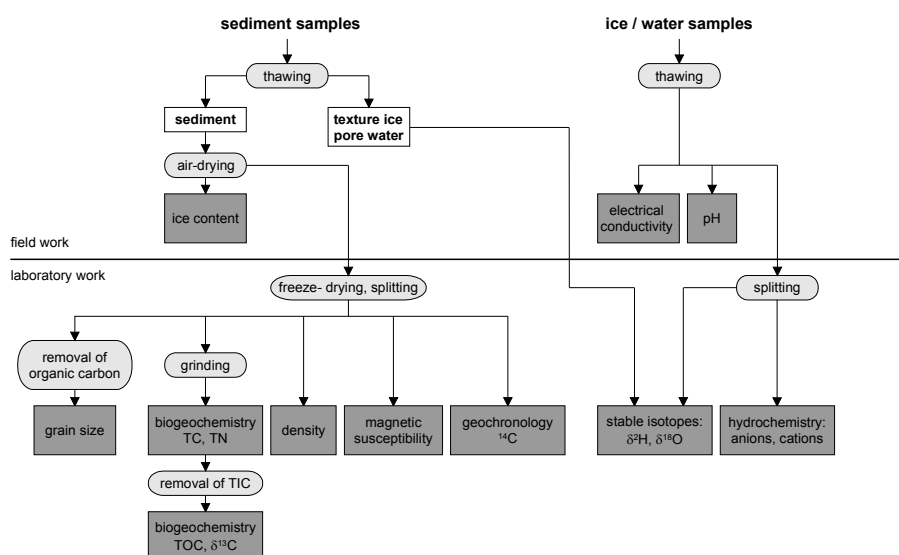


Fig. 3-1: Organisation chart of methods and preparation for the majority of samples.

3.2 Field work

The field work at the Duvanny Yar section was done by L. SCHIRRMEISTER and S. WETTERICH in the period of 2nd until 23rd of August 2008 (expedition report “Beringia/Kolyma 2008”, in press). The whole section of Duvanny Yar was mapped for a size estimation of alas and Ice Complex sections. Two long composite profiles of Ice Complex sections (DY-01, DY-05) and three smaller separate profiles of lake

deposits underlying the Ice Complex sequence (DY-02, DY-03, DY-06) as well as one section of an alas (DY-04) were studied and sampled.

3.2.1 Sediments studies and sampling

The profiles were mostly exposed on thermokarst mounds in thaw slumps or at the lower riverbank. After cleaning the walls of thermokarst mounds from thawed material, the exposed sequences were examined, described, photographed and sketched according to sediment- and cryostructures. In addition, frozen deposits were sampled for further laboratory studies using hammers and small axes. The sediment samples were packed into plastic bags. Some samples were collected unfrozen. Various subprofiles from different thermokarst mounds were stacked together to create composite profiles. The correlation of the sampling position in neighbouring subprofiles was realised by height estimation using a measuring tape.

3.2.1.1 Field measurements

Frozen samples were taken in aluminum boxes in order to determine the absolute and gravimetric ice content. After thawing and weighing, the fresh samples were dried using a portable oven to measure the dry weight subsequently in order to compute the absolute ice content. The difference between the two weights related to the dry weight results in the gravimetric content of the containing ice. Due to the definition, some ice supersaturated samples have gravimetric ice contents of more than 100 % (VAN EVERDINGEN 1998).

3.2.2 Studies and sampling of ground ice and recent waters

The ice wedges were sampled at horizontal transects in distances of 0.01 to 0.4 m using ice screws (\emptyset 14 mm). The ice wedges were described by the following characteristics: development (syngenetic or epigenetic), altitude, width, ice structure, width of single ice veins, content of organic material and sediment as well as amount, size, orientation and distribution of gas bubbles and other remarkable features. Samples of texture ice were taken as supernatant water from thawed sediment samples. In addition, samples from different modern surface waters (lake and river water) and summer precipitation (fog, rain) were taken near the study area in order to compare data sets from ground ice to the actual hydrochemical and climatic conditions. The samples were collected for stable isotopes analyses ($\delta^{18}\text{O}$ and $\delta^2\text{H}$) and hydrochemistry (pH, EC, anions, cations). The $\delta^{18}\text{O}$ and $\delta^2\text{H}$ isotope samples were kept in narrow mouth PE-plastic bottles (30 ml) and immediately closed to avoid evaporation. In total, this study analysed altogether 107 water samples (41 ice wedge and fissure ice samples, 49 texture ice samples, 10 lake water samples, 5 precipitation/fog samples and 2 river water samples).

Thereof, five ice wedge, seven fissure ice and twelve recent waters samples were measured at the field for electrical conductivity and pH. The pH and electrical conductivity were quantified using a WTW 340i pocket meter.

3.3 Sedimentological analysis

The following laboratory analyses were all performed at the AWI Potsdam except from density measurements (AWI Bremerhaven) and radiocarbon dating (Leibniz-Laboratory for Radiometric Dating and Stable Isotope Research, Kiel). As a first common step all samples were freeze dried (Sublimator 3-4-5, ZIRBUS technology), manually homogenised and split.

3.3.1 Mass specific magnetic susceptibility

The magnetic susceptibility describes how magnetisable a material is. It indicates the amount of ferri- and ferromagnetic minerals in a sample, like iron oxide or iron sulphite. This measurement allows the detection of differences between samples caused by sediment layers with different mineral composition. Thus, assumptions about distinctive genetic strata within a sediment profile can be made. The mass specific magnetic susceptibility (χ) is defined as the ratio of the volume magnetic susceptibility (κ) to the sample bulk density (ρ) (Eq. 3.1) (BUTLER 1992; DEARING 1999; SOFFEL 1991).

$$\chi = \frac{\kappa}{\rho_b}$$

Eq. 3.1

χ	mass specific magnetic susceptibility	$10^{-8} \text{m}^3 \cdot \text{kg}^{-1}$
κ	volume magnetic susceptibility	$\text{m}^3 \cdot \text{m}^{-3}$; dimensionless
ρ_b	bulk density	$\text{kg} \cdot \text{m}^{-3}$

The mass specific magnetic susceptibility was measured with a Magnetic Susceptibility Meter (Model MS2, Sensor Type MS 2B, Bartington Instruments) on the raw sample filled into a 12.5 ml vessel. The unit of the susceptibility is mentioned in the further text as ‘SI’, referred to the standardised unit $10^{-8} \text{m}^3 \cdot \text{kg}^{-1}$.

3.3.2 Grain size analysis

The grain size parameters are fundamental to describe the sediment structure and its variations. They allow the determination of accumulation areas and the medium of transportation (e.g. glaciers, water or wind) and are used to reconstruct environmental and energetic conditions during sediment transport and deposition (FÜCHTBAUER et al. 1988; TUCKER 1996).

The grain size was analysed using a laser particle sizer (Coulter LS 200, Beckmann Coulter GmbH). In order to measure only clastic grains, organic components were removed by shaking and adding three times a week 10 ml of concentrated hydrogen peroxide (35 % H_2O_2) per sample. The organic-free samples were diluted with about one litre of water and ‘washed’ to neutral pH value by centrifugation twice for 15 minutes at a speed of 5050 rpm at 20 °C. After that the samples were centrifuged again for water volume reduction. This centrifugation was done for 20 minutes at 4000 rpm and 2-4 times per sample. Afterwards the samples were dried for at least 2 days in a drying oven at 50 °C. Finally, 1.3 g of the dry sample was transferred into a 1000 ml PE-bottle with about 0.5-1 g of dispersing agent ($\text{Na}_4\text{P}_2\text{O}_7 \cdot 10 \text{H}_2\text{O}$) and filled with ca. $\frac{1}{2}$ to $\frac{3}{4}$ litre of 1 % ammonia solution (NH_3). The PE-bottles were placed in an overhead shaker for at least 6 hours. The liquid samples were split into eight homogenous subsamples and the sediment fraction >1 mm was sieved out because of measurement limitations of the laser. The particles >1 mm were exam-

ined by microscopy to determine whether it is an inorganic component and included into the grain size fraction.

The grain size distribution was displayed in volume percentage. Grain sizes between 0.375 and 1000 µm were derived. The sediments were classified according to Table 3-1. The results of the grain size analysis were entered into the software SEDIVISION 2.0 and average diameter, sorting after TRASK (1932) and fractions of sand, silt and clay were calculated.

Table 3-1: Fine grain size fractions according to EN ISO 14688/ DIN 4022 (SCHEFFER and SCHACHTSCHABEL 2002), modified.

Phi (-log ₂ mm)	9	7	6	4	2	1	-1
µm (10 ⁻³ mm)	<2.0	<6.3	<20	<63	<200	<630	<2000
mm	<0.002	<0.0063	<0.02	<0.063	<0.2	<0.63	<2.0
		fine	middle	coarse	fine	middle	coarse
	clay	silt			sand		

3.3.2.1 Interactive peak fitting

The peak fitting is used to differentiate the grain size fractions. The background for this is the detection of changes in the processes of weathering, transport and accumulation. The grain size distribution curve can be regarded as a response of many overlapping sedimentological signals. To consider different modes of the grain size curve separately, the Interactive Peak Fitter (IPF, Version 4.1, O’HAVER 2009) was used. The software is a Matlab extension for time-series signals. It uses an unconstrained non-linear optimisation algorithm to break apart a complex, overlapping peak signal into its component parts. This is done to determine whether a signal can be represented as the sum of fundamental underlying peaks shapes. The method was applied to the two Ice Complex profiles. The grain size in µm needed to be converted into Phi (Φ) values according to Eq. 3.2 (FÜCHTBAUER et al. 1988) before an import into the Interactive Peak Fitter software was possible.

$$d_{\Phi} = -\log_2 \frac{d_{\mu m}}{1000} \quad \text{Eq. 3.2}$$

d_{Φ} grain diameter Φ

$d_{\mu m}$ grain diameter µm

The Phi scale was used because of its logarithmic definition. For use with the interactive peak fitter the data table had to be sorted in ascending order. The equivalence with µm scale is shown in Table 3-2.

Table 3-2: Equivalence of Φ and µm scales.

Φ	0	1	2	3	4	5	6	7	8	9	10	11
µm	1000	500	250	125	62.50	31.25	15.63	7.81	3.91	1.95	0.98	0.49
	coarse ←—————→ fine											

After the data was imported, a baseline of the grain size distribution was defined and the number of peaks was set to 4 or 5 depending on the number of peaks at specific grain size distributions. In addition, the

estimated position of peaks was defined approximately. The peak type was set to Gaussian distribution and the grain size distribution was fitted applying several Gauss curves until the RMS error has been < 2 and the curve parameters (position, height, width and area) reasonable. Finally, the mode position, height, width, area and error of each curve were exported. Moreover, percentage of its mode area to the total curve area was calculated. The error, which is reported by the interactive peak fitter, is the RMS difference between the best-fit model and the raw data over the fitted segment. Fig. 3-2 explains the interactive peak fitter output and the position of the different peaks (chapter 4.5.1).

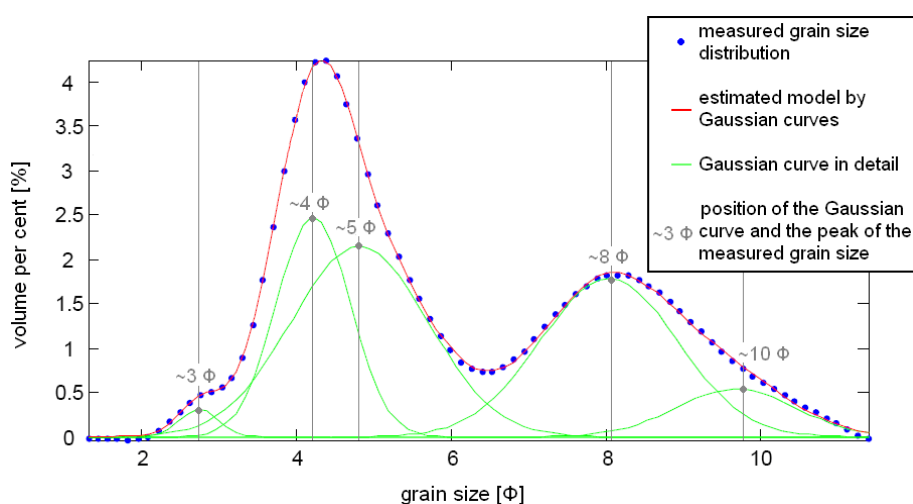


Fig. 3-2: Example of the peak fitting for sample DY-05-H-48 and the explanation of the interactive peak fitter outputs.

3.3.3 Determination of TC, TOC and TN values

Sediments are the quantitative most important depositions and reservoirs of organic carbon (DEGENS 1968). The determination of organic carbon is of high relevance, because it could preserve the molecular, elemental and isotopic composition of carbon from living plants (MEYERS 1994, 2003). Paleoenvironmental conditions can be reconstructed concerning e.g. temperature regimes. In addition, conclusions on biological productivity and the metabolic category of plants (e.g. C_3 , C_4 , algae etc.) are possible.

The biogeochemical parameters total carbon (TC), total organic carbon (TOC), total nitrogen (TN) and TOC/TN ratio were determined. The TOC/TN ratio could be used as an indicator for mineralisation rate of the organic components (Table 3-3).

Table 3-3: Approach of a classification of TOC/TN values; after WALTHERT et al. (2004).

TOC/TN- ratio	Description	Rate of mineralisation
<10	very narrow	high
10-12	narrow	
13-16	moderately narrow	
17-20	moderate	moderate
21-25	moderately wide	
26-35	wide	low
>35	very wide	

The sediment samples were analysed with a CNS analyser (Vario El III, Elementar Analysensysteme). The analytical process is based on the principle of catalytic tube combustion with oxygen supply at high temperatures. Samples were homogenised by grinding (planetary mill Pulverisette 5, Fritsch). Five milligram were taken from each pulverised sample and encapsulated twice in zinc capsules for TC and TN determination. In each series of measurements a blank capsule for background detection and measuring of standards after every 20 samples ensures correct analytical values with a device-specific accuracy of $\pm 0.1\text{wt } \%$. For the TOC measurements the procedure was the same except from use of different calibration standards and the removal of carbonate content by hydrochloric acid (1.3 molar).

In addition to the quantitative measurement of the inorganic carbon content, the existence of calcium carbonate (CaCO_3) was estimated using a field test with hydrochloric acid (10 %). The measurements were based on the classification of the ‘Bodenkundliche Kartieranleitung’ (AD-HOC-ARBEITSGRUPPE-BODEN 2004) (Table 3-4).

Table 3-4: Carbonate content in soil (AD-HOC-ARBEITSGRUPPE-BODEN 2004, Table 40, S. 169), shortened.

CO ₂ -development and its impact on cohesive soils	Carbonate content		
	approx. carbon content in wt. %	Abbreviation	Characterisation
no reaction	0	c ₀	free of carbonate
very weak reaction: not visible, only audible	< 0.5	c ₁	very low carbonate
weak reaction, hardly visible	0.5 – <2	c ₂	low carbonate
not continuous flare-up	2 – <10	c ₃	carbonaceous
weak, not continuous, but visible CO ₂ bubbling	2 – <4	c _{3,2}	weakly carbonaceous
clear, not continuous CO ₂ bubbling	4 – <7	c _{3,3}	medium carbonaceous

3.3.4 Bulk density and organic carbon ratio

The density of the solid matter was measured to calculate the bulk density of the sediment samples. The bulk density is a standard parameter describing the mass of a unit volume of soil. The volume includes both solid and pore volume. The density was measured by using a helium gas displacement pycnometer (Accu-Pyc-1330, Micromeritics). The principle of this measurement is that helium penetrates into the pores and permits to approach the real volume (Eq. 3.3).

$$V_{\text{sample}} = V_{\text{sample cell}} - \frac{V_{\text{exp cell}}}{\left(\frac{P_r}{P_f}\right) - 1} \quad \text{Eq. 3.3}$$

V_{sample}	volume of the sample	cm ³
$V_{\text{sample cell}}$	volume of the sample cell	cm ³
$V_{\text{exp cell}}$	volume of the expansion cell	cm ³
P_r	run fill pressure	Pa
P_f	the final pressure	Pa

The size of the sample ($V_{\text{sample cell}}$) and expansion ($V_{\text{exp cell}}$) cells are determined by calibration and automatically stored in the instrument’s set-up parameters. Given that the sample weight has been specified, the density is derived automatically (Eq. 3.4).

$$\rho_s = \frac{m_{sample}}{V_{sample}}$$

Eq. 3.4

ρ_s	density of the solids	$\text{g} \cdot \text{cm}^{-3}$
m_{sample}	weight of the sample	g
V_{sample}	volume of the sample	cm^3

Further details are described in VIANA et al. (2002). The bulk density of the samples were calculated according to SCHEFFER and SCHACHTSCHABEL (2002). Therefore the volume of the solids (V_s) was derived first (Eq. 3.5). After that, the porosity (n) was calculated (Eq. 3.6). The negative linear correlation with the sediment porosity allows calculation of the bulk density as shown in Eq. 3.7.

$$V_s = \frac{m_s}{\rho_s}$$

Eq. 3.5

$$n = \frac{V_p}{V_p + V_s}$$

Eq. 3.6

$$\rho_b = (n - 1) \cdot (-\rho_s)$$

Eq. 3.7

ρ_s	density of the solids	$\text{g} \cdot \text{cm}^{-3}$
m_s	weight of the solids	g
V_s	volume of the solids	cm^3
n	porosity	dimensionless
V_p	volume of the pores	cm
ρ_b	bulk density	$\text{g} \cdot \text{cm}^{-3}$

Assuming that in the studied deposits all pores are saturated with ice, the absolute ice content gives an estimation of the volume of the pores. For the determination of ice volume ($V_{ice} = m_{ice} \cdot \rho_{ice}^{-1}$) an ice density of $0.9127 \text{ g} \cdot \text{cm}^{-3}$ was assumed.

The aim of the density measurement was a quantification of a ratio of organic carbon in the permafrost deposits. As a reference volume a $1 \text{ m} \times 1 \text{ m} \times 1 \text{ m}$ (1 m^3) cube was taken. The calculation of the organic carbon content in $\text{kg TOC} \cdot \text{m}^{-3}$ was accomplished with Eq. 3.8.

$$\text{organic carbon content} = V_{ref} \cdot \rho_b \cdot 1000 \cdot \frac{TOC_{wt\%}}{100}$$

Eq. 3.8

V_{ref}	reference volume	1 m^3
ρ_b	bulk density	$\text{t} \cdot \text{m}^{-3}$
$TOC_{wt\%}$	TOC content	wt %

3.4 Geochronology

The dating of sediment samples is essential for chronological classification of former events and stages (AHNERT 2003). In addition, it is possible to estimate the duration and rates of processes within a sediment profile. In an ideal case, the sedimentation rate ($\text{sedimentation} \cdot \text{time}^{-1}$) can be estimated from the time span between dated samples if correlated with the sediment thickness.

The age determination was realised with the radiocarbon dating method on macroscopic plant remains while using the radioactive decay of the ^{14}C nuclide. The analytical principle is based on the fact that the radioactive carbon isotopes (^{14}C) are released from the reaction of stable nitrogen isotopes (^{14}N) with solar neutrons in the upper atmosphere. Together with oxygen, ^{14}C isotopes form a steady-state equilibrium (about one ^{14}C isotope per 10^{12} stable C atoms) of $^{14}\text{CO}_2$, next to the stable forms of $^{13}\text{CO}_2$ and the most abundant $^{12}\text{CO}_2$. Certainly, the ^{14}C isotopes take part in the global carbon cycle. Atmospheric $^{14}\text{CO}_2$ mixes into biomass through photosynthetic processes and so there exists a constant proportion between the radioactive ^{14}C and the stable isotope ^{12}C . After the organisms death this stable proportion underlies a constant

decay of ^{14}C to ^{14}N . The radioactive half-life of ^{14}C amounts to 5730 ± 40 a (CLARK and FRITZ 1997; GODWIN 1962).

According to LIBBY (1955; 1961) and STUIVER et al. (1977) the time since organism death, that corresponds to the radiocarbon age, can be calculated as follows:

$$t = \frac{1}{\lambda} \cdot \ln \frac{{}^{14}\text{C}_{t=0}}{{}^{14}\text{C}_{t=1}} \quad \text{Eq. 3.9}$$

t	calculated age	a BP
${}^{14}\text{C}_{t=0}$	original ${}^{14}\text{C}$ content	pMC
${}^{14}\text{C}_{t=1}$	${}^{14}\text{C}$ content after a certain time span	pMC
λ	decay constant	a^{-1}
$t_{1/2}$	half time of ${}^{14}\text{C} = 5730 \pm 40$	a

There is a detection limit due to the half-life time of radiocarbon. Despite special enrichment techniques and the possibility of using small sample volumes, the AMS (Accelerator Mass Spectrometry) dating method has a limit of 40000-50000 a, not exceeding 60000 a at its best (WAGNER 1995). The measured radiocarbon ages are reported in years before present (a BP) related to 1950 AD. Moreover radiocarbon ages within the time span of 0 until ~26000 a BP were converted into calendar years (cal BP) using calibration data sets, which are based on dendrochronology and uranium/thorium series measured on corals (REIMER et al. 2004). The age determination measurements within this study were performed at the Leibniz-Laboratory for Radiometric Dating and Stable Isotope Research, Kiel. The detailed measurement procedure is described by GROOTES et al. (2004).

3.5 Stable isotope geochemistry

Stable isotope geochemistry analyses were applied for organic carbon and ice. In this study particularly information about metabolic plant category ($\delta^{13}\text{C}$ of sediment samples) and the paleotemperature ($\delta^{18}\text{O}$, $\delta^2\text{H}$) are of importance.

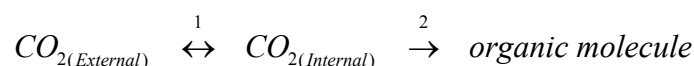
3.5.1 Carbon isotopes ($\delta^{13}\text{C}$)

Carbon has two stable isotopes, ^{12}C (98.9 %) and ^{13}C (1.1 %) (HOEFS 1997; NIER 1950). It is generally assumed that plant biomass reflects environmental conditions during their growth period. So paleoclimatic information is stored in organic carbon, even after its deposition. Analysing organic sedimentary properties may provide information about prevailing temperature regime, water availability, soil properties and biogeochemical mechanisms of decay. The preservation of characteristic elemental and isotopic composition allows plant identification (e.g. marine or land plants) (MEYERS 1994). The carbon isotopes content ($\delta^{13}\text{C}$) is calculated by the ratio of ^{13}C to ^{12}C atoms and reported as per mill difference against the international reference standard VPDB (Eq. 3.10) (CRAIG 1953; NIER 1950).

$$\delta^{13}\text{C} = \left(\frac{R_{\text{sample}}}{R_{\text{VPDB}}} - 1 \right) \cdot 1000 \quad \text{Eq. 3.10} \quad \text{R atomic ratio between the heavy and light isotope } ({}^{13}\text{C}/{}^{12}\text{C})$$

The standard VPDB is a limestone belemnite from the Pee Dee Formation in South Carolina, which is depleted but replaced by an adequate material.

Generally, plants take carbon for photosynthesis from two major sources, the atmospheric CO_2 and from CO_2 and HCO_3^- (hydrocarbonate), dissolved in the hydrosphere. Kinetic isotope effects during photosynthesis (step 2, scheme below) concentrate the light isotope ^{12}C in the synthesised organic matter (PARK and EPSTEIN 1960). A simplified two step scheme of carbon uptake is assumed:



Plants using the C_3 pathway (first product of synthesis is a C_3 chain: phosphoglyceric acid), called Calvin-Benson pathway, preferentially incorporates ^{12}C into organic matter, leading to a significantly negative shift from the isotope ratio (Fig. 3-3). Another photosynthetic pathway, the Hatch-Slack pathway, is used by C_4 plants (first product of synthesis is a C_4 chain: oxalacetate). In this case a smaller carbon isotope fractionation is associated (Fig. 3-3). A third group of plants is characterised by a hybrid pathway (CAM, crassulacean acid metabolism), which can use both Calvin-Benson and Hatch-Slack pathway and consequently results in intermediate carbon fractionation (HOEFS 1997). Aquatic plants use dissolved CO_2 and the ^{13}C enriched HCO_3^- as carbon source, which is more important in sea water than on land. This explains why marine algae are enriched in ^{13}C relative to land plants (Fig. 3-3).

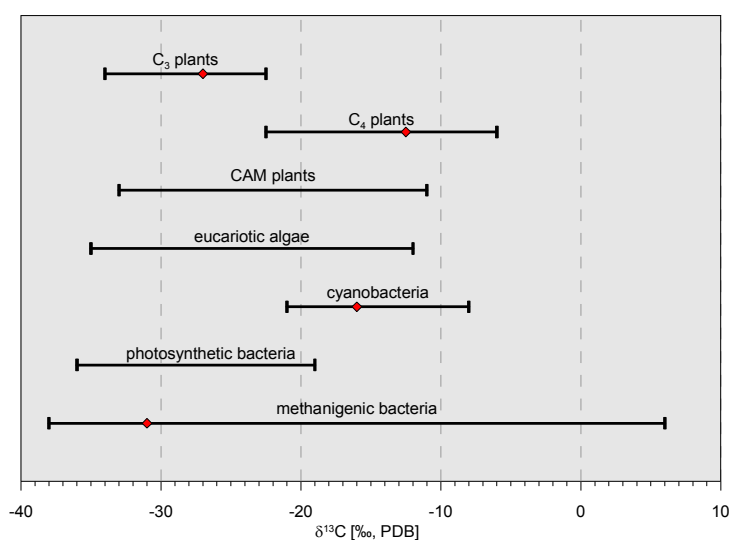


Fig. 3-3: Rough estimation of carbon isotope composition of higher plants, algae and autotrophic prokaryotes; the red dots are estimated means for some groups, in HOEFS (1997) after SCHIDLOWSKI et al. (1983), modified.

Measurement technique

The $\delta^{13}\text{C}$ ratio was measured with a Thermo Finnigan MAT Delta-S mass spectrometer. Due to the analytical method which requires a gaseous state (CO_2) of the sample, an element analyser (Flash EA 1112 Series, Thermo Finnigan) and a gas mixing device (CONFLO III) were linked to the mass spectrometer. As only the $\delta^{13}\text{C}$ value of the organic carbon was of relevance to this study, carbonate free samples which were prepared for TOC determination were used. The required sample weight for the measurement was calculated as shown in Eq. 3.11.

$$\text{sample weight [g]} = \frac{45}{\text{TOC}} \quad \text{Eq. 3.11}$$

Similar to the TN, TC and TOC analysis, the sample material was encapsulated in silver capsules. Measuring control standards and performing repeated determination after every seventh measurement ensured correct analytical values. First, the samples were combusted at ~ 950 °C. The generated CO₂ was induced into the sample tube of the mass spectrometer while other gases (by-gases) were reduced. A standard gas (also CO₂) of known isotopic composition was measured against the sample to determine the isotopic ratio. After that, the CO₂ was put into the mass spectrometer, where it was ionised, accelerated and focused in an electrostatic field resulting in a single beam. A magnetic field separates the ions according to their mass and they were neutralised by hitting a collector. The released mass specific electrical currents were used to calculate the individual isotopic contents and the ¹³C/¹²C ratios (CRAIG 1953; DEGENS 1969). Measurements at AWI Research Unit Potsdam were reproducible with accuracy better than ± 0.15 ‰.

3.5.2 Oxygen & hydrogen isotopes ($\delta^{18}\text{O}$, $\delta^2\text{H}$)

Given that ground ice is fed by meteoric waters, it provides valuable information for paleoclimatic reconstructions. The temperature conditions, precipitation sources and the genesis of ground ice (DEREVIAGIN et al. 2002) can be studied with stable water isotopes in permafrost on ground ice.

Natural water consists to nearly 99.73 % of ¹H₂¹⁶O isotopes, but it also contains other stable isotopic molecules, in particular ¹H₂¹⁸O (~ 0.205 ‰), ¹H₂¹⁷O (~ 0.035 ‰) and ¹H²H¹⁶O (~ 0.015 ‰) (HÖLTING and COLDEWEY 2009). Due to slight differences in physical properties of these molecules, which mainly affect their saturation vapour pressure and their molecular diffusivity in air, fractionation processes occur at phase changes of water (JOUZEL 2003). As a result, these processes divide light and heavy isotopes. The lighter isotopes stay/move predominantly in the more volatile fraction (Fig. 3-4) (DANSGAARD 1964). The fractionating processes are subdivided into two major effects:

1. Equilibrium effects, which have forward and backward reaction rates and are part of a well mixed system in a chemical equilibrium. Those effects are reversible.
2. Kinetic isotopes, which are in the sum unidirectional (e.g. isolation of the reaction product from the reactant) (Kendall and Doctor 2003).

The isotope distribution in the precipitation varies according to latitudes, altitudes and continents and, in turn, in the various reservoirs of the hydrosphere and cryosphere. Globally, the oceans serve as the main source for atmospheric water vapour and the initial isotopic composition of 0 ‰ is termed as Vienna Standard Mean Ocean Water (VSMOW). The formation of vapour masses from the oceans is dominated by kinetic non-equilibrium fractionation and mainly influenced by the relative humidity. As the vapour mass starts drifting and gets cooler, condensation and hence precipitation are also subjected to isotope partitioning, which operates under equilibrium conditions. This process is strongly controlled by temperature. The isotopic evolution of precipitation can be understood as Rayleigh distillation process, leading to a progressive decrease in the heavy isotope concentration within the remaining vapour and thus to a relative enrichment in ¹H₂¹⁶O (DANSGAARD 1964).

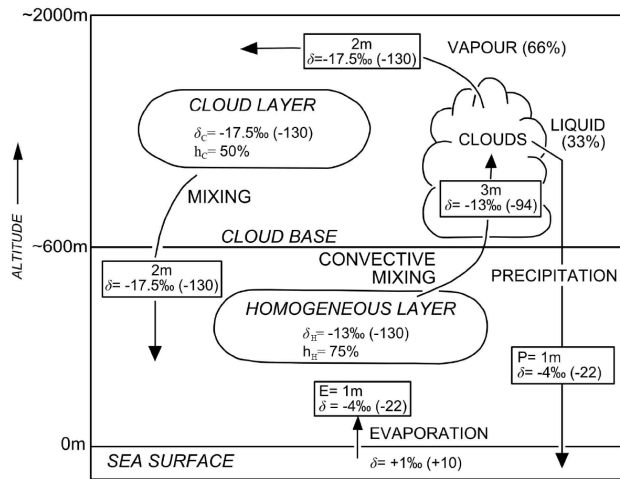


Fig. 3-4: CRAIG and GORDON (1965) model for isotopic fractionation in marine-atmosphere cycle. δ -values are reported for ^{18}O (^2H in parenthesis), relative mass fluxes in metres of water; E: evaporation, P: precipitation, h: humidity, H: homogeneous layer (in GAT 1996).

The isotope ratios, $^2\text{H}/^1\text{H}$ and $^{18}\text{O}/^{16}\text{O}$, are reported using the δ -notation described as per mil (‰) against VSMOW:

$$\delta^{18}\text{O}, \delta^2\text{H} = \left(\frac{R_{\text{sample}}}{R_{\text{VSMOW}}} - 1 \right) \cdot 1000 \quad \text{Eq. 3.12}$$

R atomic ratios between the heavy and light isotope ($^{18}\text{O}/^{16}\text{O}$ and $^2\text{H}/^1\text{H}$, respectively)

Negative δ -values indicate a depletion of heavy isotopes relative to the reference standard. CRAIG (1961) observed that $\delta^2\text{H}$ and $\delta^{18}\text{O}$ values of precipitation are linearly related throughout the world. This is shown by the correlation of ^2H and ^{18}O concentrations in worldwide fresh surface water and is called the Global Meteoric Water Line (GMWL, Eq. 3.13).

$$\delta^2\text{H} = 8 \cdot \delta^{18}\text{O} + 10 \quad \text{Eq. 3.13}$$

Referring to the position relative to the GMWL, DANSGAARD (1964) defined the parameter d to describe the deuterium (d) excess in global precipitation and hence express the corresponding deviation from the GMWL (Eq. 3.14).

$$d = \delta^2\text{H} - 8 \cdot \delta^{18}\text{O} \quad \text{Eq. 3.14}$$

This divergence is caused by kinetic non-equilibrium processes during evaporation from the ocean surface and accordingly is a consequence of ^{18}O being more sensitive to kinetic fractionation than ^2H . The fact that the d excess of a precipitation is influenced by the conditions prevailing in the oceanic moisture source region (temperature, relative humidity and wind speed) is used to reconstruct the changes in the temperature of the evaporative source and potential switches of precipitation sources (JOUZEL 2003). Craig's GMWL is an average of different meteoric water lines. To a regional scale, the local factors affect both d excess and slope, which justify the introduction of Local Meteoric Water Lines (LMWL) (CLARK and FRITZ 1997). It offers detailed regional specific information for e.g. trajectory of storms secondary changes in isotopic composition. With regard to this theoretical concept and the related assumptions, in particular the dependence of the isotopic composition from the condensation temperature, some general implications can be made (CLARK et al. 1997; DANSGAARD 1964):

1. Isotopically depleted meteoric waters are associated with cold regions.
2. Areas of high latitude receive isotopically more depleted precipitation than areas of lower latitude. This phenomenon is known as “latitude effect”.
3. Precipitation on continental sites in regions with seasonal temperature variations exhibits a seasonal cycle with isotopically depleted precipitation in winter and enriched in summer. This case is called “seasonal effect”.
4. Progressive Rayleigh rainout causes a depletion of heavy isotopes in continental areas compared to regions which are closer to the vapour source. This phenomenon is called “continental effect”.
5. High altitudes favour isotopically more depleted precipitation than lower elevations, which is known as “altitude effect”.

Moreover, the formation of snow within a cloud has, in contrast to rain, a non-equilibrium fractionation effect additional to the equilibrium process (JOUZEL and MERLIVAT 1984). This partly kinetically fractionation is a consequence of vapour deposition in an environment supersaturated over ice. This is responsible for elevated values for the d excess of winter precipitation in high latitudes (GAT 1996). Additionally, once the snow is formed as ice crystals no further isotope exchange with the surrounding moisture occurs during snowfall and the isotopic composition of the cloud is preserved (GAT 1996). This is only true for fast freezing processes, where isotope fractionation during freezing is negligibly low. Slower freezing rates of lower $2 \text{ mm} \cdot \text{h}^{-1}$ (VAIKMÄE 1991) cause the typically enrichment in ^2H and ^{18}O in the less volatile phase, the ice. As rates for ice wedge freezing are faster than $2 \text{ mm} \cdot \text{h}^{-1}$, fractionation during freezing is negligible.

Ice wedges are mainly fed by winter precipitation (VAIKMÄE 1989), so that the water filling frost cracks gives a winter temperature signal. In contrast, texture ice is postulated to form syngenetically in the active layer. It consists of refrozen soil water, which is a mixture of waters of various origins: summer and winter precipitation, surface waters and last winter’s ice. Repeated seasonal thawing and freezing adds numerous cycles of phase change and fractionations, mixes the isotopic signal in the active layer and generally reduces the variations of isotopic composition in texture ice. Even though preservation of soil moisture in texture ice occurs in a complex way, it still reflects environmental and climatic changes (MEYER et al. 2002a; SCHWAMBORN et al. 2006).

Measurement technique

The determination of deuterium ($\delta^2\text{H}$) and oxygen ($\delta^{18}\text{O}$) isotope contents within a sample is based on mass spectrometric detection of atoms. Atoms with a different mass cause specific ion beams and motions in a magnetic field (HOEFS 1997). For this purpose a Finnigan MAT Delta-S mass spectrometer is combined with two equilibration units (MS Analysetechnik, Berlin). The equilibration technique, based on HORITA et al. (1989), allows measurements of $\delta^2\text{H}$ and $\delta^{18}\text{O}$ on one single subsample in one run (MEYER et al. 2000).

The hydrogen isotope measurement was carried out first according to MEYER et al. (2000). The equilibration for oxygen isotope detection was performed on the same sample after finishing the hydrogen isotope

measurement. Before measuring a sequence of water samples, the laboratory reference standard NGT1 (snow from the North Greenland Traverse) was measured to serve as reference material. The sample gas passed, alternating with the reference gas, the mass spectrometer and was consequently measured against the reference gas. Additionally, control standards of different isotopic composition were employed for each equilibration unit for quality control. Standard deviations were generally better than 0.8 ‰ for $\delta^2\text{H}$ and 0.1 ‰ for $\delta^{18}\text{O}$. The detected values of $\delta^2\text{H}$ and $\delta^{18}\text{O}$ were further recalculated to the VSMOW standard with the software ISODAT[®].

3.6 Hydrochemistry

By gaining knowledge about the chemical composition of water samples, it is possible to draw conclusions about origin and the flow path of the water for instance (HÖLTING and COLDEWEY 2009). The hydrochemistry of ice wedges and recent waters allows inferring the probable origin of the water prior to freezing. In addition, the dominant water type, hydrochemical facies and possible changes over time were determined. Before conserving the samples for hydrochemical measurements, all samples were filtered through a cellulose-acetate filtration set (pore size 0.45 μm) already in the field.

The mass concentrations in $\text{mg} \cdot \text{l}^{-1}$ of the major cations (Na^+ , K^+ , Ca^{2+} , Mg^{2+}) and anions (Cl^- , SO_4^{2-} , HCO_3^-) were transformed into equivalent concentrations in $\text{mmol} \cdot \text{l}^{-1}$ (expressed as $\text{mmol}(\text{eq}) \cdot \text{l}^{-1}$ for the distinction with the molar concentration) using Eq. 3.15.

$$c_{\text{mmol}(\text{eq}) \cdot \text{l}^{-1}} = c_{\text{mg} \cdot \text{l}^{-1}} \cdot \frac{z}{M} \quad \text{Eq. 3.15}$$

$c_{\text{mmol}(\text{eq}) \cdot \text{l}^{-1}}$	equivalent concentration	$\text{mmol} \cdot \text{l}^{-1}$
$c_{\text{mg} \cdot \text{l}^{-1}}$	mass concentration	$\text{mg} \cdot \text{l}^{-1}$
z	valence of the ion	
M	molar mass	$\text{mg} \cdot \text{mmol}^{-1}$

Furthermore, the Normalised Inorganic Charge Balance (NICB, in %) was calculated. The NICB can be used as quality control for the hydrochemical analyses, indicating a charge imbalance. The underlying assumption of the NICB is that the sum of equivalent concentrations ($\text{mmol}(\text{eq}) \cdot \text{l}^{-1}$) (Eq. 3.15) of dissolved anions in natural water should equalise the cation concentration. Relative to half the total sum of anions and cations, the charge imbalance should not exceed 5 % for concentrations $<2 \text{ mmol}(\text{eq}) \cdot \text{l}^{-1}$ and 2 % for concentrations $>2 \text{ mmol}(\text{eq}) \cdot \text{l}^{-1}$ (HÖLTING and COLDEWEY 2009).

$$\text{NICB} [\%] = \frac{\sum c_{\text{cations}} - \sum c_{\text{anions}}}{\frac{1}{2} \cdot (\sum c_{\text{cations}} + \sum c_{\text{anions}})} \times 100 \quad \text{Eq. 3.16}$$

c_{cations}	equivalent concentration of the cations	$\text{mmol} \cdot \text{l}^{-1}$
c_{anions}	equivalent concentration of the anions	$\text{mmol} \cdot \text{l}^{-1}$

3.6.1 Alkalinity measurements

Alkalinity measurements were taken from a subset of the prepared anion samples using a digital titrator (Metrohm 794 Basic Titrino). The analytical principle is based on potentiometric titration. The equivalence point was determined by using a standard reagent of known concentration. At this point of titration the

standard reagent had completely reacted with the measured sample. Via the consumption of standard reagent the HCO_3^- content could be calculated. To ensuring a complete reaction, the pH was permanently measured (HEINRICHS and HERRMANN 1990). This reaction was completed when the measured liquid was pH neutral. For this purpose the assumption was made, that in most natural waters other ions besides carbonate (CO_3^{2-}) and hydrocarbonate (HCO_3^-) are found in low concentrations. This means that the carbonate alkalinity is nearly equivalent to the total alkalinity (EN ISO 9963-1). Before starting the alkalinity measurements, the digital titrator and the pH electrode were calibrated with two buffer solutions. After that, a control standard of known concentration (1000 μmol Standard HCO_3^-) was titrated. Then a 2.5 ml sample was titrated with 0.01 $\text{g} \cdot \text{mol}^{-1}$ HCl solution in μl -intervals until the endpoint of pH = 4.3, where all CO_3^{2-} and HCO_3^- contained in the sample was converted to H_2CO_3 . Afterwards, the volume of HCl (standard reagent) was used for the alkalinity calculation described as the concentration of HCO_3^- in $\text{mg} \cdot \text{l}^{-1}$. For this purpose, the software Tinet and Eq. 3.17 (EN ISO 9963-1) were used:

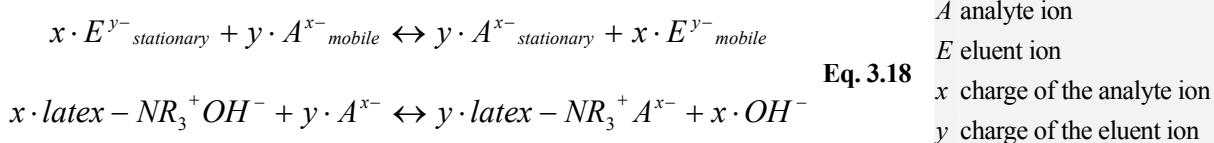
$$\text{Alkalinity}_{\text{sample}} = \frac{V_{\text{std reagent}} \cdot c_{\text{std reagent}}}{V_{\text{sample}}} \quad \text{Eq. 3.17}$$

$V_{\text{std reagent}}$	volume of the standard reagent	ml
$c_{\text{std reagent}}$	known concentration of the standard reagent	$\text{mg} \cdot \text{l}^{-1}$
V_{sample}	known sample volume	ml

Each measurement was accomplished 2 times to minimise the measurement error.

3.6.2 Determination of anion concentration

The determination of dissolved anions (F^- , Cl^- , SO_4^{2-} , Br^- , NO_3^- , PO_4^{3-}) concentrations was carried out with an ion chromatograph (Dionex DX-320). Ion chromatography based on anion separation through ion exchange processes between a mobile phase and a stationary phase (column). The liquid mobile phase contained about 25 μl sample fluid and an eluent (KOH), which functions a carrier and moves the chemicals through the different columns. The stationary phase consisted of two columns. The first column (guard column) purified the mobile phase of any contaminants (e.g. organic compounds). After that, the purified mobile phase entered the separation column, which is coated with ionic functional groups (here latex- NR_3^+) that reversibly interact with the analyte ions of opposite charge (Eq. 3.18). In this column the separation of anions took place. Depending on their specific affinity towards the stationary phase, the anions were retained for a certain time. Those components which were strongly retained moved slowly with the flow of the mobile phase. As a consequence of differences in mobility, the different anions were separated into discrete bands or zones.



In the next step, the mobile phase passed a suppression column to amplify and clarify the signal. Therefore, ion exchanger membranes converted the eluent into H_2O and thereby lowered its electrical conductivity, while the sample anions were converted into their corresponding strong acids. (HANDBOOK DIONEX

2000; WEIB 2001). A conductometric detector recognised these anion signals automatically according to the positions of peaks in the chromatogram displayed against time. Finally, the anion concentrations were calculated based on the anion peaks against time by using the PEAKNET[®] software. To ensure a precise measurement, a blank sample was analysed in order to detect the background noise. Moreover, a certified reference standard (QCP 051) was measured in regular intervals between the samples to validate the recorded values. The standard deviation of the target value for the control standard was better than 2.5 %.

3.6.3 Determination of cation concentration

Samples for cation analyses (15 ml) were acidified with 200 µl HNO₃ straight after field sampling to prevent precipitation. In the laboratory the cation concentrations of Al, Ba, Fe, Mn, Sr (in µg · l⁻¹) and Ca, K, Mg, Na, P and Si (in mg · l⁻¹) were analysed by Inductively Coupled Plasma Optical Emission Spectrometry (ICP-OES) using a Perkin-Elmer ICP-OES Optima 3000 XL. The measuring principle is based on the detection of element specific emissions of radiation after the excitation through plasma.

The plasma is formed from argon gas, which is ionised by an electric spark and reaches temperatures of 5000-10000 °K (NÖLTE 2001). For the whole duration of the analysis, the sample was continuously introduced into a cross-flow nebuliser. The nebuliser converted the sample into a mist of droplets (aerosols) by a stream of compressed argon gas. Applying a steady flow-through, the sample was injected into the plasma stream, which atomised and ionised the aerosols. This procedure resulted into a higher hybrid orbital of the samples. Electromagnetic radiation was emitted by ions, which dropped back to the lower energy level, which resulted in the release of energy as photons. The whole electromagnetic spectrum was separated in the characteristic wavelengths of the different elements. The intensity of a characteristic wavelength was used as a proxy for the elemental concentration. A polychromator and photodiodes were used to detect the electromagnetic radiation (NÖLTE 2001). The element concentrations were calculated with the software AA WinLab[®].

A control standard for surface water (SPS-SW-2, Spectrapure Standards Norway) was measured in regular intervals between samples to ensure an accuracy of <5 % for elements detected in the range of mg · l⁻¹ and 5-10 % for elements detected in the range of µg · l⁻¹. Furthermore, a blank containing water and HNO₃ was measured to detect background noise.

4 Results

The results are subdivided according to the genetic origin of the sediments. Lake sediments (DY-02, DY-03 and DY-06), Ice Complex deposits (DY-01 and DY-05) and alas deposits (DY-04) are presented in separate sections following the chronological manner from old to young deposits. Within the profiles the results are presented from bottom to top.

4.1 General composition of the Duvanny Yar section

According to SHER et al. (1979) the Duvanny Yar section is divided stratigraphically into four main units (unit 1 to 4) and alas deposits (Fig. 2-13). In August 2008, six profiles along the riverbank were sampled (DY-01 to DY-06, Fig. 4-1).

The sediment profiles analysed in this study comprise SHER's unit 2 (here DY-02) assumed as Eemian deposits. Middle and Late Weichselian Ice Complex deposits of unit 3 (DY-05 and DY-01) and unit 4, the Holocene covering layer (topmost samples of DY-01) were sampled as well. Furthermore, alas deposits described by SHER et al. (1979), were sampled at profile DY-04 (Fig. 4-1). The below and next to profile DY-01 located profiles DY-03 and DY-06 are probably of Eemian/Weichselian transition and Holocene age, respectively. Following SHER's classification, DY-03 could be related to unit 1 lake deposits at the bottom beds (Fig. 2-13 and Fig. 4-1).

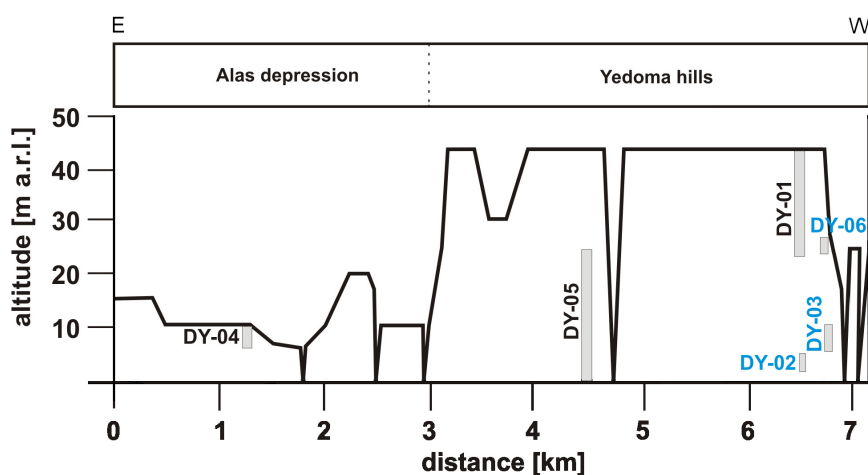


Fig. 4-1: Scheme of the Duvanny Yar section with positions of the studied profiles; from SCHIRRMAYER et al. (in press), modified.

4.2 Lake deposits below/next to the Ice Complex sequence

4.2.1 Profile DY-02

The profile DY-02 was located 2.0 to 5.5 m a.r.l. below the composite profile DY-01 (Fig. 4-1). A temporal thermo-erosional gully exposed a three metre high steep wall of frozen sediments and a large ice wedge. Ten sediment samples (DY-02-A-01 to 10, Fig. 4-2) were taken from this profile.

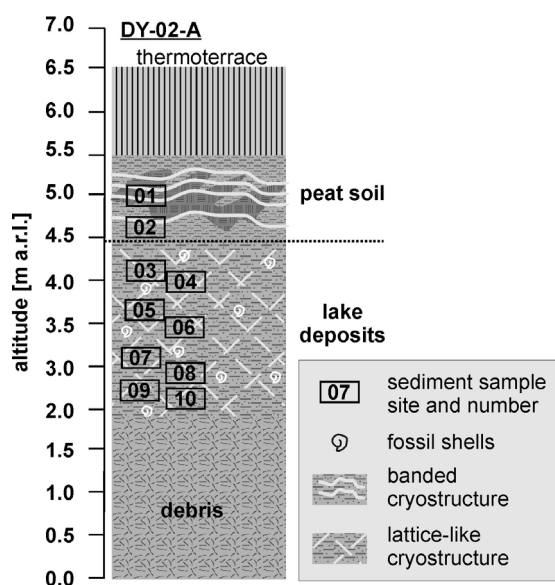


Fig. 4-2: Scheme of the lake profile DY-02; from SCHIRRMEISTER et al. (in press), modified.

4.2.1.1 Sediments of profile DY-02

The profile DY-02 consisted of a lower lake sequence overlain by a peat soil layer (Fig. 4-2). The sediments were alternate bedded and composed of a grey fine-laminated silty fine sand and brown plant detritus layers. In addition, wood fragments (\varnothing 2 cm), separate plant remains and shell fragments were observed. The cryostructure was mostly reticular with diagonal and vertical ice veins (1 to 2 mm thick, 2 to 10 cm long, 1 to 5 cm distance). The gravimetric ice content of this part ranges between 30 und 68 wt % (Fig. 4-3). At some sites the lacustrine sediment and along ice veins parts of the boundary zone were coloured brownish by iron oxide.

The lake sequence was covered by a cryoturbated peat soil layer (>4.3 to 5.5 m a.r.l., Fig. 4-2), which was composed of grey-brown silty fine sand and dark brown tongue-like peat inclusions (10 to 20 cm, roots, wood fragments). The cryostructure was banded with 1 to 2 cm thick ice bands in a distance of 5 to 10 cm. Interlayers between ice bands showed lenticular structures (lenses 2 to 3 cm long, 1 mm thick). The gravimetric ice content is about 250 wt %.

The boundary between the two parts is reflected in the sedimentary properties (Fig. 4-3). In the lower part, the magnetic susceptibility decrease from 52 to 38 SI. At the boundary zone to the upper part, it increases to 58 SI and decreases again to 31 SI at the top. From 2.1 to 4.2 m a.r.l. the TOC content is on a constant low level between 0.4 and 1.4 wt %, which indicates more or less constant formation conditions for the lake sediments. A few centimetres higher, there is a steep increase up to ~4 wt % in the boundary zone and high values of nearly 18 wt % in the peat soil layer. The same increase, although less pronounced, is reflected in the TOC/TN ratio, where the ratio increases from 7 to 11 over the boundary zone between lake sequence and peat soil layer. An inverse pattern is shown in the $\delta^{13}\text{C}$ ratios, which decrease from -25.5 to -32.8 ‰.

This shows periods of increased organic matter accumulation and its limited decomposition. The carbonate content in this profile is very low (max. c_2 : 0.5-2 wt %).

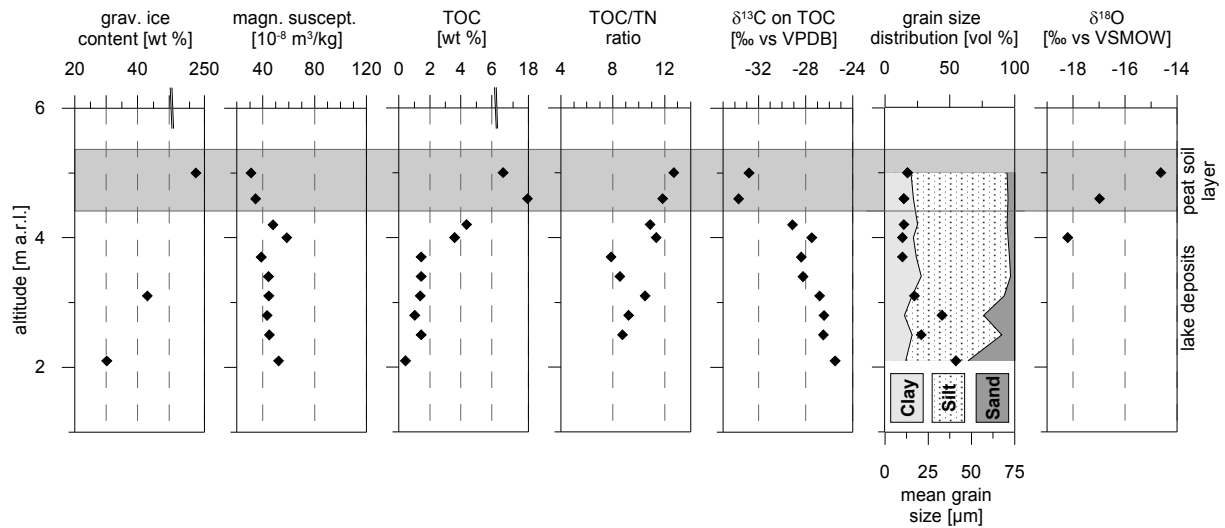


Fig. 4-3: Summary of cryolithological and sedimentological parameters for the lake sediment profile DY-02.

In general, the profile is dominated by silt-sized material with a bias from fine sand/coarse silt towards fine silt. As shown in the triangle diagram after SHEPARD (1954), all sediments except of two in the lower part (sandy silt at DY-02-A-08 and -10) can be described as clayey silt (Fig. 4-4 B). The mean grain size decreases from 41 μm at the lowermost sample to 10 to 11 μm in the middle part of the profile (Fig. 4-3). All sediments in DY-02 are very poorly sorted (2.7 to 4.4) with the major grain size peak in the silt fraction. Only the peak of the lowermost sample is shifted into the fine sand fraction. For the grain size distribution curves the classification into two parts is slightly different as mentioned above. The grain size distribution curves reveal an increase of the middle silt fraction. The increase sets in already in the middle part of the lake deposits.

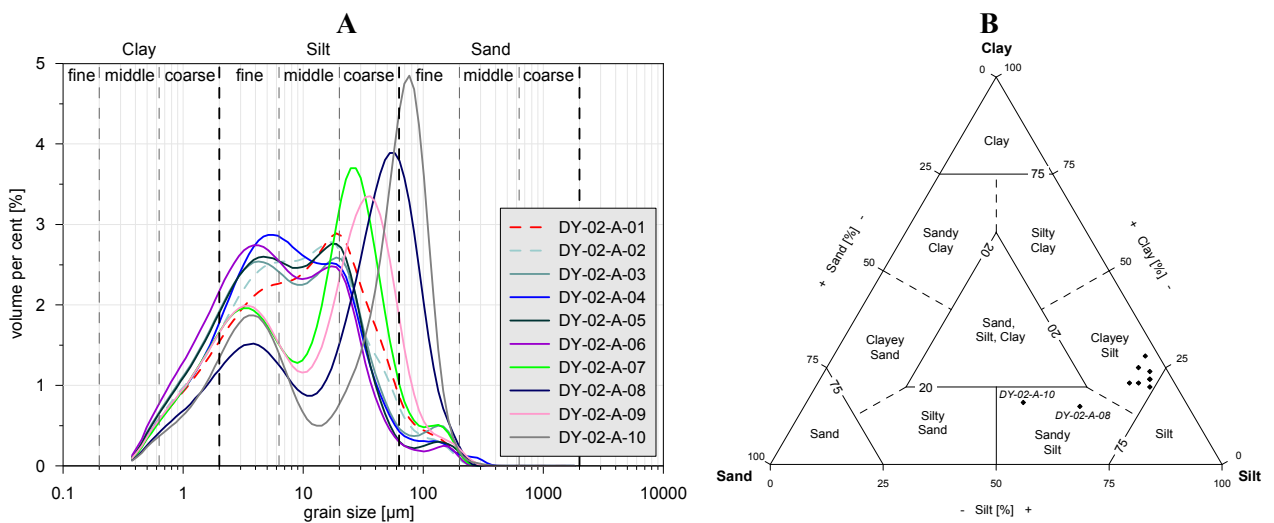
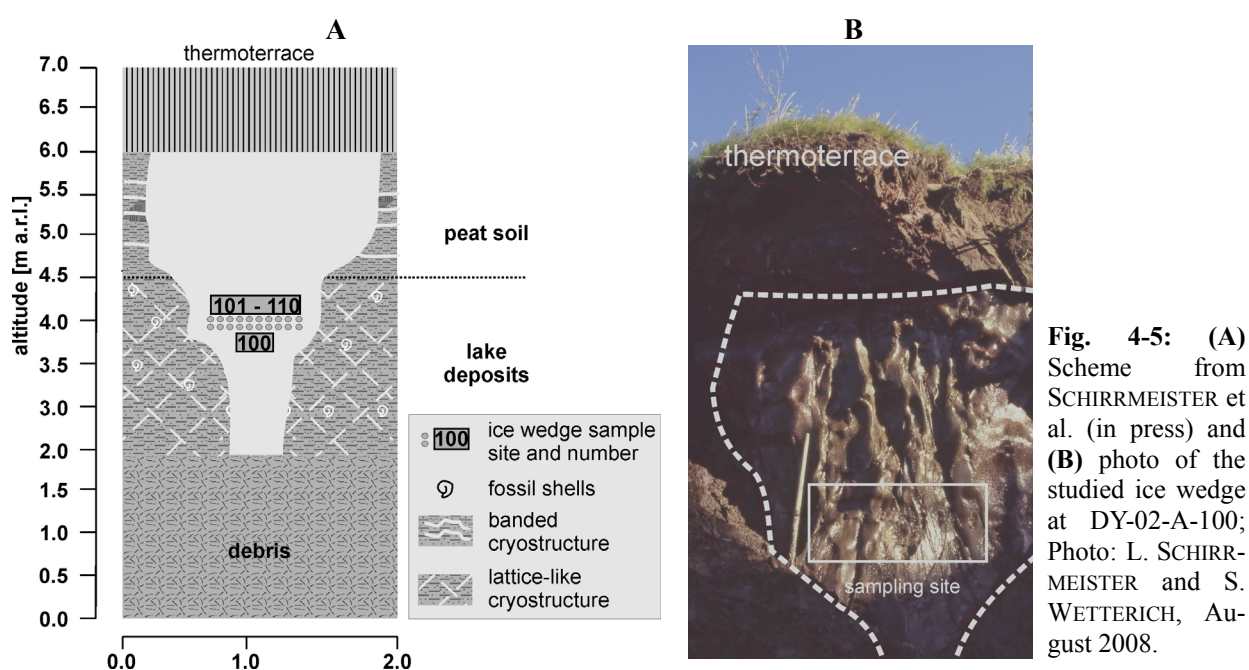


Fig. 4-4: (A) Grain size distribution and (B) sediment triangle after SHEPARD (1954) of the lake sediment profile DY-02. In A, the peat soil part is shown as dashed curves.

The lowermost four samples are characterised by two distinct major peaks in the fine silt and the coarse silt/fine sand fraction. This grain size distribution changes from a cluster of distinct bimodal distributions (DY-02-A-10 to 07) into a cluster of less distinct bi- to trimodal distribution from the upper area of the lower part to the top (DY-02-A-06 to 01 Fig. 4-4 A).

4.2.1.2 Ground ice DY-02

An about 1.5 m wide ice wedge penetrating the above mentioned sequence was exposed between 2.0 and 6.0 m a.r.l. at the opposite wall of the gully. The ice wedge was covered by thermoterrace deposits. It consisted of a smaller epigenetic part within the lower lake deposits and a wide syngenetic part in the upper peat soil layer (Fig. 4-5). It was composed of alternation of milky and clear ice veins (2 to 10 mm thick) and contained irregular distributed gas bubbles (\varnothing 1 to 2 mm). The ice wedge was sampled for hydro-chemical and isotope geochemical studies (ten samples, DY-01-101 to 110).



The mean isotopic composition of the ice wedge DY-02 is -28.6‰ for $\delta^{18}\text{O}$ and -225.4‰ for $\delta^2\text{H}$ (Fig. 4-6). The heaviest values -27.4‰ ($\delta^{18}\text{O}$), -216.4‰ ($\delta^2\text{H}$) and -26.3‰ ($\delta^{18}\text{O}$), -209.2‰ ($\delta^2\text{H}$) can be affected by exchange processes with the surrounding texture ice, because their values are very different from the main cluster and they were located at the edge (Fig. 4-6). The low isotope values relative to recent summer precipitation ($\delta^{18}\text{O}$: -15.9‰ ; $\delta^2\text{H}$: -123.3‰) indicate cold temperatures during ice wedge formation. The distinct offset of the ice wedge ratios (d excess: between 1.3‰ and 4.3‰) has a small range. Due to the missing reference for winter precipitation data (expected interval approximately within the dashed lines in Fig. 4-6) at Duvanny Yar, it is not possible to draw solid conclusions on the precipitation source of the ice wedge water. All samples of this ice wedge are linearly correlated in the $\delta^2\text{H}$ - $\delta^{18}\text{O}$ diagram (Fig. 4-6) with a slope of 7.2 and an intercept of -20 ($R^2=0.996$).

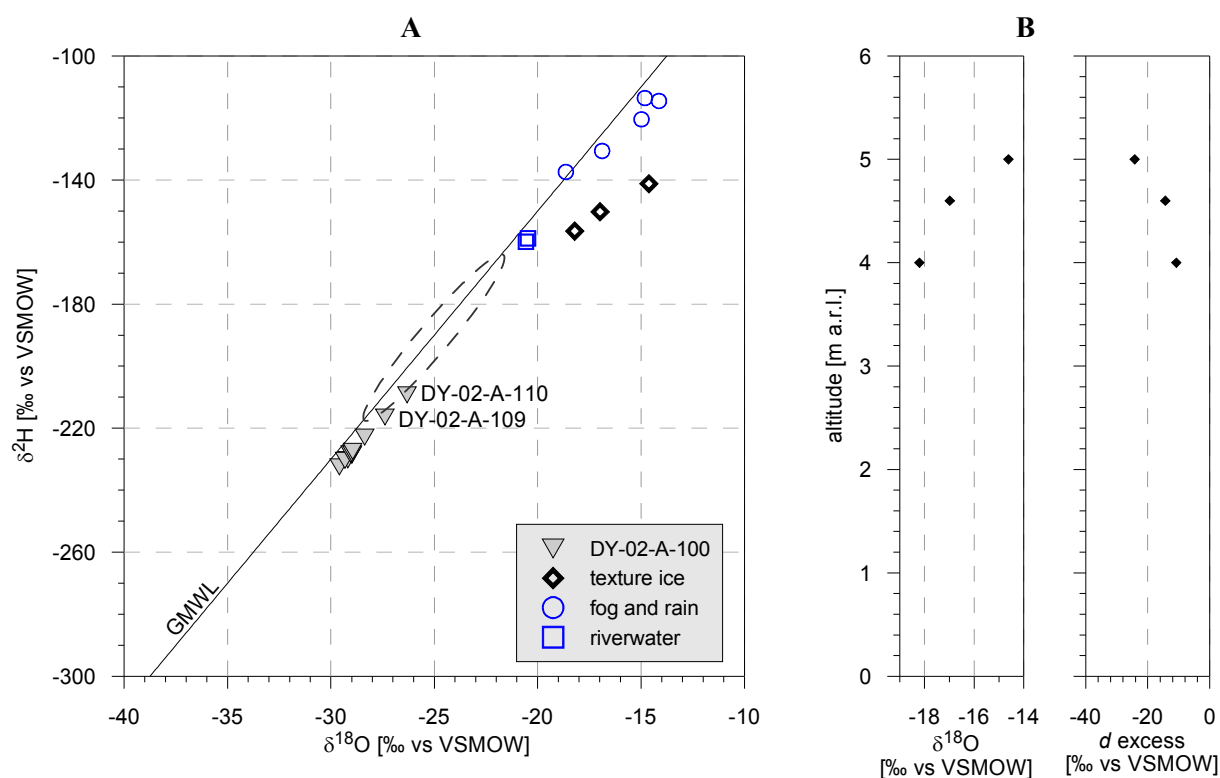


Fig. 4-6: Stable isotope signature of ground ice in DY-02. **A:** $\delta^2\text{H}$ - $\delta^{18}\text{O}$ diagram for ground ice samples related to modern precipitation data, the dashed line is the expected isotopic composition of winter precipitation, based on studies on Bol'shoy Lyakhovsky Island by MEYER et al. (2002b); **B:** $\delta^{18}\text{O}$ and d excess of three texture ice samples.

Additionally to the ice wedge samples, three texture ice samples were taken at the profile DY-02. Their mean $\delta^{18}\text{O}$ value is -16.6 ‰ and for $\delta^2\text{H}$ it is -149.3 ‰. These values are much heavier than the ice wedge ratios. The texture ice reflects probably a warm temperature signal (Fig. 4-6). The decrease of the slope of 4.2 compared to the GMWL (8, Fig. 4-6) and an increasing d excess (-10.8 to -24.2 ‰) for the texture ice indicates important fractionating effects during texture ice formation. Despite the use of only three data points, a linear correlation ($R^2=0.99$) indicates a consistently fractionation process.

4.2.2 Profile DY-03

The profile DY-03 was exposed between 5.0 and 10.5 m a.r.l. 150 m further west of DY-02 (Fig. 4-1). At this profile seventeen sediment samples were taken (DY-03-A-01 to 17, Fig. 4-7). A large segment of DY-03 was unfrozen. The lower part of the sequence (5.0 to 6.0 m a.r.l.) consisted of disturbed bedded dark-grey, silty fine sand with light-grey streaks (likely thawing or drying structures). The sediment was crumbly and contained shells and black spots (Ø 1 to 2 mm). The section between 6.0 and 9.5 m a.r.l. was composed of alternate partly disturbed bedding of brown plant detritus layers, grey silt layers and light-grey fine sand.

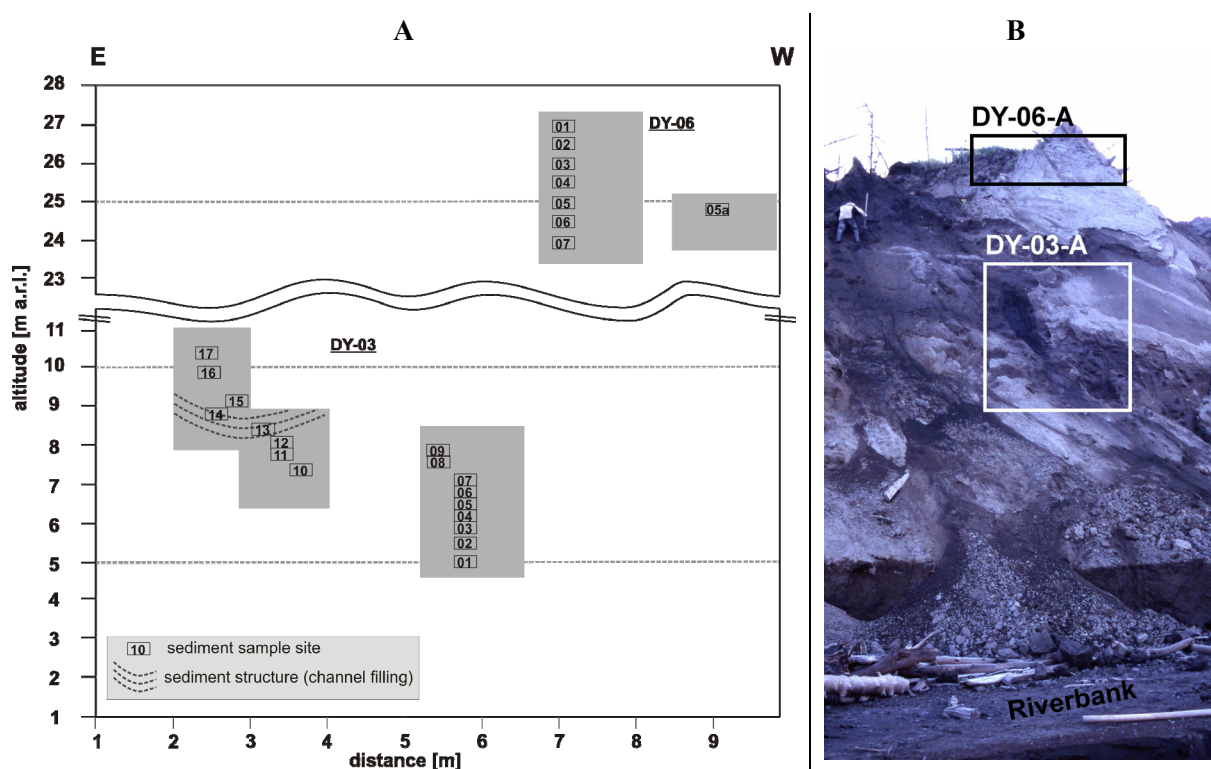


Fig. 4-7: (A) Scheme from SCHIRRMEISTER et al. (in press) and (B) photo of the lake sediment profiles DY-03 and DY-06; Photo: L. SCHIRRMEISTER and S. WETTERICH, August 2008.

The individual layers had various thicknesses of only some millimetres up to several centimetres and were internal laminated. The sediment contained some larger trunks of 10 to 20 cm in diameter and several smaller wood fragments of twigs and roots. A cryoturbated peaty part existed in 8.0 to 8.8 m a.r.l. (Fig. 4-8).



Fig. 4-8: Peat inclusions (white frame) in silty matrix (sample DY-03-A-14), Photos: L. SCHIRRMEISTER and S. WETTERICH, August 2008.

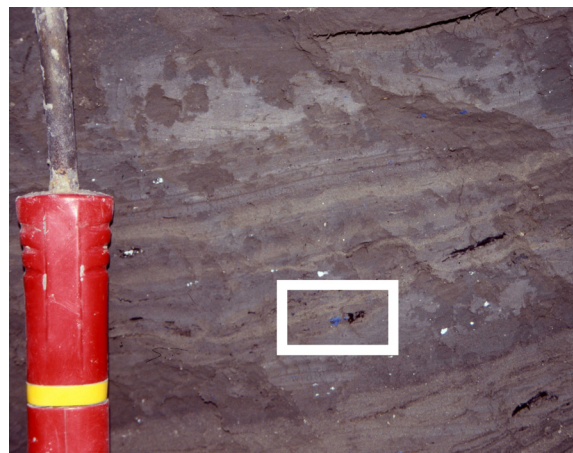


Fig. 4-9: Alternate bedding of silty fine sand and plant detritus layers close to the samples DY-03-10 to 13. The white frame marks an oxidised blue vivianite.

The studied deposits at DY-03 were only frozen in the uppermost part of profile between 9.3 m and 10.3 m a.r.l. The sediments were similarly composed as the sediments below. The cryostructure was massive and

the gravimetric ice content is low (24 to 29 wt %, Fig. 4-3). Two diagonal ice veins (probably fissure ice) crossed this frozen segment. Moreover, at the upper part of the profile (DY-03-A-13 and 14), vivianite minerals were included in a 2 cm wide zone near DY-03-A-12 and 13 (Fig. 4-9). Vivianite is formed in lakes under reducing conditions. Because of the close connection to lake environments, this mineral is an evidence for the sediments to be lake deposits.

In the lower part until 8.1 m a.r.l. the magnetic susceptibility is constant between 39 and 52 SI with a slight decreasing trend from the bottom to 8.1 m (Fig. 4-10 B). At the next two samples (8.4-8.8 m a.r.l., DY-03-A-13, -14) the values reach a minimum with ~26 SI. Afterwards a sharp increase to 117 SI takes place within only 1 m distance.

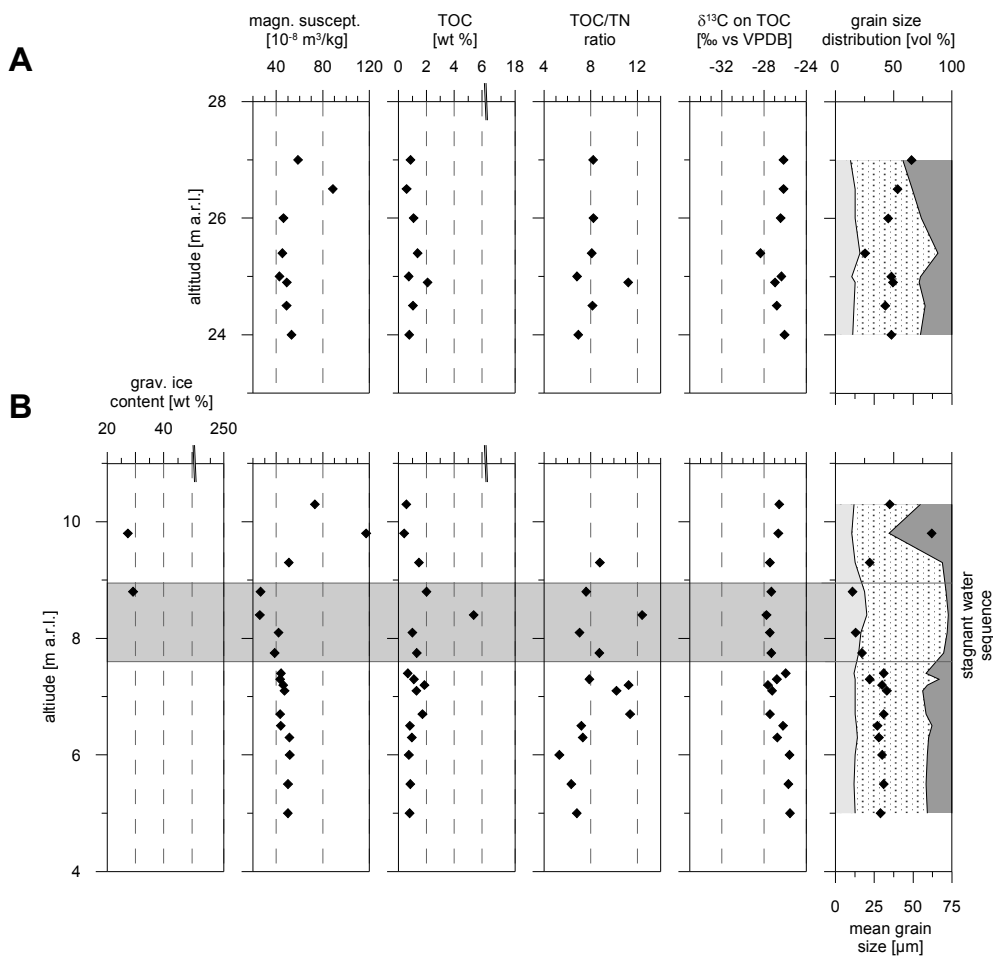


Fig. 4-10: Summary of cryolithological and sedimentological parameters for the lake sediment profiles (A) DY-06 and (B) DY-03. The TOC axis is broken for comparability with profile DY-02. The legend of the grain size diagram is shown in Fig. 4-3.

Moreover, at the lower part (up to 8.1 m) the TOC content range between 0.7 and 1.7 wt %. Next to the peaty cryoturbated part (at DY-03-A-13 and -14, Fig. 4-8 and Fig. 4-9) the organic content increases to 5.9 wt % and decreases subsequently to the level of the lower part (Fig. 4-10 B). The TOC/TN ratios scatter in this profile between 5.3 and 12.4 because of the generally low TOC contents. Thus, a high degradation rate of the organic material is indicated. In combination with low TOC values, only slight changes in TN have a great effect on the TOC/TN ratio and the peak in TOC at 8.4 m a.r.l. altitude also relates to the highest TOC/TN ratio (12.4). The relatively constant $\delta^{13}\text{C}$ values between -25.6 ‰ and -27.8 ‰ show a constant

source for the organic matter at this profile. The carbonate content in this profile is low (max. $c_{3.2}$: <4 wt %).

As shown in Fig. 4-11 B, all samples of profile DY-03 are very poorly sorted. The amount of clay is nearly constant between 16 and 19 vol %, with an exception in the interval between 7.75 and 8.8 m a.r.l. (grey bar in Fig. 4-10 B). At this site, the clay content is slightly increased to 20 to 27 vol %. In addition, the silt fraction increases from ~60 vol % to 70 to 75 vol %. Consequently, the sand fraction is low (4-8 vol %) between 8 and 9 m a.r.l. Directly adjacent at 9.8 m height (DY-03-A-16) the sand fraction set a peak with 54 vol %. With the exception of the latter described sample (silty sand) all other sample are sandy or rather clayey silts (Fig. 4-11 B). The mean values of the grain size covary with the magnetic susceptibility ($R^2 = 0.8$). Larger grain size occurs with higher susceptibility. The grain size distribution is similar, especially at the first peak at ~4 μm . A deviant grain size distribution occurs from a height of 7.75 (DY-03-A-11) to 8.8 m a.r.l. (DY-03-A-14). Firstly, the gap between the first and the second peak decrease from DY-03-A-11 to 14 (Fig. 4-11 A). The middle silt fraction is relatively enriched at this interval likely because of stagnant waters. Adjacent to this, DY-03-A-15 and -16 show different grain size distributions. DY-03-A-15 has a remarkable high peak in the coarse silt fraction, which shifts into the fine sand fraction at DY-03-A-16 (Fig. 4-11 A). The uppermost sample DY-03-A-17 has a similar grain size distribution like the lower part of the profile.

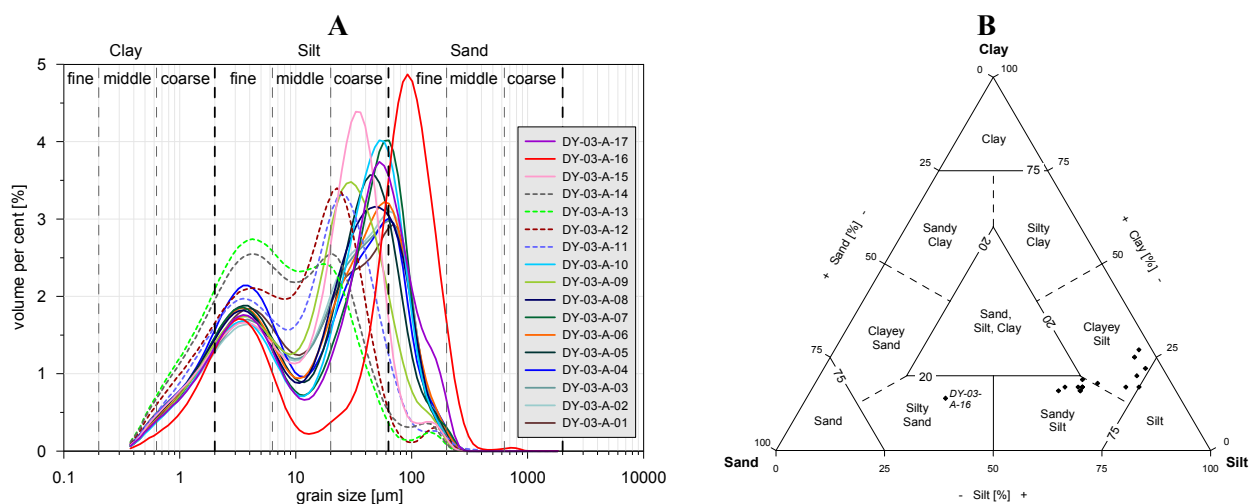


Fig. 4-11: (A) Grain size distribution and (B) sediment triangle after SHEPARD (1954) of the lake sediment profile DY-03.

4.2.3 Profile DY-06

The profile DY-06 was studied between 24.0 and 27.5 m a.r.l. about 15 m higher than profile DY-03 (Fig. 4-7 A and B). Eight unfrozen sediment samples were taken from this profile. The unfrozen sequence consisted of alternate bedding of brown-grey laminated fine sand (1 to 4 cm thick), laminated grey silt (1 to 2 cm) and dark-brown plant detritus (2 to 10 mm) (Fig. 4-12). The detritus layers were irregular distributed (5 to 10 cm long segments). In addition, cross and ripple bedding structures, rusty-brown coloration in sand

layers as well as small twigs (\varnothing 1 to 2 cm), shell fragments and vivianite minerals (at DY-06-A-05) were observed. Moreover, charcoal fragments were contained in this profile.

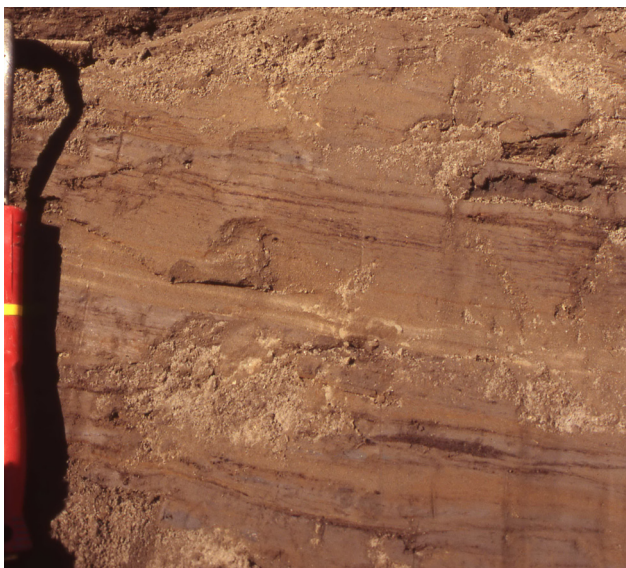


Fig. 4-12: Alternate bedding of brown-grey laminated fine sand, laminated grey silt and dark brown plant detritus; Photo: L. SCHIRRMESTER and S. WETTERICH, August 2008.

From 24 to 26 m a.r.l. the magnetic susceptibility is within a narrow range between 43 and 53 SI. Only one sample in 26.5 m a.r.l. (DY-06-A-02) shows nearly double the susceptibility (89 SI) than DY-06-A-03 (26 m a.r.l.; Fig. 4-10 A). The magnetic susceptibility decreases to 59 SI in the last sample, which is within the same range of the lower part of the profile. The TOC content is quite stable between 0.6 and 1.4 wt %. Only DY-06-A-5a, which was situated right of the other samples (Fig. 4-7 A) and lay within a wood fragments, has a higher value with 2.1 wt %. The same results are shown by TOC/TN values (Fig. 4-10 A). The TOC/TN ratio of DY-06-A-5a (11.2) is slightly higher compared to other values of the profile (6.9 to 8.2). The $\delta^{13}\text{C}$ ratio has a minimum of -28.3 ‰ at DY-06-A-04 (25.4 m a.r.l.), whereas all other values range between -27.0 and -26.1 ‰. Like in DY-03, the carbonate content in this profile is low (max. <4 wt %).

The profile DY-06 is characterised by very poorly sorted sediments (3.7 to 4.6). The per cent amount of clay is similar to DY-03 and shows constant values around ~ 16 vol %. DY-06-A-04 (25.4 m altitude, Fig. 4-10 A) differs in grain size composition (Fig. 4-13 A). It stands out having a relative enrichment of clay (21 vol %) and silt (67 vol %) and a depletion of the sand fraction (12 vol %). Its mean grain size is remarkably lower ($19\ \mu\text{m}$) than other values at DY-06. At the lower part of DY-06 (up to 26 m a.r.l.), the dominating silt fraction is between 57 and 61 vol % and increases to 49 and 45 vol % at the uppermost two samples. Coarser grain sizes from bottom to top are also shown by mean grain sizes. All sediment samples, except from DY-06-A-04 (clayey silt) can be described as sandy silts (Fig. 4-13 B), which is a bit more sandy than in the other two lake deposits. The grain size distribution curves are bi- to trimodal with two clearly separated main peaks. The first peak is uniformly at $\sim 4\ \mu\text{m}$. At the lower part of the profile (up to 26 m a.r.l.) the second peak is near the silt-sand border ($\sim 55\ \mu\text{m}$), whereas the two uppermost samples are relatively depleted in the middle silt fraction. Instead of being near the silt-sand border, the remarkably high second peak of DY-06-A-01 and DY-06-A-02 is located at the fine sand fraction. DY-06-A-04 (Fig. 4-13 A)

is characterised by two nearly similar sized peaks, whereas the second peak occurs at $\sim 30 \mu\text{m}$ and differs from the surrounding samples.

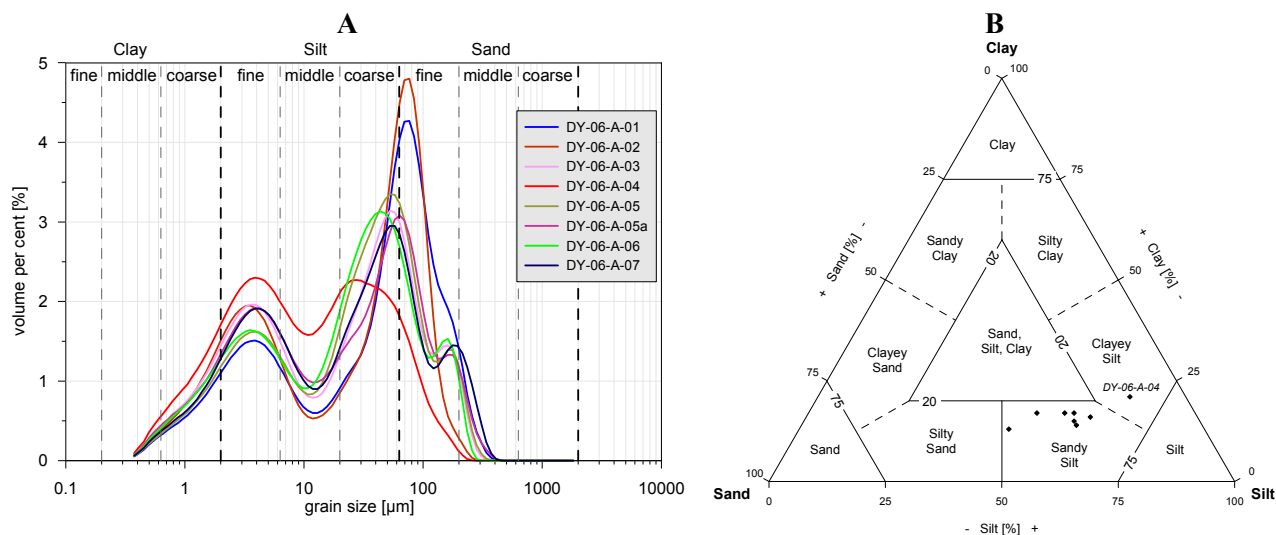


Fig. 4-13: (A) Grain size distribution and (B) sediment triangle after SHEPARD (1954) of the lake sediment profile DY-06.

4.3 Ice Complex

4.3.1 Profile DY-05

The lower part of the exposed Ice Complex sequence was studied in a thaw slump about 2 km east of DY-01 (Fig. 4-1). A 25 m long sequence was surveyed upwards starting at the river level, crossing the thermoterrace and ending below the steep ice wall at about 18 m below the surface level (Fig. 4-14, Fig. 4-15). The composite profile consists of eight subprofiles (DY-05-A to H) mostly exposed at thermokarst mounds (Fig. 4-14). At this profile 48 sediment samples were analysed.



Fig. 4-14: Thermo-cirque of the composite profile DY-05. The Photo was taken from campsite location, the Dresvyanny Island. The height of the profile is ~ 40 m; Photo: L. SCHIRRMEISTER and S. WETTERICH, August 2008.

The lowermost subprofile DY-05-A was exposed between 1 and 2 m a.r.l. at the wall of a temporary thermo-erosional gully. It was covered by deposits of a thermoterrace. At this site, an ice wedge and frozen sediments of light-brown fine sand with filament roots were studied.

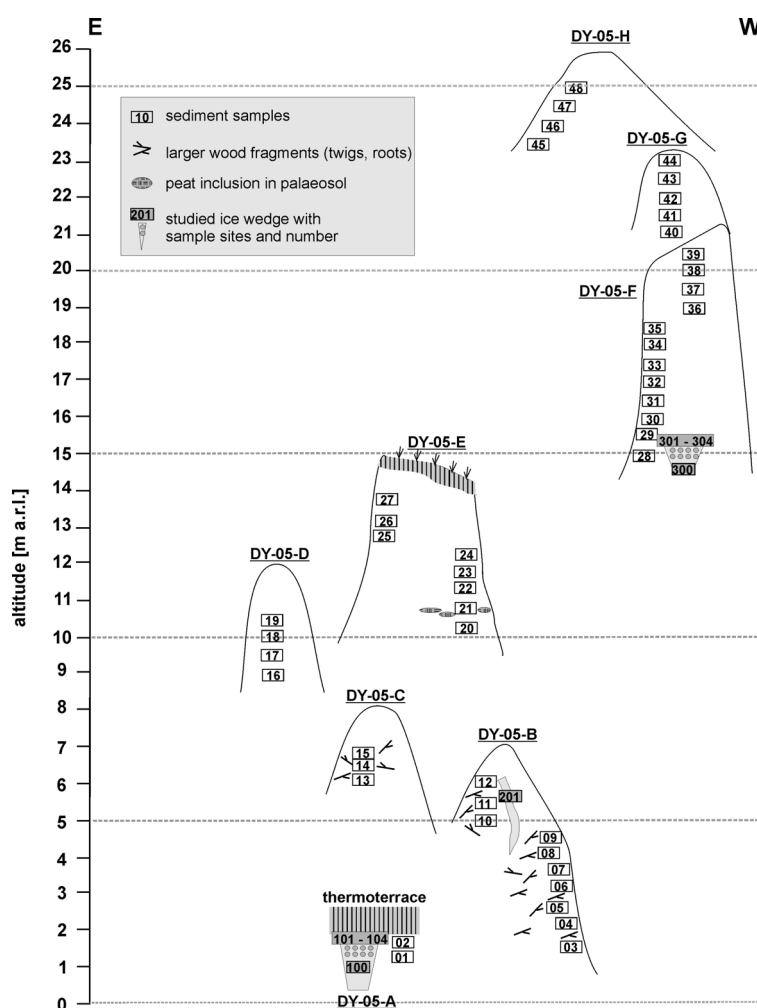


Fig. 4-15: Scheme of the composite Ice Complex profile DY-05; from SCHIRRMEISTER et al. (in press), modified.

The cryostructure was banded and micro to fine lens-like ice bands (distance 10 to 15 cm) composed of numerous micro lenses led into the ice wedge shoulders. The gravimetric ice content in this lower part is 70-75 wt % (Fig. 4-16). The following subprofile DY-05-B between 2.0 and 6.0 m a.r.l. was characterised by dark-brown patches and the occurrence of wood fragments like twigs or roots (\varnothing 2 to 4 mm, max. 20 mm long). The matrix of light-brown fine sand contained numerous filament grass roots and separate black spots (\varnothing 2 to 3 mm). This part is considered to be a paleocryosol sequence. The cryostructures were different and changed between laminated lenticular and micro lenticular. Clear segregation ice occurred around larger wood fragments. At some spots, ice bands of 2 to 3 cm thickness and separate \sim 3 cm long ice veins occurred. Here, the gravimetric ice content varies between 40 and 100 wt % (Fig. 4-16). The paleocryosol sequence of DY-05-B seemed to continue in subprofile DY-05-C (6.0 to 6.8 m a.r.l.). Its cryostructure was banded. Ice bands were 0.5 to 1.0 cm thick and had a distance of 2.0 to 4.0 cm. The cryostructure in the interbeds were micro to fine lenticular structured. The gravimetric ice contents range between 50 and 180 wt % (Fig. 4-16). Further upwards between 10 and 25 m a.r.l., the sequence was more homogenous (sub-profiles DY-05-D to H). The sediments consisted of lightgrey-brown silty fine sand with filament roots, single black spots (\varnothing 1 to 2 mm). The cryostructure was massive to micro lenticular and the gravimetric ice

content varies around 40 wt % (Fig. 4-16). Some separate parts contained larger amounts of plant fragments (stems). In addition, small layers of 5 cm thickness in 10.8 m a.r.l. (DY-05-E-21) containing dark-brown peat inclusions were considered as a cryoturbated paleocryosol. Here, the gravimetric ice content is higher and ranged between 60 to 80 wt % (Fig. 4-16). Separate ice-filled fissures of 1 to 2 mm width crossed the upper subprofiles.

In the previous mentioned paleocryosol sequence (1.3 to 6.8 m a.r.l.) the magnetic susceptibility is changeable (Fig. 4-16). It starts at 53 SI and decreases to 44 SI, before increasing to 57 SI again. Following a second decrease to the profile minimum (35 SI), the susceptibility increases within ~1 m to the maximum susceptibility of 77 SI at DY-05-C-13.

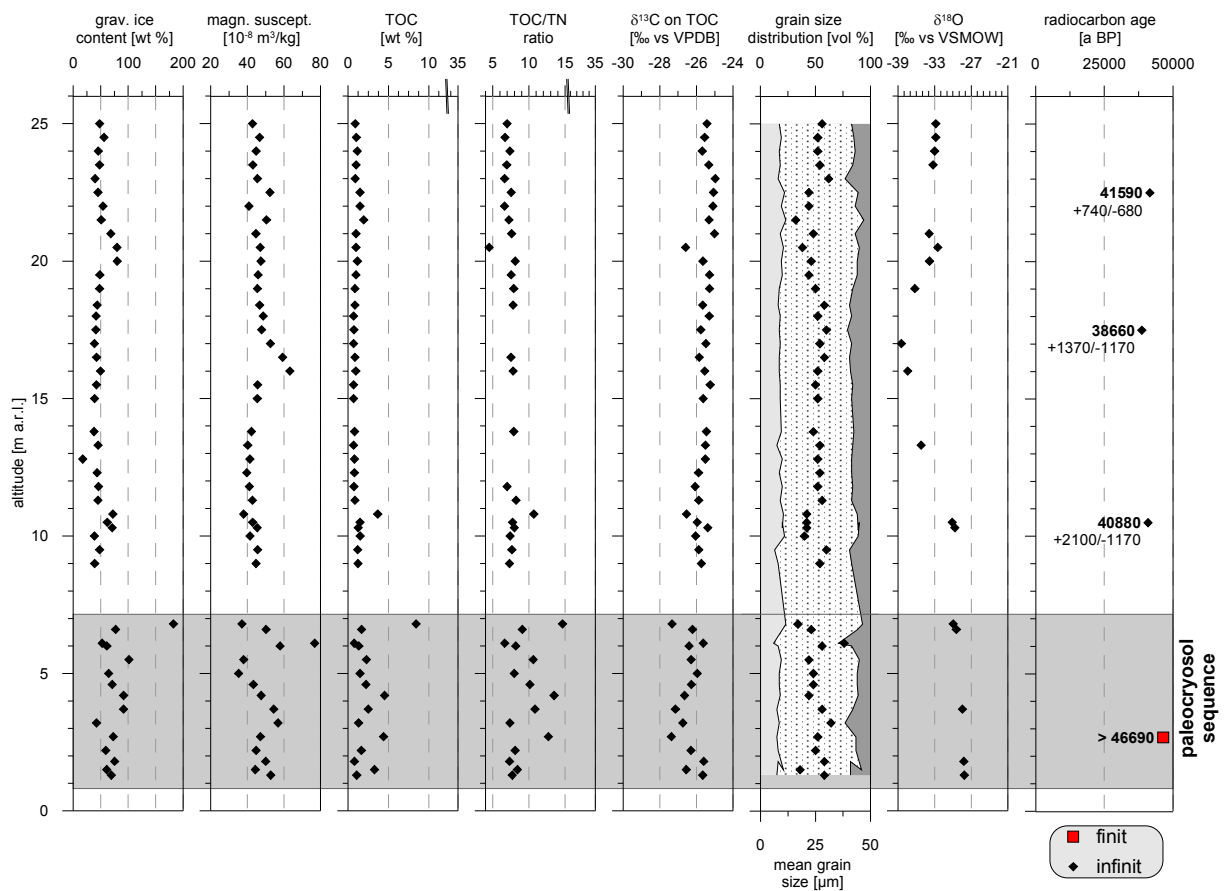


Fig. 4-16: Summary of cryolithological and sedimentological parameters for the Ice Complex profile DY-05. The TOC and TOC/TN axes are broken, because of high values in the Ice Complex profile DY-01. The axes of DY-05 and DY-01 are labelled identically. The legend for the grain size diagram is shown in Fig. 4-3.

Similar to the susceptibility, the TOC values and TOC/TN ratio in the paleocryosol sequence show an alternating behaviour. High values of TOC >4 wt % and TOC/TN ratios of >12 indicate paleocryosols, like in DY-05-B-05 (2.7 m a.r.l.; TOC 4.4 wt %), DY-05-B-08 (4.2 m a.r.l.; TOC 4.5 wt %) and DY-05-C-15 (6.8 m a.r.l.; TOC 8.4 wt %). Generally, the organic carbon content in this part of DY-05 is remarkably high with a mean value of 2.5 wt %. The TOC/TN ratios reach values of 12.7, 13.5 and 14.7 at the described maxima of TOC. These values are the highest measured for Duvanny Yar, except the litter horizon samples

on top of DY-01. The $\delta^{13}\text{C}$ values up to DY-05-C-15 (6.8. m a.r.l.) range from -27.4 to -25.6 ‰ (mean -26.4 ‰), which is lighter than the mean value at upper part of the profile. The carbonate content is rather low with maxima <2 wt % at the paleocryosol sequence.

The observed homogenous impression of the sediments above 9 m a.r.l. to the end of the profile at 25 m altitude (DY-05-D-16 to DY-05-A-01) is also reflected by the measured sediment properties. The magnetic susceptibility reaches about 60 SI at 16 m a.r.l.; all other values are on a narrow range between 38 and 53 SI. The TOC content in the sequence from 9 to 25 m altitude stays remarkably constant between 0.7 and 1.9 wt % (Fig. 4-16), with an exception at 10.8 m height. Here probably a paleocryosol sample is indicated, because the TOC value (3.7 wt %) and the TOC/TN ratio (10.7) are differed from the prevailing homogeneity. Another deviation is observed for the TOC/TN ratio at DY-05-F-39 at 20.5 m a.r.l.. Here the ratio is lower (4.5) than the adjacent samples (Fig. 4-16). Also the $\delta^{13}\text{C}$ value of -26.6 ‰ is the lowest at the sequence above 9 m a.r.l.. All other values except the mentioned paleocryosol sample (-26.5 ‰) range in a small distance from the mean -25.5 ‰ (standard deviation 0.3 ‰). The carbonate content shows maximum values <4 wt %, but most samples have low carbonate content values <0.5 wt %.

All profile samples are very poorly sorted (3 to 4.1). The percentages of the clay (between 12 and 23 wt %) and silt (59 to 72 wt %) fractions stay more or less constant. The sand fraction shows a wider range between 6 and 29 wt %. The sand maximum at DY-05-C-13 (black line in Fig. 4-17 A and B) at 6.1 m height shows the maximum grain size mean value of 38 μm at the DY-05 profile. The other mean grain size values range between 16 to 32 μm , which show a remarkable uniformity for a ~24 m high profile. This homogeneity is also shown by the sediment triangle diagram (Fig. 4-17 B), in which all samples cluster around the clayey silt/sandy silt border. The only deviant sample from this cluster is the sandy DY-05-C-13 sample (Fig. 4-17 B).

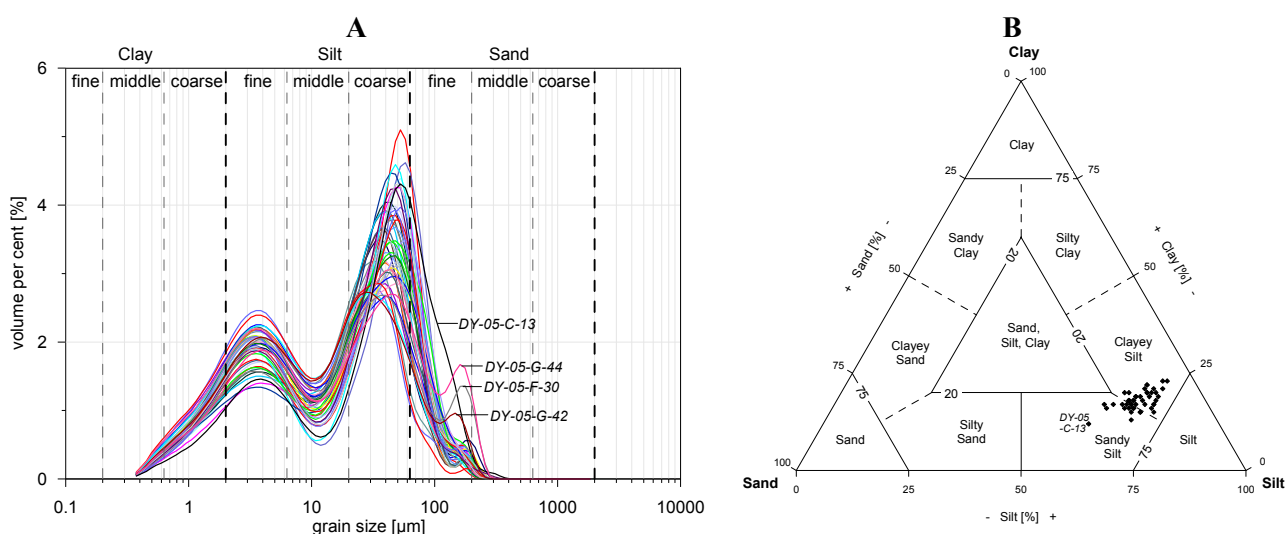


Fig. 4-17: (A) Grain size distribution and (B) sediment triangle after SHEPARD (1954) of the Ice Complex profile DY-05.

This high degree of homogeneity in mean grain sizes (Fig. 4-16) is also reflected in the grain size distribution curves (Fig. 4-17 A). All samples shows a distinct two major peak distribution, with a smaller peak in the fine silt fraction (between 3 and 4 μm) and a greater peak at ~ 40 to 60 μm (coarse silt fraction).

A less distinct third peak in the fine sand fraction is found for nearly all samples. Two characteristics can be seen in Fig. 4-17 A. Firstly, the sand peak sample DY-05-C-13 (black and labelled distribution, Fig. 4-17 A), which has the maximum sand content of DY-05, shows a wider curve width at the coarse silt peak than the other samples and this peak reaches considerable into the fine sand fraction. Secondly, the samples DY-05-F-30 (grey distribution, 16 m a.r.l.), DY-05-G-42 (dark red distribution, 22 m a.r.l.) and DY-05-G-44 (pink distribution, 23 m a.r.l.) show a small third peak.

Age determinations at the basis of the DY-05 profile yields an infinite ^{14}C age of >446690 a BP (Table 4-1). Therefore, it can be concluded that the formation of the Ice Complex profile begun during the Middle Weichselian interstadial. The youngest ^{14}C age at DY-05 is $38660 \pm 1370 / -1170$ a BP.

Table 4-1: Radiocarbon accelerator mass spectrometer (AMS) dating results of DY-05.

Lab. N ^o	Sample	Description	Altitude [m a.r.l.]	^{14}C age [a BP]
KIA39776	DY-05-G-43	plant remains	22.5	$41590 \pm 740 / -680$
KIA38383	DY-05-F-33	plant remains	17.5	$38660 \pm 1370 / -1170$
KIA38382	DY-05-D-19	plant remains	10.5	$40880 \pm 2100 / -1660$
KIA38381	DY-05-B-05	plant remains	2.7	> 46690

4.3.1.1 Ground ice of DY-05

At DY-05 two ice wedges and one fissure ice structure were studied (Fig. 4-15). The lowermost ice wedge was of syngenetic origin and 0.5 to 0.8 m wide (DY-05-A-100; Fig. 4-18 A). It was cut diagonally (real width: 0.35 m) and had an exposed height of 1.8 m as well as numerous irregular gas bubbles (\varnothing 1 mm).



Fig. 4-18: Ice wedges in the Ice Complex deposits of DY-05 framed by dotted with lines; (A) DY-05-A-100; (B) ice wedge DY-05-F-300; Photos: L. SCHIRRMEISTER and S. WETTERICH, August 2008.

At this ice wedge four subsamples were taken. The stable isotope composition of this ice wedge plots near the GMWL ($\delta^{18}\text{O}$: -31.6 ‰ to -29.9 ‰, $\delta^2\text{H}$: -244.3 ‰ to -229.1 ‰, mean d excess: 7.9 ‰; Fig. 4-19 A).

The fissure ice sample comprises ground and ice layers (DY-05-B-200, width: 0.7 m) and was sampled at 5.7 m a.r.l.. It consisted of 5 to 10 mm wide ice veins and 1 to 2 mm wide ground veins. DY-05-B-200 shows $\delta^{18}\text{O}$ and $\delta^2\text{H}$ values of -30.3 ‰ and -228.5 ‰, respectively. The d excess is remarkable high (14.1 ‰). As shown in Fig. 4-19 A, the isotopic signal is similar to the texture ice and the high d excess indicates either exchange processes with the surrounding sediment or a different origin of this ice. It could be a texture ice influenced ice wedge, a fissure filled with texture ice melt water or texture ice influenced precipitation, but in any case it is fossil ground ice.

The uppermost ice wedge samples (DY-05-F-300) were taken at 15.0 m a.r.l. (Fig. 4-18 B, 4 subsamples, width: 0.7 m). It had single ice veins, which were 0.5 to 3.0 cm wide and two to three ground veins of <1 mm width, which were bundled in millimetre distance. The clear ice contained numerous gas bubbles (\varnothing 1 to 2 mm). The isotopic values for this ice wedge spans a range between -34.5 ‰ to -33.5 ‰ for $\delta^{18}\text{O}$ and -273.0 ‰ to -264.5 ‰ for $\delta^2\text{H}$, respectively. These values are the most negative values determined for ice wedges within this study. The wide range in d excess (-0.2 to 11.4 ‰; high standard deviation of 4.4 ‰) indicates secondary alteration processes in this ice wedge. The outlier (DY-05-F-304, d excess: 11.4 ‰) has a peripheral position.

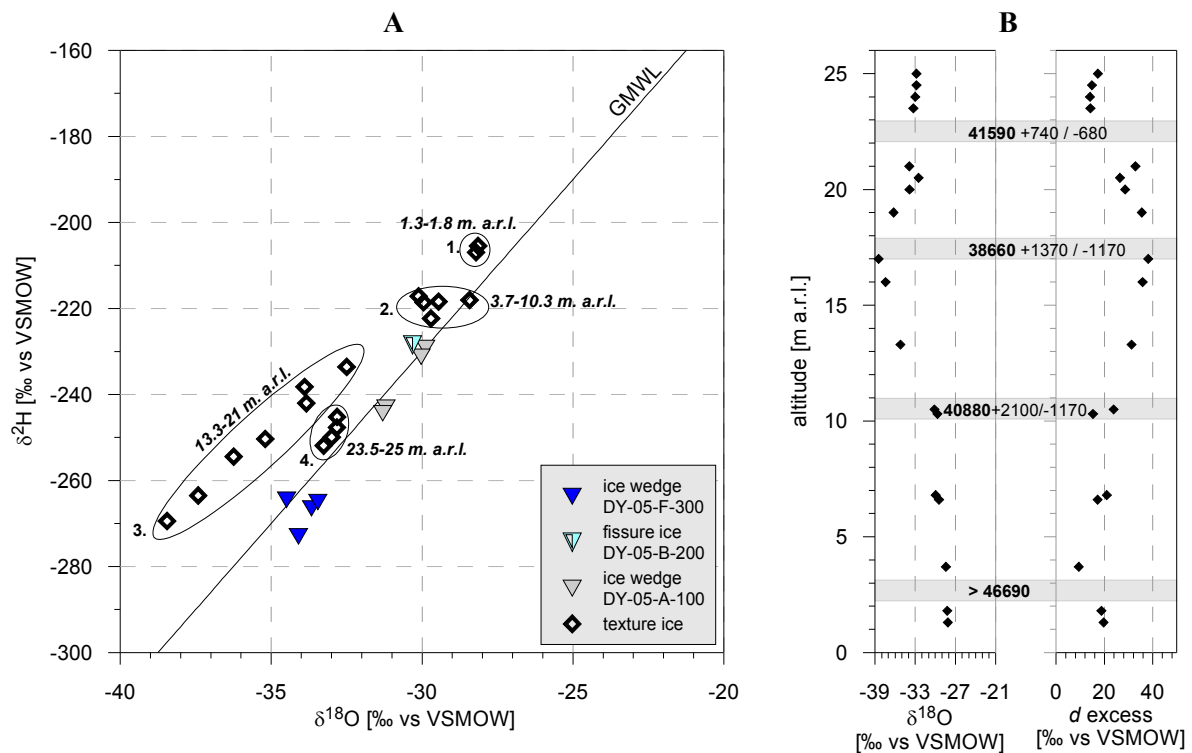


Fig. 4-19: Stable isotope signature of ground ice in DY-05. **A:** $\delta^2\text{H}$ - $\delta^{18}\text{O}$ diagram for ground ice of the Ice Complex profile DY-05; **B:** $\delta^{18}\text{O}$ and d excess variations of the 18 texture ice samples. For a geochronological orientation the ^{14}C ages [a BP] are added.

The isotopic results for texture ice in DY-05 show four different clusters. Three of these clusters lie on an imaginary regression line (1.3 to 21 m a.r.l.), whereas one cluster seems to be separated (23.5 to 25 m a.r.l., Fig. 4-19). The first cluster (1.3 to 1.8 m a.r.l.) is characterised by a relatively heavy isotope composition of -28.2‰ ($\delta^{18}\text{O}$) and -206.2‰ ($\delta^2\text{H}$). The isotopic compositions of the second cluster (3.7 to 10.3 m a.r.l.) range between -28.4 to -30.1‰ for $\delta^{18}\text{O}$ and -218.0 to -222.4‰ for $\delta^2\text{H}$. The third cluster (13.3 to 21 m a.r.l.) is characterised by a high linearity (R^2 : 0.98, slope 5.5). This linearity is apparently generated randomly, because as shown in Fig. 4-19 B, the isotopic values firstly decrease (13.3 to 17 m a.r.l.), thereafter they increase (17 to 20.5 m a.r.l.) and finally they decrease again. Because of a lack in altitude correlation this isotopic cannot be explained by freezing fractionation. In contrast to these three clusters the separate fourth cluster (23.5 to 25 m a.r.l.) shows an isotopic constancy of $\delta^{18}\text{O}$ between -33.3‰ and -32.8‰ and $\delta^2\text{H}$ between -251.9‰ and -245.2‰ . Additionally, the fourth cluster has a small offset relative to the GMWL (mean d excess 15.1‰ ; Fig. 4-19 A).

4.3.2 Profile DY-01

The studied 20 m long exposure of Ice Complex deposits reached from a thermoterrace above DY-02 (Fig. 4-1), where older permafrost deposits were buried by modern debris, up to the upper edge of the thaw slump (Fig. 4-20). The composite profile DY-01 consists of eight subprofiles (DY-01-A to DY-01-H) exposed in neighbouring thermokarst mounds (Fig. 4-21). At this profile, 47 sediment samples were taken.



Fig. 4-20: Overview of the thermocirque of the composite profile DY-01; Photo: L. SCHIRRMESTER and S. WETTERICH, August 2008.

The lowermost subprofiles DY-01-H to lower portions of DY-01-F (24.0 to 28.0 m a.r.l.) consisted of light-brown fine sand with filamentous grass roots. The cryotexture was micro lenticular and laminated. The gravimetric ice content ranges between 37 to 53 wt %. A dark brown coloured paleocryosol with wood fragments and peaty organic patches occurred at 28 to 29.5 m a.r.l. (DY-01-F-34 to 37). The cryostructures were irregular lenticular (Fig. 4-22). Diagonal ice veins and ice segregation around wood fragments occurred. The gravimetric ice content at this site ranges between 81 to 113 wt %.

Large parts of the following sequences from 29.5 to 41.5 m a.r.l. (DY-01-E to DY-01-B) were relatively homogenous composed of grey-brown and light brown fine sand with filamentous grass roots. Numerous small black patches were frequently observed. The gravimetric ice content ranges between 40 and 65 wt %, but without any ice super saturation.

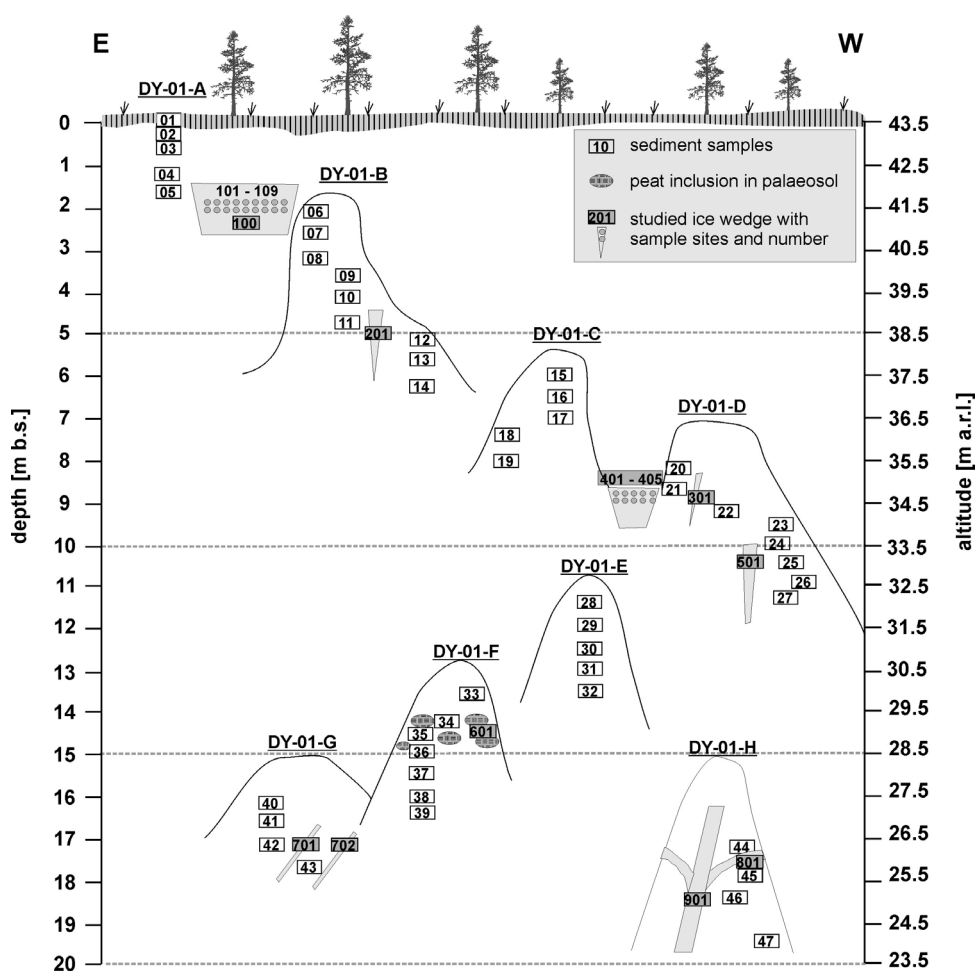


Fig. 4-21: Scheme of the composite Ice Complex profile DY-01; from SCHIRRM-EISTER et al. (in press).

The observed cryostructures at DY-01-E to DY-01-B were generally massive or micro lenticular. At some spots micro lenses were organised to laminated structures (Fig. 4-23).



Fig. 4-22: Irregular lenticular to laminated cryo-structures near sample point DY-01-F-35.



Fig. 4-23: Laminated cryostructures in subprofile DY-01-C (DY-01-C-15); Photos: L. SCHIRRM-EISTER and S. WETTERICH, 2008.

The uppermost samples were exposed at a steep wall on top of the outcrop of about 2 m thickness (Fig. 4-25). It consists of a grey-brown silty paleocryosol with a banded and lenticular cryostructure (subprofile DY-01-A).



Fig. 4-24: Thermokarst mounds at the composite profile DY-01. In front the subprofile DY-01-G is exposed.



Fig. 4-25: Topmost part of the Ice Complex profile, where ice wedges are covered by ice-banded deposits (subprofile DY-01-A); Photos: L. SCHIRRMESTER and S. WETTERICH, August 2008.

The samples of the main part of DY-01 range between 32 and 55 SI. The paleocryosol sequence fits well into this data range (~42 SI). On top, at DY-01-A-03, the susceptibility decreases to a value of 31 SI and at the next higher sample it decreases even more to the profiles minimum of 25 SI. At the uppermost DY-01-A-01 sample the magnetic susceptibility (46 SI) increases again.

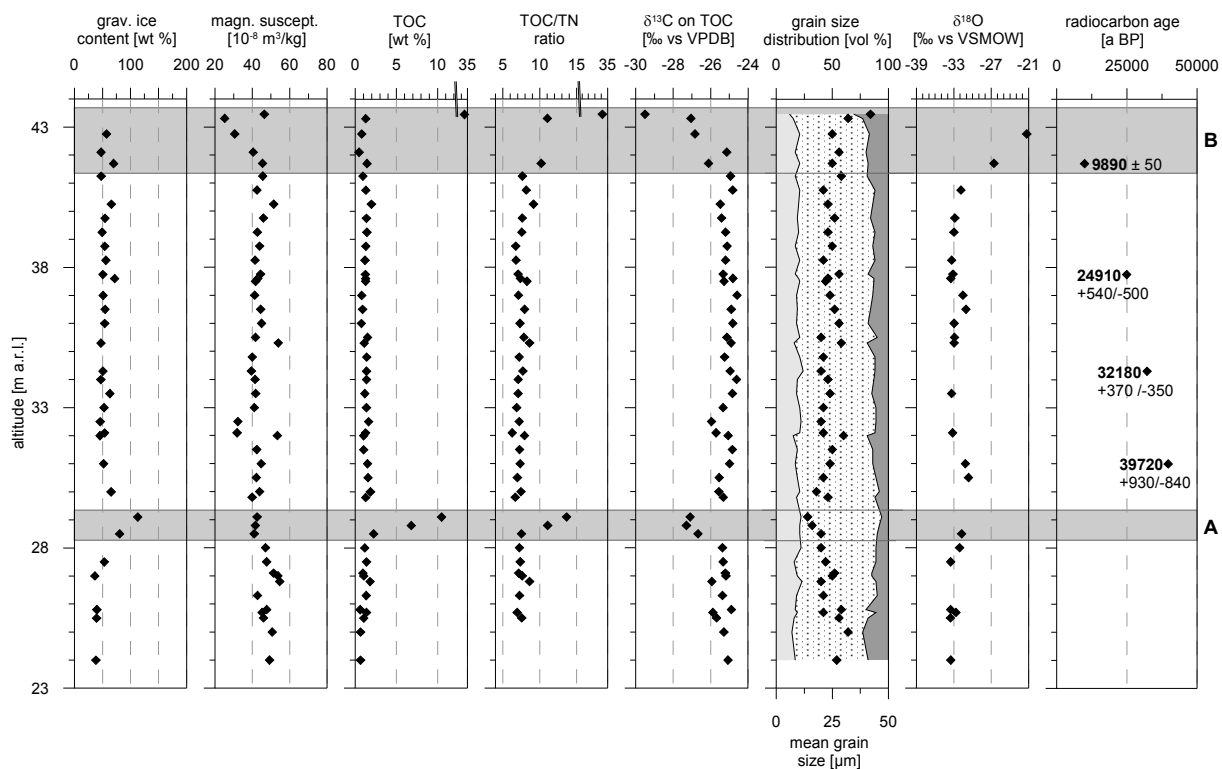


Fig. 4-26: Summary of cryolithological and sedimentological parameters for the Ice Complex profile DY-01. The TOC and TOC/TN axes are broken. The grey bars show (A) the paleocryosol sequence and (B) the Holocene formed sediments. The axes of DY-01 and DY-05 are labelled identically.

The main part of the profile shows uniform biogeochemical parameters. The TOC values range between 0.6 and 2 wt % with a mean of 1.2 wt %. The TOC/TN ratios range between 6.3 and 9.2 and the mean $\delta^{13}\text{C}$ ratio is -25.2 ‰ (range -25.9 to -24.6 ‰). The paleocryosol sequence shows increased values for TOC values ranging from 2.2 over 6.8 to 10.5 wt % (28.5 to 29.1 m a.r.l., Fig. 4-26) and TOC/TN values of max. 13.6 at 29.1 m a.r.l.. The $\delta^{13}\text{C}$ values are within a range of -27.3 to -26.7 ‰ being lighter than the adjacent samples. At DY-01-A, the uppermost sample are deviant due to extremely high TOC (34.5 wt %) and TOC/TN (34.2) values. Here, the stable carbon isotope ratio is light (-29.5 ‰). The high TOC and TOC/TN values are the result of a moderate degree of mineralisation compared to a high mineralisation rate at the adjacent samples (values <10). The light $\delta^{13}\text{C}$ values indicate a different origin of the organic matter. The carbonate content is low for all samples at DY-01 showing maxima of <2 wt %

As the profile DY-01 is considered as the continuation of the DY-05 profile, the sedimentological parameters are similar. The very poorly sorted character of the Duvanny Yar profile occurs at profile DY-01 as well (3.2 to 4.2). The clay fraction ranges from 12 to 24 vol %, whereby the lower boundary (12 vol %) is set by the lowermost sample DY-01-H-47 at 24 m a.r.l.. The next higher sample DY-01-H-46 shows the second lowest content of clay with 14 vol %. The silt fraction has lowest its values in the uppermost subprofile DY-01-A (57 to 63 vol %). The paleocryosol sequence (28.8 to 29.1 m a.r.l.) shows increased silt contents at DY-01-F-34 and DY-01-F-35 (72 and 71 vol % silt) compared to other samples, which has silt contents between 63 and 79 vol %. The sand content of the main part ranges between 8 vol % at DY-01-E-32 and 23 vol % at DY-01-H-46. The mean grain sizes of the main part of the profile ranges between 18 μm (DY-01-E-32) and 32 μm (DY-01-H-46). The already mentioned differentiation the paleocryosol sequences at 28.5 to 29.1 m a.r.l. and the uppermost samples is indicated in the sand fraction, too. The lowest sand content occurs at the paleocryosol sequence (6 vol % at DY-01-F-34 and 8 vol % at DY-01-F-35), whereas the maximum occurs at DY-01-A-02 and DY-01-A-01 with 31 and 23 vol % sand, respectively. Similarly, the lowest value of mean grain size occurs in the paleocryosol sequence at DY-01-F-35, showing a mean value of 14 μm followed by a mean value of 16 μm at DY-01-F-34. The maximum is at DY-01-A-02, having a value of 42 μm . The following sample DY-01-A-01 has a mean value of 32 μm .

All samples are categorised as clayey or sandy silts according to the sediment triangle after SHEPARD (1954) (Fig. 4-27 B). The sample DY-01-A-01 differs slightly from the main cluster (Fig. 4-27 B), because this sample is part of the Holocene litter horizon. Fig. 4-27 A shows a homogeneous picture of the grain size distribution curves. All curves are at least bimodal with well distinct major peaks at the ~ 4 μm (fine silt fraction) and ~ 40 to 60 μm (coarse silt fraction). The paleocryosol sequence (28.8 m a.r.l., green colour and 29.1 m a.r.l., pink distribution in Fig. 4-27) stands out from the general pattern of grain size distributions, because of a relative enrichment at the middle silt fraction. Together with increased TOC value (Fig. 4-26) this could be an indication for water ponding, which had allowed the middle silt fraction to settle. DY-01-E-28 at 32 m a.r.l. (grey curve in Fig. 4-27) and DY-01-D-20 at 35.3 m a.r.l. (blue distribution in Fig. 4-27) show a remarkably high second major peak in the coarse silt fraction. DY-01-A-01 (red labelled curve in

Fig. 4-27 A) has because of its position close to the recent surface a deviant distribution. Here, the recent vegetation is a sediment trap, whereby coarser grain size can be enriched.

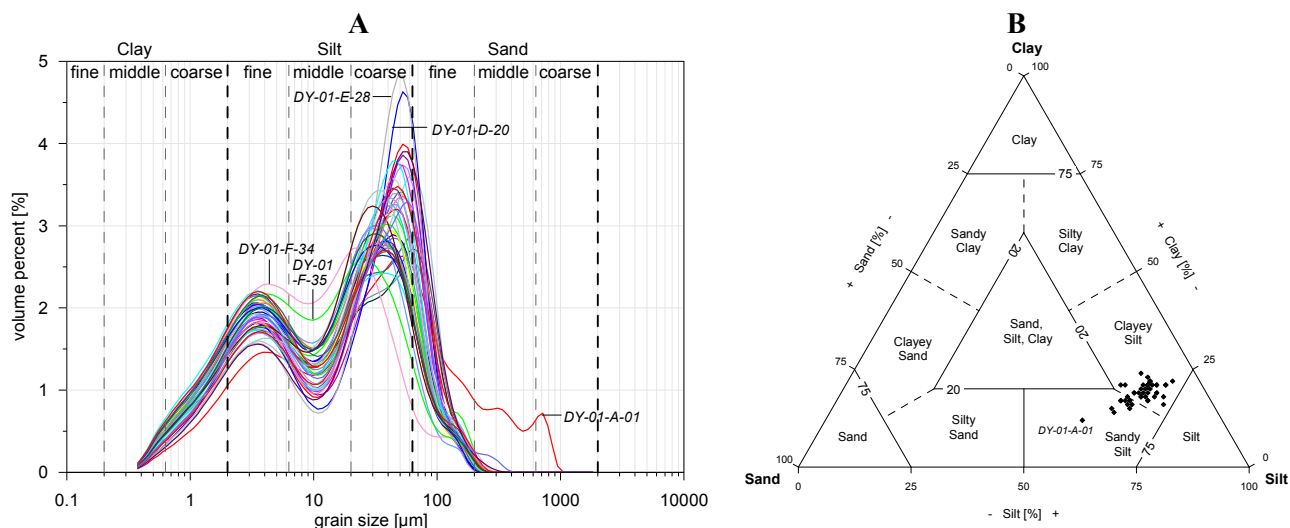


Fig. 4-27: (A) Grain size distribution and (B) sediment triangle after SHEPARD (1954) of the Ice Complex profile DY-01.

As an upper Ice Complex deposits continuation, the radiocarbon ages of DY-01 are younger than at DY-05. The deposition period of DY-01 is between $39720 + 930 / -840$ and 9890 ± 50 a BP (Table 4-2), thus during the Middle/Late Weichselian till the Early Holocene.

Table 4-2: Radiocarbon AMS dating results of DY-01.

Lab. N ^o	Sample	Description	Altitude [m a.r.l.]	¹⁴ C age [a BP]
KIA39774	DY-01-A-05	plant remains	41.7	9890 ± 50
KIA38378	DY-01-B-13	plant remains	37.75	$24910 + 540 / -500$
KIA39775	DY-01-D-22	plant remains	34.3	$32180 + 370 / -350$
KIA38380	DY-01-E-30	plant remains	31.0	$39720 + 930 / -840$

4.3.2.1 Ground ice DY-01

For the several small fissure ice samples of 0.03 to 0.80 m width (DY-01-H-900, H-800 (Fig. 4-28 A), G-700, D-500, D-300 and DY-01-B-200) the same phenomenon like at DY-05-B-200 occurs. The origin of these ground ice sample is probably different. It could be texture ice derivate or just small through exchange processes influenced ice wedges. Their composition was characterised by ice veins (1 to 10 mm wide) and thin sediment veins (1 to 2 mm wide). The clear ice contained numerous non-oriented gas bubbles (\varnothing 1 to 2 mm). The isotopic composition of the two lowermost fissure ice samples (Fig. 4-28 A) range between -33.5 to -32 ‰ for $\delta^{18}\text{O}$ and -248.7 to -241.2 ‰ for $\delta^2\text{H}$. Their mean d excess is high (17.3 ‰). The four small fissure ice samples above (DY-01-D-300, DY-01-D-500 and DY-01-G-701/702) have similar to slightly heavier values ranging from -32.8 to -32.5 ‰ ($\delta^{18}\text{O}$) and -246.7 to -229.3 ‰ ($\delta^2\text{H}$), respectively. These ground ice samples have the highest d excess values (25.1 to 30.4 ‰) at the Duvanny Yar section measured for fissure ice. The small fissure ice sample DY-01-B-200 ($\delta^{18}\text{O}$: -32.7 ‰, $\delta^2\text{H}$: -239.9 ‰, d excess: 21.8 ‰) can be grouped with the four ground ice samples from DY-01-G-701/702, DY-01-D-

500 and DY-01-D-300. As shown in Fig. 4-29 A, the isotopic signals of fissure ice samples are similar to texture ice and the high d excess indicates either exchange processes with the surrounding sediment or a different origin of this ice.

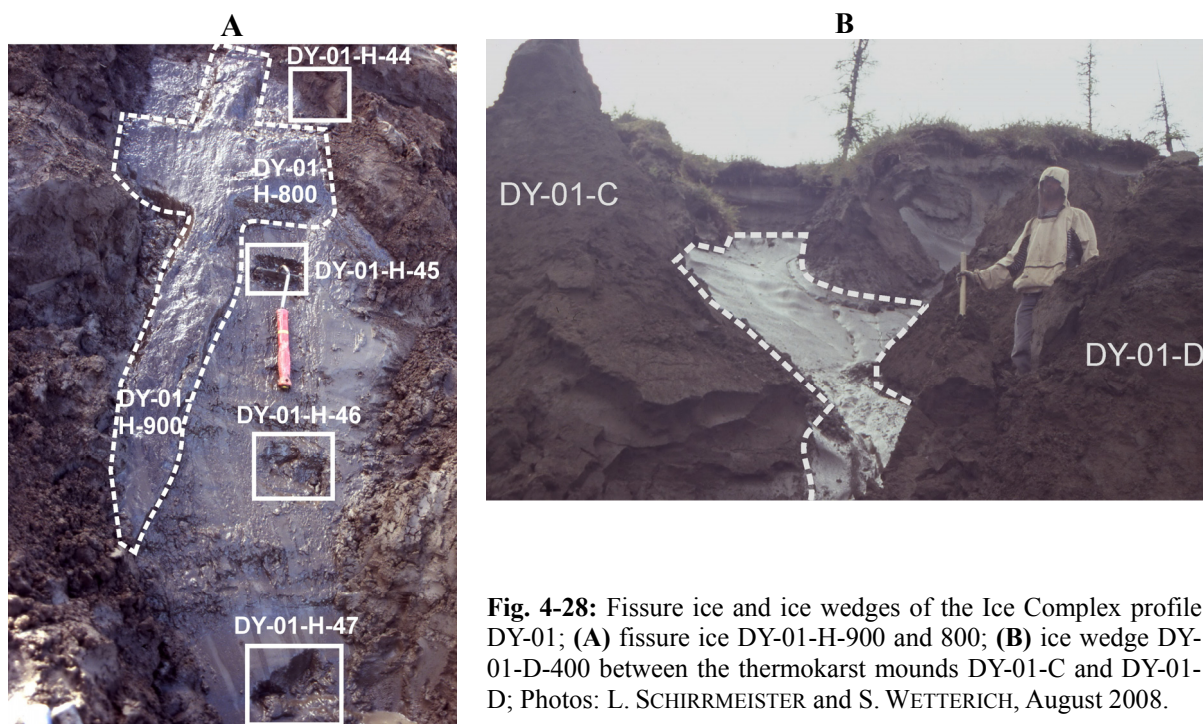


Fig. 4-28: Fissure ice and ice wedges of the Ice Complex profile DY-01; (A) fissure ice DY-01-H-900 and 800; (B) ice wedge DY-01-D-400 between the thermokarst mounds DY-01-C and DY-01-D; Photos: L. SCHIRRMEISTER and S. WETTERICH, August 2008.

Ice wedge DY-01-D-400 plots close to the GMWL (Fig. 4-29 A; mean d excess: 5.5 ‰) and its mean isotopic values are -32.3 ‰ for $\delta^{18}\text{O}$ and -253.2 ‰ for $\delta^2\text{H}$. A four metre wide ice wedge was sampled in 41.5 m a.r.l. (DY-01-A-101 to 109). This ice wedge was composed of numerous separate ice (\varnothing 1 to 2 cm) and ground veins ($\varnothing < 1$ mm). The ice was clear and contained numerous non-oriented gas bubbles. DY-01-A-100 is characterised by a narrow range in the isotopic composition with mean values of -31.5 ‰ for $\delta^{18}\text{O}$, -248.5 ‰ for $\delta^2\text{H}$ and a mean d excess of 3.3 ‰. The slope of the regression is 8.1 and therefore it shows a parallel course to the GMWL.

Despite the uncertainties at the narrow fissure ice samples, all nine ground ice sample locations span a narrow range of isotopic values ranging from -33.5 ‰ to -30.6 ‰ ($\delta^{18}\text{O}$) and -256.8 ‰ to -229.2 ‰ ($\delta^2\text{H}$), respectively (Fig. 4-29 A).

The isotopic composition of the texture ice is in the same range (except the two uppermost samples) as the ice wedges (Fig. 4-29 A). As shown at Fig. 4-29 B, the $\delta^{18}\text{O}$ ratio from 24.0 to 40.75 m a.r.l. ranges around a mean of -32.6 ‰ (-33.5 ‰ to -30.6 ‰). At the same level of altitude the $\delta^2\text{H}$ values are between -246.4 and -219.1 ‰. The texture ice from sample DY-01-D-27 (32.1 m a.r.l.) is deviant through an extremely high d excess of 44.0 ‰. The d excess values for DY-01-H-47 to DY-01-B-07 (up to 40.75 m a.r.l.) have a mean value of 25.6 ‰ with a low standard deviation (3.0 ‰).

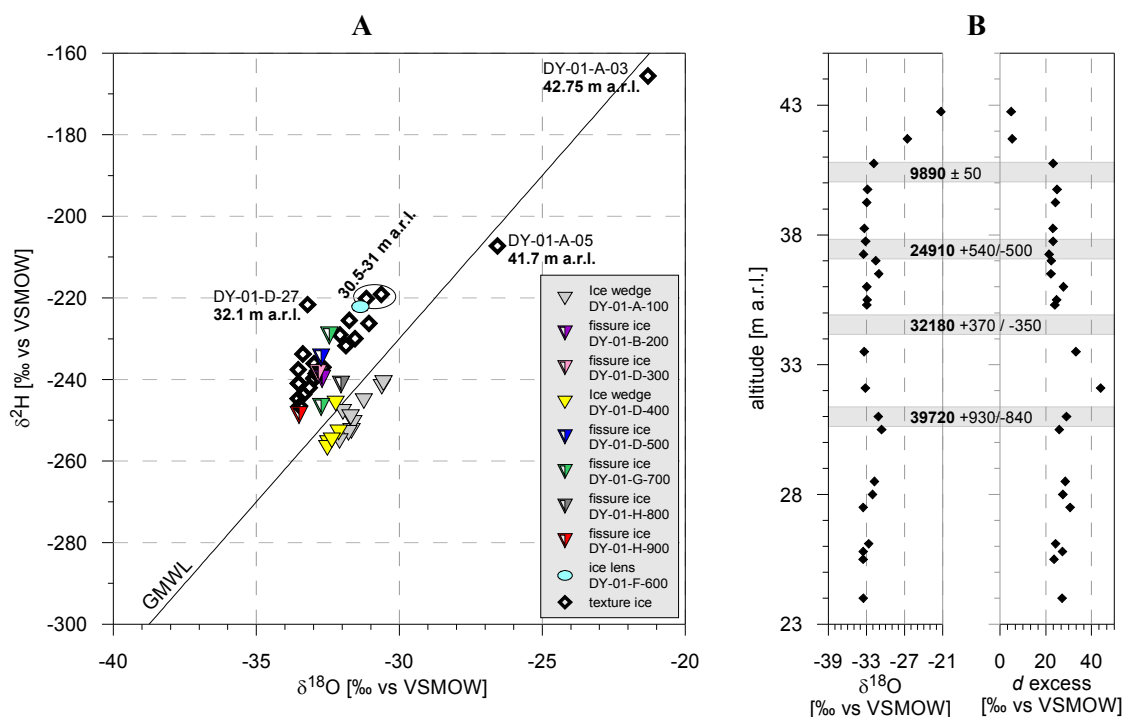


Fig. 4-29: Stable isotope signature of ground ice in DY-01. **A:** $\delta^2\text{H}$ - $\delta^{18}\text{O}$ diagram for ground ice of the Ice Complex profile DY-01; **B:** $\delta^{18}\text{O}$ and d excess variations of 24 texture ice samples; AMS ^{14}C ages are given in a BP.

A light isotopic composition is obvious at an altitude of 30.6 to 31 m a.r.l. (DY-01-E-30 and DY-01-E-31, upper circled area in Fig. 4-29 A). The sampled ice lens (DY-01-F-600; 28.5 m a.r.l.) matches well into the surrounding texture ice isotopic signal of DY-01-E-31 ($\delta^{18}\text{O}$: -30.6 ‰; $\delta^2\text{H}$: -219.1 ‰) and DY-01-F-36 ($\delta^{18}\text{O}$: -31.6 ‰; $\delta^2\text{H}$: -225.5 ‰) by showing values of -31.4 ‰ ($\delta^{18}\text{O}$) and -222.1 ‰ ($\delta^2\text{H}$). This is evidence for a genetic connection of this two ground ice types. The two uppermost texture ice samples, DY-01-A-05 in 41.70 and DY-01-A-03 in 42.75 m a.r.l. show heavier values (Fig. 4-29 B). The difference of DY-01-A-05 and DY-01-A-03 relative to samples of DY-01 below 40.75 m a.r.l. (Fig. 4-29 B) is caused by Holocene deposition conditions.

4.4 Alas deposits

The easternmost profile of this study was located in a thermokarst depression about 3.2 km east of the Ice Complex section DY-05 (Fig. 4-1). The eight metre high steep wall of the riverbank cut the frozen alas deposits (Fig. 4-30, Fig. 4-31) and the upper four metres were well exposed.

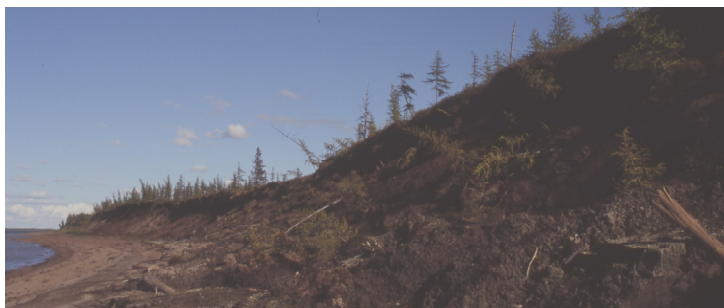


Fig. 4-30: Overview of the alas into eastern direction; Photo: L. SCHIRRMEISTER and S. WETTERICH, August 2008.

The profile started at 3.75 m a.r.l. above a cavern, probably a wave cut niche, which was buried by talus material (Fig. 4-31). At this sequence, twelve sediment samples were taken (DY-04-A-12 to 01).

A great part the sediment consisted of grey and brown patched silty fine sand. The sediment was crumbly (1×1 to 2×2 cm crumbs) and contained white spots (\varnothing 2 to 3 mm). Twigs and plant detritus layer were observed. The cryostructure was complex. Diagonal and horizontal 2 to 3 mm thick ice veins formed a reticulate structure of various sizes.

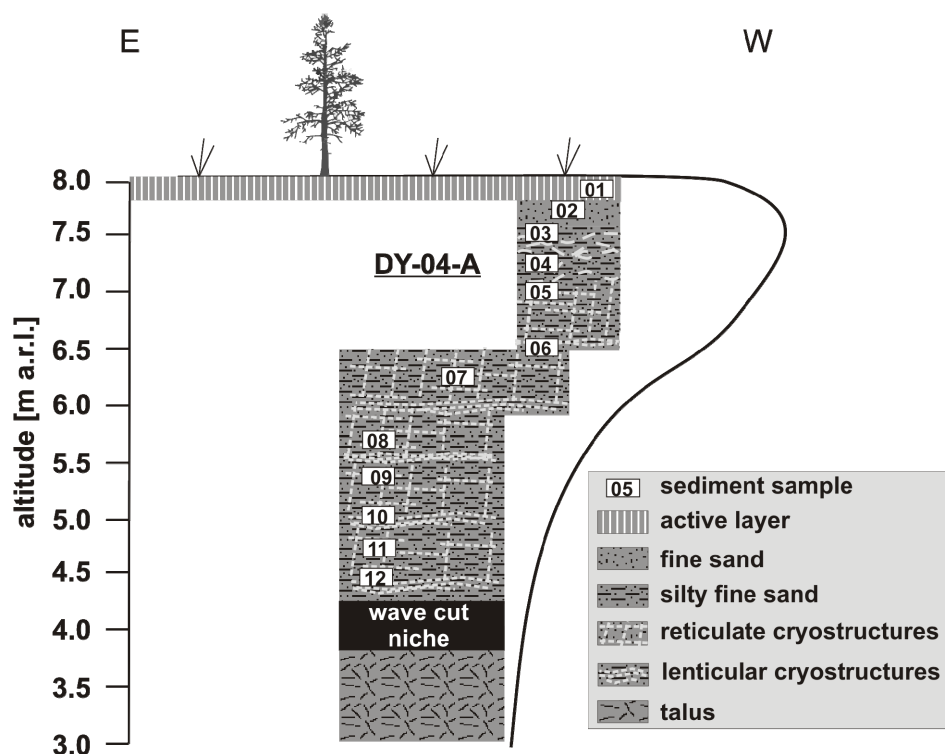


Fig. 4-31: Scheme of the alas profile DY-04; from SCHIRRMESTER et al. (in press), modified.

At some places zones with horizontal ice bands and broken lenticular structures occurred as well as vertical ice veins and a massive cryostructure. From 4.4 to 7.2 m a.r.l. the gravimetric ice content varies between 40 and 150 wt % (Fig. 4-32). Up to 7.5 m a.r.l. the cryostructure was reticular and the gravimetric ice content increases to 227 wt % (Fig. 4-32). The studied sequence ended at the surface with an unfrozen moss cover, underlain by frozen silty fine sand with roots that belongs to the transition zone of the active layer. The cryostructure here was lenticular with 10 to 20 mm long and <1 mm thick ice lenses. At 7.7 m a.r.l. horizontal ice veins, composed of small vertical ice needles, occurred. The gravimetric ice content amounts to 136 wt % (Fig. 4-32).

The majority of the magnetic susceptibility values range between 38 and 63 SI without any obvious significant trend. The second and third highest samples at 7.5 and 7.7 m a.r.l. (DY-04-A-03 and -02) have a magnetic susceptibility of 30 and 32 SI and formed a cluster of minimum values (Fig. 4-32). The TOC content seems to have an increasing trend from the bottom to the top with a local maximum of 6.9 wt % at 6.1 m a.r.l. (DY-04-A-07). The TOC contents increase from 4.4 at 7.2 m a.r.l. to 13 wt % at 7.5 m a.r.l. (DY-04-A-

04 to DY-04-A-03). Within the two uppermost samples at 7.7 to 7.85 m a.r.l. the TOC contents increase even more from 13.1 wt % to 40.3 wt %. This extremely high content is common for a moss layer in the active layer and samples below with recent root penetration. The TOC/TN ratios show a similar pattern like the TOC content. Ranging between 7.4 and 11.5 at the lower part (4.4 to 7.2 m a.r.l.), the TOC/TN ratio increases to ~14 (7.5 and 7.7, Fig. 4-32) and has a maximum of 32.6 on top. The $\delta^{13}\text{C}$ values have a wide range from -31.4 to -27.2 ‰ with a mean isotopic composition of -29.4 ‰ (Fig. 4-32). Carbonate could be detected in samples from DY-04-A-09 (0.5 to 2 wt %) and DY-04-A-12 (<0.5 wt %) only. All other samples are free of carbonate.

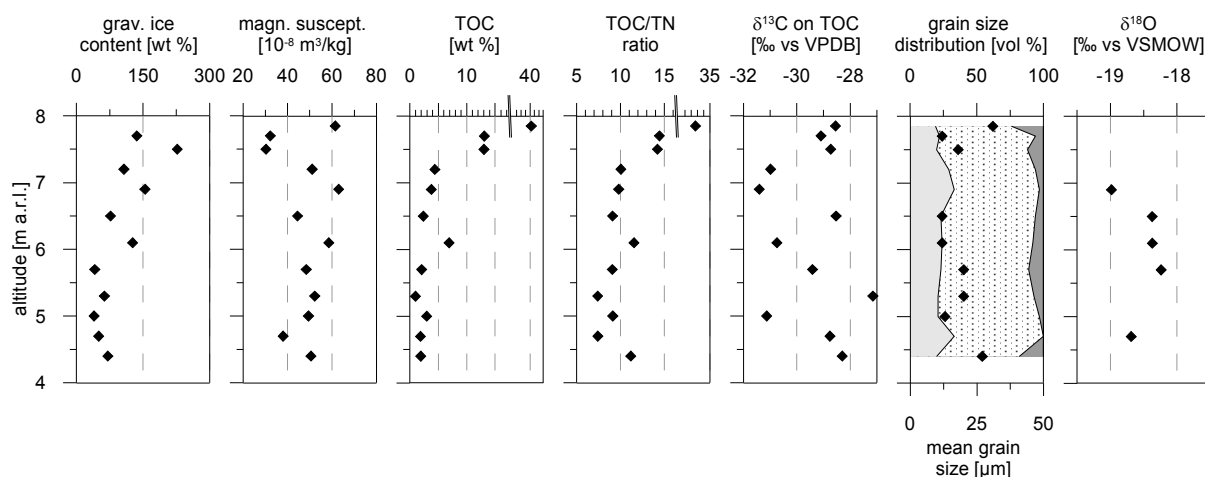


Fig. 4-32: Summary of cryolithological and sedimentological parameters for the alas profile DY-04. The TOC and TOC/TN axes are broken. The legend of the grain size diagram is shown in Fig. 4-3.

All samples are very poorly sorted (2.6 to 4.6). The percentages of different grain size fractions show two distinct features. Firstly, there is no sand at DY-04-A-11, but a increased clay fraction of 33 vol %. Secondly, the lowermost and the uppermost samples, DY-04-A-12 and DY-04-A-01, are deviant by maxima in the sand fraction showing values of 18 vol % and 24 vol % sand, respectively. The grain sizes of all other samples range between 20 and 33 vol % clay, 64 and 76 vol % silt and 3 and 12 vol % sand. All samples, except DY-04-A-10 (silt) and DY-04-A-01 (sandy silt), are categorised as clayey silts according to the sediment triangle (Fig. 4-33 B)

The grain size fraction at DY-04 is less homogeneous compared to the other profiles at Duvanny Yar. This is reflected by the unimodal grain size distribution at DY-04-A-11, the bimodal distribution at DY-04-A-12, DY-04-A-09 and DY-04-A-08 and the grain size distributions at DY-04-A-05/04, which were depleted in the coarse silt fraction. Moreover, the grain size distribution of the uppermost sample DY-04-A-01 shows multiple peaks. The other samples are more or less distinct trimodal in their grain size distributions with a first peak in the fine silt fraction, a second peak in the coarse silt fraction and a small third peak in the fine sand fraction. The grain size distributions of DY-04 have similarities to the Ice Complex deposits DY-05/01 and to lake deposits DY-03/06 as well.

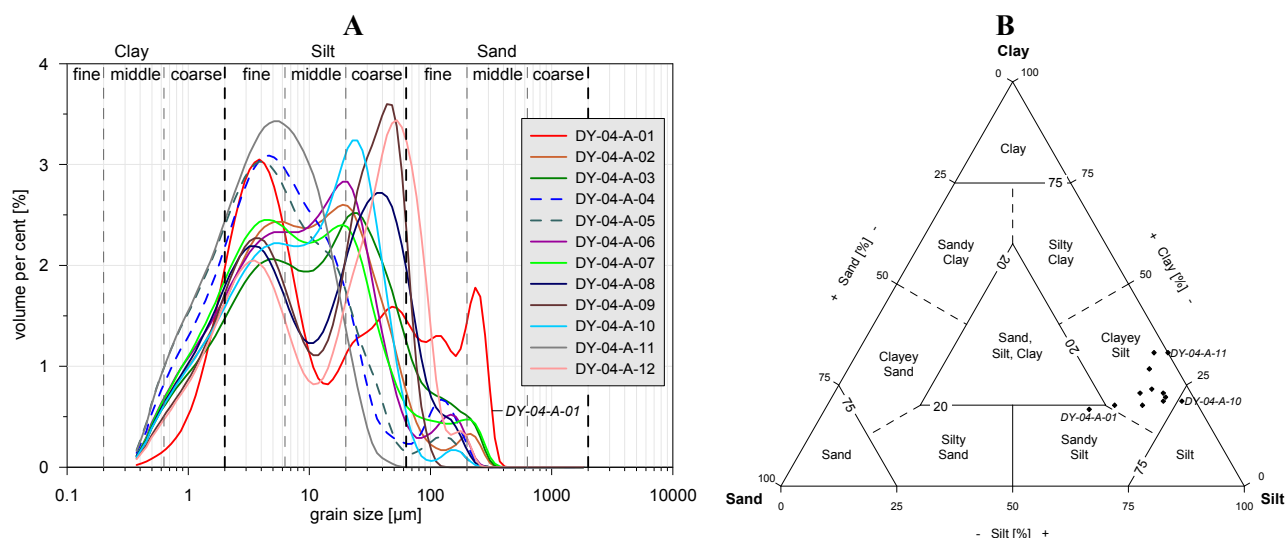


Fig. 4-33: (A) Grain size distribution and (B) sediment triangle after SHEPARD (1954) of the alas profile DY-04.

4.4.1.1 Texture ice at DY-04

The isotopic values for texture ice range between -19.0 ‰ to 18.2 ‰ for $\delta^{18}\text{O}$ and -244.3 ‰ to -229.1 ‰ for $\delta^2\text{H}$. The mean d excess is -7.4 ‰ and shows freeze thaw fractionating processes (Fig. 4-34 B). In addition to freeze thaw fractionating processes, water in alas show an evaporation signal (WETTERICH et al. 2008a). Possibly, the d excess between -10.0 and -2.2 ‰ vs VSMOW is caused by lake water evaporation. The texture ice of the alas has an akin isotopic signal to thermokarst lakes at Duvanny Yar (Fig. 4-34 A).

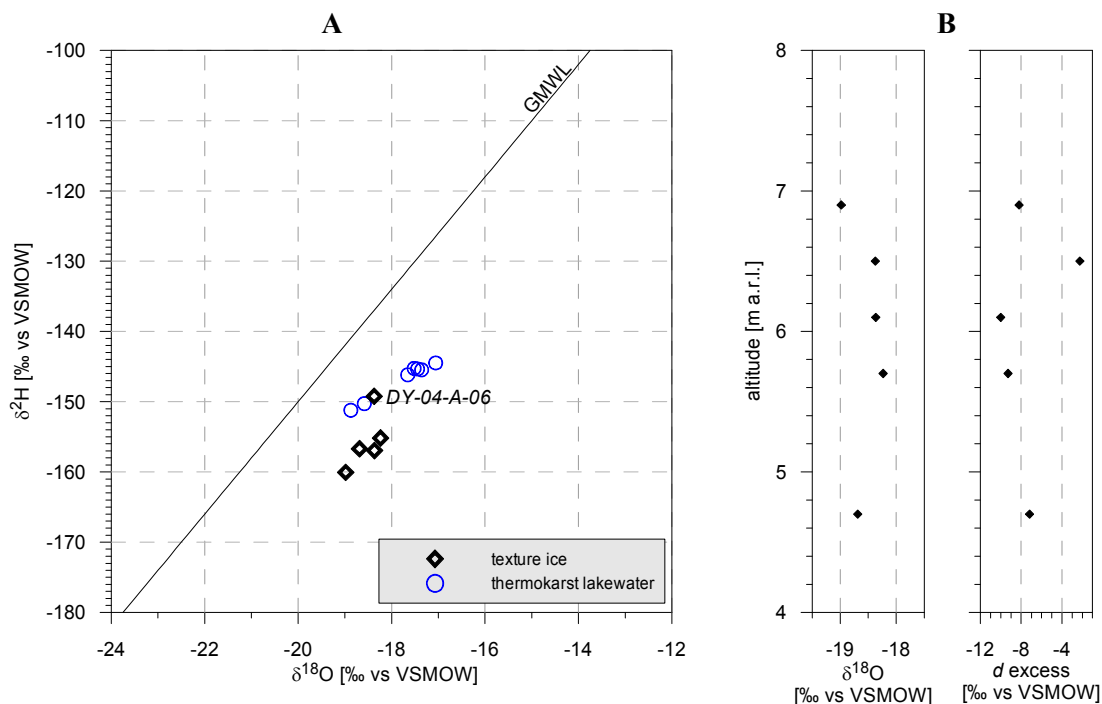


Fig. 4-34: Stable isotope signature of ground ice of DY-04. A: $\delta^2\text{H}$ - $\delta^{18}\text{O}$ diagram for texture ice of the alas profile DY-04; B: $\delta^{18}\text{O}$ and d excess variations of the 5 texture ice samples.

4.5 Specific studies on Ice Complex and alas deposits

Extra methodical tests were accomplished additional to the sedimentological and isotope geochemistry analysis. For the Ice Complex deposits, the grain size distribution curve was decomposed in Gaussian curves through peak fitting. Moreover, the organic carbon content was calculated for the Ice Complex and alas deposits.

4.5.1 Peak fitting at the Ice Complex grain size distributions

The polymodal curves were split into five Gaussian distributions at modal values of 3, 4, 5, 8, 10 Φ (chapter 3.3.2.1, Fig. 3-2), except from eleven exceptional cases, which could only split into four.

4.5.1.1 Peak fitting at DY-05

The coarse peak at $\sim 3 \Phi$ is characterised by a relatively stable position of its mode between 2.3 and 3.3 Φ (mean mode 2.6 Φ). The area of the Gaussian distribution is, except from three outliers, between 0.3 % and 4.0 % (Fig. 4-35). The mode position and the area of the Gaussian distributions of the small coarse peak at $\sim 3 \Phi$ are correlated. This means that a finer grain size shows a relative enrichment of the fraction and vice versa.

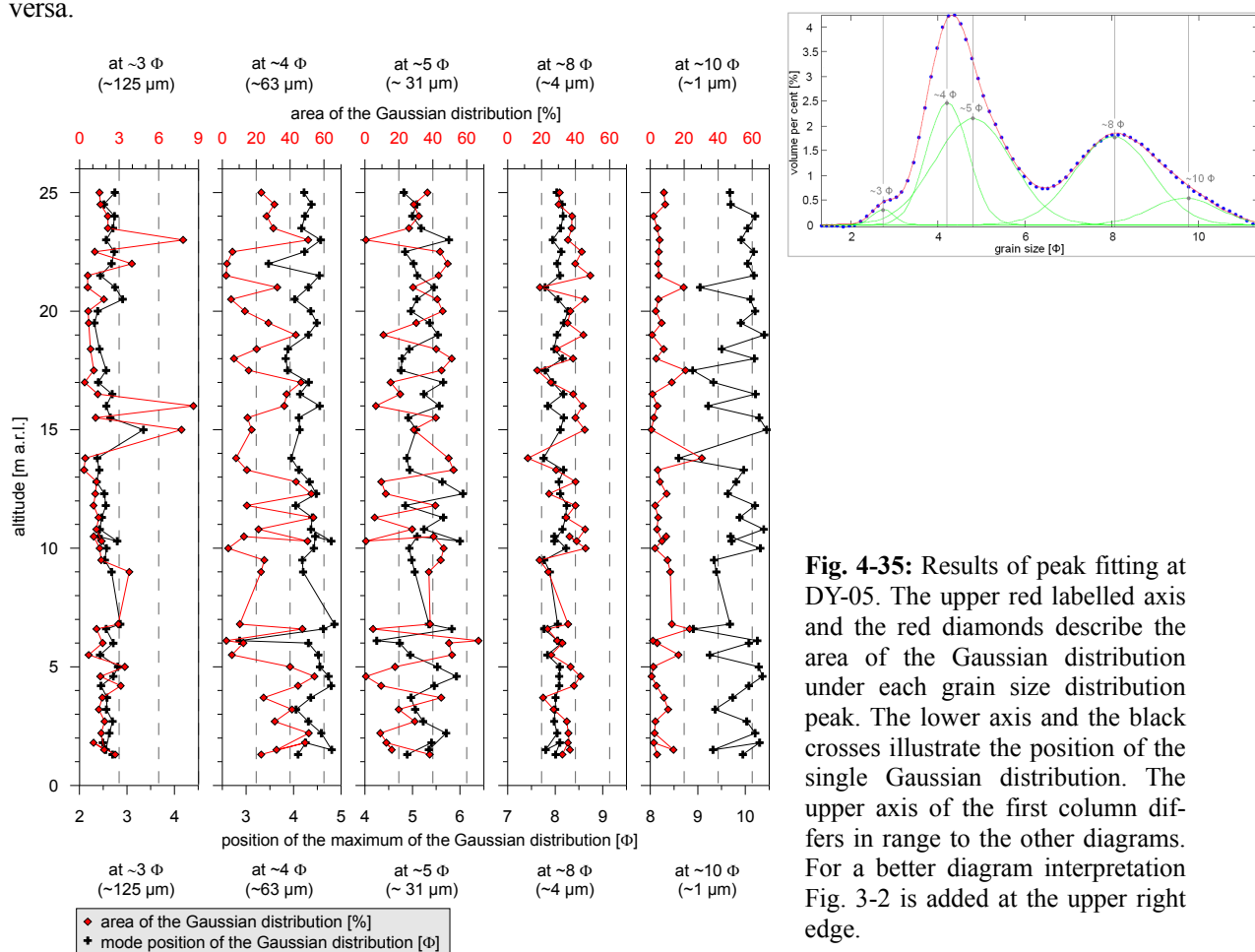


Fig. 4-35: Results of peak fitting at DY-05. The upper red labelled axis and the red diamonds describe the area of the Gaussian distribution under each grain size distribution peak. The lower axis and the black crosses illustrate the position of the single Gaussian distribution. The upper axis of the first column differs in range to the other diagrams. For a better diagram interpretation Fig. 3-2 is added at the upper right edge.

The peak at $\sim 4 \Phi$ shows a range in its mode position between 3.5 and 4.9 Φ . An outlier occurs at DY-05-C-13 (6.1 m a.r.l.), showing a value of 2.9 Φ . The area of the Gaussian distributions varies between 2.4 and 54.2 % (mean area 26.7 %) over the whole height of the profile. The position of the 5 Φ mode varies a little more, especially in the paleocryosol sequence, which reaches from the bottom of the profile to DY-05-C-15 at 6.8 m a.r.l.. The area of this peak ranges between 0.5 and 66.9 %. The mean area is slightly higher compared to the previous peak (30.1 %). Its position and area are anticorrelated. The position at the mode around 8 Φ is nearly constant between 7.8 and 8.3 Φ (mean mode 8 Φ). This constancy is an indicator for a stable sedimentation process. The area ranges between 11.9 and 48.7 %. The last and finest grain size peak around 10 Φ shows a wide range in mode position between 8.6 and 10.6 Φ with alternating values over the whole profile. The area is between 0.7 and 30.3 % and is anticorrelated with the peak position. A coarser peak position seems to cause an enrichment of this grain size fraction.

4.5.1.2 Peak fitting at DY-01

The coarsest grain size peak at $\sim 3 \Phi$ is characterised by a relatively stable mode position between 2.1 and 3.3 Φ (mean mode position 2.7 Φ). The uppermost value is deviant because of a low mode of 0.4 Φ . The area of the Gaussian distribution has one outlier at 34.3 m a.r.l. (7.9 %). Its minimum is 0.4 % and the maximum is 6.2 % (Fig. 4-36). The mode position and the area of the Gaussian distributions are correlated. The uppermost sample has a remarkable lower position values for both, the 3 and the 4 Φ peaks. This can be expected because of the different grain size distribution curve.

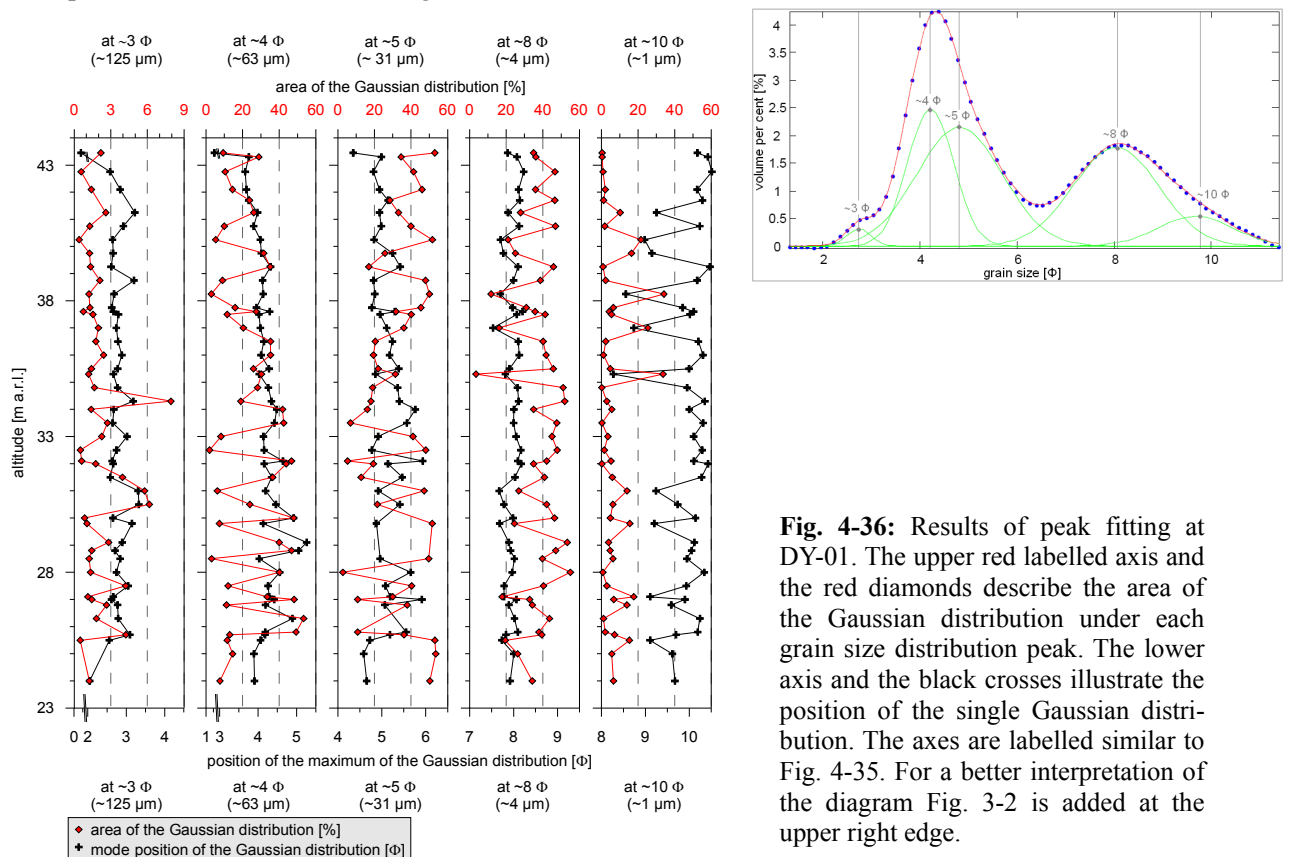


Fig. 4-36: Results of peak fitting at DY-01. The upper red labelled axis and the red diamonds describe the area of the Gaussian distribution under each grain size distribution peak. The lower axis and the black crosses illustrate the position of the single Gaussian distribution. The axes are labelled similar to Fig. 4-35. For a better interpretation of the diagram Fig. 3-2 is added at the upper right edge.

The mode position of the $\sim 4 \Phi$ peak is between 3.7 and 5.3 Φ . The area ranges between 2.0 and 53.4 %. From 24.0 to 33.1 m a.r.l. the area alternates more often and on shorter intervals than in the upper part above 33.1 m a.r.l.. The 5 Φ peak ranges between 4.4 and 5.9 Φ and the mean value is 5.1 Φ . The area of the Gaussian distribution alternates between 2.7 and 53.5 % with a mean area of 32.5 %. The position of the $\sim 8 \Phi$ peak ranges between 7.5 and 8.2 Φ . The range of the area at $\sim 8 \Phi$ peak is 3.5 to 55.0 %. Its mean value of 36.8 ‰ is the highest for DY-01. The finest peak at $\sim 10 \Phi$ has the widest range in mode position, showing values between 8.3 and 10.5 Φ . The area is anticorrelated with the position and ranges between 0.1 and 34.1 %.

Summing up the results of the peak fitting, it was difficult and uncertain to separate the noise and the competition between the Gaussian distributions from the transportation and deposition signal.

4.5.2 Bulk density and organic carbon content for Ice Complex and alas deposits

The bulk density of Ice Complex and alas deposits was calculated (Eq. 3.5 to Eq. 3.7) and combined with the TOC content to estimate the organic carbon content in $\text{kg TOC} \cdot \text{m}^{-3}$ (Eq. 3.8). At the Ice Complex profile DY-05 the ice content was measured for every sample.

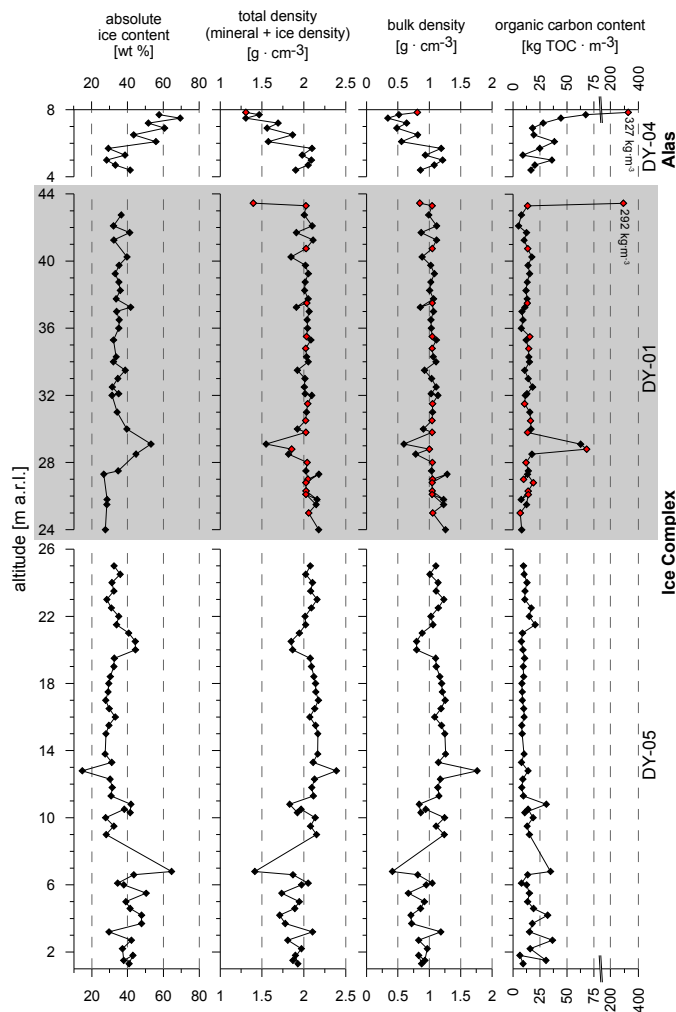


Fig. 4-37: Relevant parameters for the bulk density calculations and organic carbon content estimations. The red diamonds are samples, where no ice content was measured. Here the mean value of 34 wt % was used. The profiles are sorted in a stratigraphical order.

The lower paleocryosol sequence from 1.3 to 6.8 m a.r.l. (chapter 4.3.1) is characterised by an alternating bulk density between 0.4 to 1.2 g · cm⁻³ (mean 0.8 g · cm⁻³). The organic carbon contents span a relatively wide range between 6 and 37 kg TOC · m⁻³ (Fig. 4-37). The mean value of 19 kg TOC · m⁻³ at the paleocryosol sequence is increased for the Ice Complex deposits. As mentioned above, the upper part of DY-05 was homogeneous. Over the entire range from 9 to 25 m a.r.l. the organic carbon content at this site is between 8 to 21 kg TOC · m⁻³. An exception from this homogeneous sequence is a paleocryosol sample at 10.8 m a.r.l. (31 kg TOC · m⁻³). Further exceptions from this homogeneity in terms of bulk density are the sample groups DY-05-D-19 to DY-05-E-21 and DY-05-F-38 to DY-05-G-40 (0.8 to 0.9 g · cm⁻³). At DY-05-E-25 (12.8 m a.r.l.) a peak in bulk density (1.8 g · cm⁻³) occurs (Fig. 4-37).

DY-01 shows a similar picture as the upper homogeneous sequence of DY-05. The paleocryosol with its peat inclusions and the high ice content is connected with a minimum in bulk density between 28.5 and 29.1 m a.r.l. (~0.7 g · cm⁻³). At this height also a maximum of organic carbon (63 kg TOC · m⁻³) occurs. Due to its position near the recent surface, the uppermost sample (43.45 m a.r.l.) has the highest organic carbon value for Ice Complex with an organic carbon content of 292 kg TOC · m⁻³.

The alas deposits have the lowest bulk densities with a decreasing trend from bottom to top. The mean bulk density at the alas is 0.8 g · cm⁻³. Moreover, these deposits contain the highest amount of organic carbon per cubic metre with a mean value of 54 kg TOC · m⁻³. The values for organic carbon for samples from 4.4 to 7.2 m a.r.l. (DY-04-A-12 to 04) alternate between 9 and 38 kg TOC · m⁻³. Above 7.2 m a.r.l. the TOC amount rise from 44 kg TOC · m⁻³ (DY-04-A-03) over 68 kg TOC · m⁻³ (DY-04-A-02) to 327 kg TOC · m⁻³ (DY-04-A-01), the maximum for the Duvanny Yar section.

For all three high values (paleocryosol in DY-01, uppermost Holocene samples in DY-01 and DY-04) no ice content was measured directly and so the mean value of 34 wt % was used to estimate the bulk density. The real water content is assumed to be higher and consequently the calculation error became greater.

4.6 Hydrochemistry

Hydrochemical analysis of ground ice is based upon five ice wedge and seven fissure ice samples. In addition, twelve recent water samples were analysed; seven from thermokarst lakes in alasses at Duvanny Yar, three from thermokarst ponds in a floodplain of the 'Pleistocene Park' near Cherskii and two samples from the Kolyma River. The pH, electrical conductivity and major ions (cations: Ca²⁺, K⁺, Mg²⁺, Na⁺; anions: Cl⁻, SO₄²⁻ and HCO₃⁻) were analysed.

The pH value of the Pleistocene ice wedges and fissure ice range between slightly acidic (6.5) and slightly alkaline (8.2) values. The pH of recent water samples is between 5.9 and 7.8. These signals do not show a saline water influence or salinisation by evaporation. Also the low electrical conductivity shows a pure fresh water signal. The ice wedge conductivity varies between 61 and 156 μS · cm⁻¹. The fissure ice con-

tains two outliers, DY-01-G-701 (23.8 m a.r.l., 0.07 m width) and DY-01-D-501 (31 m a.r.l., 0.07 m width), which show higher values of 653 and 718 $\mu\text{S} \cdot \text{cm}^{-1}$, respectively. The other fissure ice samples have an electrical conductivity between 80 and 178 $\mu\text{S} \cdot \text{cm}^{-1}$. The increased conductivity for fissure ice is an indicator for exchange processes or genetic connection with the surrounding texture ice. The values for recent waters show a range between 26 and 153 $\mu\text{S} \cdot \text{cm}^{-1}$ with one outlier of 318 $\mu\text{S} \cdot \text{cm}^{-1}$. The ion composition of ice and water samples is shown in Fig. 4-38. The ice wedges and fissure ice of the DY-01 and DY-05 section have similar ion composition (Fig. 4-38). In comparison to lake water the ice wedge and fissure ice samples are depleted in HCO_3^- and Ca^{2+} , but enriched in Cl^- and SO_4^{2-} . In comparison to the river water the ice wedges and the fissure ice are remarkable depleted in Ca^{2+} and SO_4^{2-} but enriched in Mg^{2+} , K^+ and Cl^- .

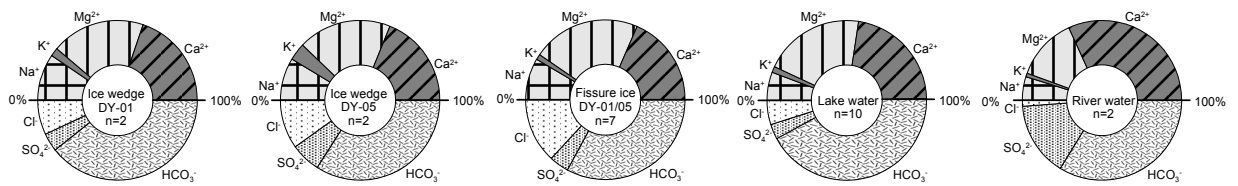


Fig. 4-38: Pie charts of the major ion of the mean for the ice wedges and fissure ice in the Ice Complex deposits and recent waters. The upper half of the pie chart shows the major cation content, the lower part the anion content in percent.

In general, the ice wedges and the fissure ice show a narrow range in their major ionic composition (Fig. 4-39). An exception from this is the concentration of chloride ions, which shows a wider range, particularly for the fissure ice in DY-01 (Fig. 4-39).

water type (after FURTAK and LANGGUTH)

earth-alkalic

- a high hydrogencarbonate content
- b hydrogencarbonatic-sulphatic
- c high sulphate content

earth-alkalic with higher content of alkali

- d high hydrocarbonate content
- e high sulphate content

alkalic

- f high hydrocarbonate content
- g high chloride content

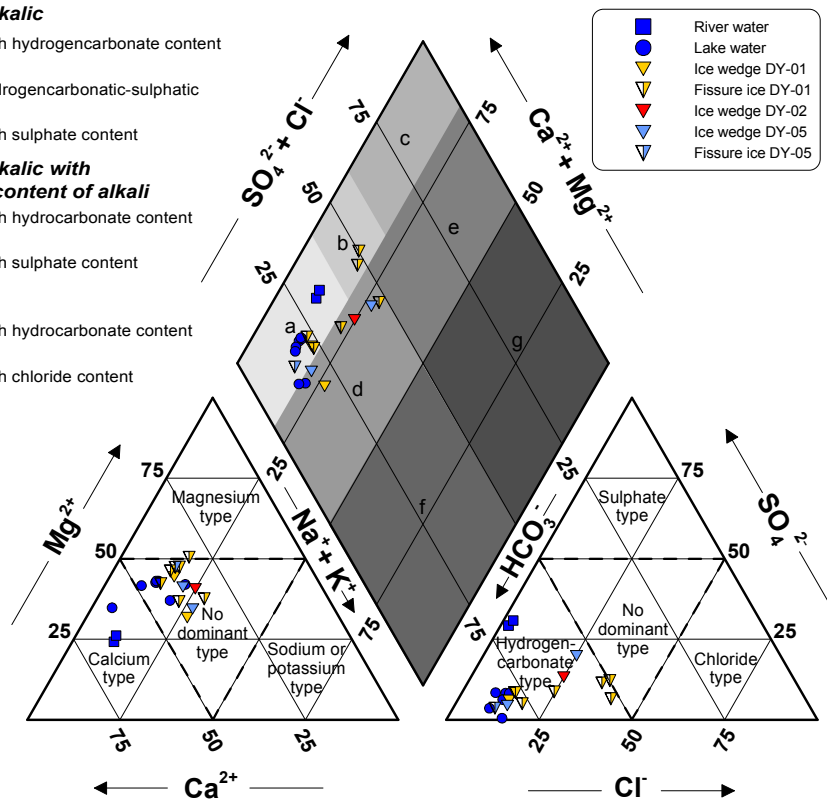


Fig. 4-39: Piper plot of the major ions. The upper rhomb contains ‘water type’ classification after FURTAK and LANGGUTH (1967), in HÖLTING and COLDEWEY (2009); the two ternary plots classify waters into ‘hydrogeochemical facies’ after KEHEW (2001).

The two river water samples, which show an increased calcium and sulphate content (Fig. 4-39), deviate from this general rule, too. The Piper plot (Fig. 4-39) is used to classify water samples to 'types' (rhomb diagram) after FURTAK and LANGGUTH (1967) and 'hydrochemical facies' (ternary diagrams) after KEHEW (2001). According to this, all ice wedges and fissure ice samples can be described as '(calcium-magnesium)-hydrocarbonate' facies. The same holds for the ionic composition of lake water and to a lesser degree for river water as well. Following FURTAK and LANGGUTH (1967), the ice wedges and fissure ice are part of the 'earth-alkalic' hydrocarbonatic (-sulphatic) water type (Fig. 4-39).

In summary, no differences in ice wedge and fissure ice and profile specific differences are obvious. Like the ice wedges and the fissure ice the recent waters are shown as 'earth-alkalic' waters. Therefore the recent hydrological situation is akin to ice wedge and fissure ice formation. The NICB for the analysed ice wedge samples from Duvanny Yar and recent waters does not fulfil the NICB criteria (chapter 3.6 and Eq. 3.16) for a large number of samples (15 out of 24 samples). Therefore, the hydrochemical results must be interpreted with caution.

5 Discussion

The discussion is structured into six parts. At the beginning, the *general geomorphology* is interpreted. The following part, the *geochronological and stratigraphical interpretation*, forms the basis for the *sediment facies discussion*. This part aims to characterise the different major paleoenvironmental conditions at Duvanny Yar. The fourth part is about the *organic carbon content calculation*. The fifth part is dealing with *climatic information* gained from ground ice. At last, a *synthesis* of the previous discussion summarises the paleoconditions for the study area and discusses Late Quaternary environmental dynamics at the Duvanny Yar.

5.1 General geomorphology

The remarkable features of the Duvanny Yar section are relicts of the Late Pleistocene floodplain of the Kolyma River. Wide and deep ice wedges are present at Duvanny Yar. Depressions caused by thermokarst processes form the Kolyma Lowland and divide the Late Pleistocene floodplain surface into Yedoma hills and alas parts (Fig. 4-1). Further periglacial geomorphologic phenomena are thermo-erosional features like thaw slumps, which are caused by the incising Kolyma River. In comparison to ice wedges, the intrapolygonal deposits are more resistant to thawing processes. Thus, small scale geomorphologic results are thermokarst mounds (Fig. 4-24). The hinterland of Duvanny Yar is characterised by wide-stretching lowlands with very low hydrological gradients. This low topographic gradients and the absence of glaciation were the basis for ice wedge polygon formation (SCHIRRMESTER et al. in review). Therefore, ice wedges are paleosurface indicators and an evidence for extremely cold and dry winters (WASHBURN 1981).

5.2 Geochronological and stratigraphical interpretation

Following VASIL'CHUK et al. (e.g. 2002), based on more than 50 radiocarbon dates for adjacent sediments, ice wedges at Duvanny Yar were formed between ~37000 to 17000 a BP. In this study direct age determinations with radiocarbon dating are done for 8 samples of the Ice Complex. The initiation of Ice Complex formation started at >46690 and ended at ~9890 ± 50 a BP. The age determinations at the lower Ice Complex profile are not very accurate, which is reflected in the plateau of the radiocarbon ages related to altitude. This kind of plateau in ¹⁴C dates and great measurement errors can occur at ages close to the detection limit. Moreover, the long safety of organic material and possibility of its repeated deposition in permafrost conditions complicates ¹⁴C dating of permafrost sediments (VASIL'CHUK et al. 2004). In particular, following NELSON et al. (1988), contaminations by old material could also be a problem in permafrost sediments. Thus, 15 % of old organic admixture can distort a ¹⁴C date of a 10000 year old sediment by 1300 years (OLSSON 1991) and a dating error of organic material older than 20000 may be more than 10000 a BP (VASIL'CHUK et al. 2001). In comparison to previous studies at Duvanny Yar, the radiocarbon dates matches with literature dates (Fig. 5-1). Due to the above mentioned uncertainties with age determinations near the detection limit, the ages at 0 to ~30 m a.r.l. scatter more than at altitudes above 30 m a.r.l.. The highest

dated sediment sample at this study is with $\sim 9890 \pm 50$ a BP the youngest radiocarbon age measured for Ice Complex deposits at Duvanny Yar.

The agreement of dates from this study with previous studies show that formation of Ice Complex deposits at Duvanny Yar must have happened since Middle Weichselian times and ended more or less at the Late Pleistocene/Holocene transition, which is supported by stratigraphical data, too.

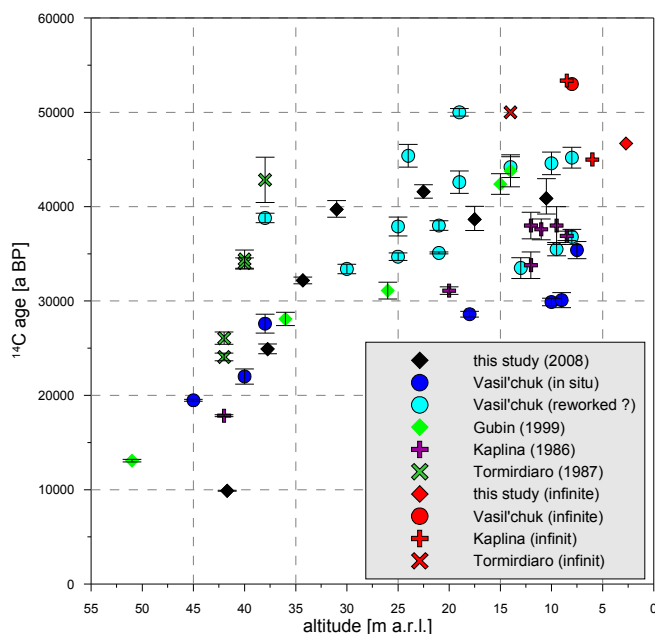


Fig. 5-1: Summary of ^{14}C dates from different authors for different kind of organic material at Duvanny Yar; the data of the previous studies were summarised by VASIL'CHUK et al. (2001).

First palynological results allow the age evaluation of other profiles besides the radiocarbon dated Ice Complex. At DY-02 *Larix* (larch), *Pinus* (pine) and *Alnus* (alder) pollen are present (ANDREEV, pers. com.). This is an indication for an interstadial period, whereas *Pinus* pollen and absence of *Ericales* (e.g. heather) point to Eemian times. Together with the stratigraphic location, a classification of DY-02 to Eemian is reasonable. At the lake sequence DY-03 the palynological conditions are not as well defined. There is neither an Eemian nor a Holocene pollen signal. Taking the stratigraphical data into account, DY-03 could be classified to the Late Eemian/Weichselian transition (\sim MIS 5d, Table 2-2). At the lake sequence DY-06 stomata of *Larix* are found. This gives evidence, that *Larix* shrubs or trees were present at the deposition time, because stomata cannot be transported by wind. Moreover, grass pollen are found, but no *Pinus* pollen. Therefore, this lake profile shows a warm time pollen signal suggesting Holocene times. Due to some *Ericales* pollen and the absence of *Pinus* pollen, the uppermost samples of DY-01 are classified as Holocene, too.

Comparison to the previous Ice Complex studies at the Laptev Sea and Dmitry Laptev Strait

The initiation of Ice Complex formation varies from >55000 a BP on the New Siberian Islands at the Dmitry Laptev Strait to about 50000 a BP at Cape Mamontov Klyk at western Laptev Sea coast (SCHIRRMEISTER et al. 2008b). The latest deposition is dated between 28000 a BP at the New Siberian

Islands and 17000 to 13000 a BP at the western Laptev Sea coast. Therefore, the Duvanny Yar section shows the youngest age for Ice Complex deposition compared to previous studies. Furthermore, at the Ice Complex sequence of Cape Mamontovy Klyk, accumulation rates of about 14 mm per year were derived (SCHIRRMESTER et al. 2008a). A similar approach is accomplished for the upper Ice Complex of Duvanny Yar (Fig. 5-2). The well correlated altitude-age-relationship allows a rough estimation of the accumulation rate of ~4 millimetres per year for the upper part of the Ice Complex profile at Duvanny Yar. It seems to be consistent over a period of about 30000 years for this part of the profile. This indicates stable deposition conditions throughout this period.

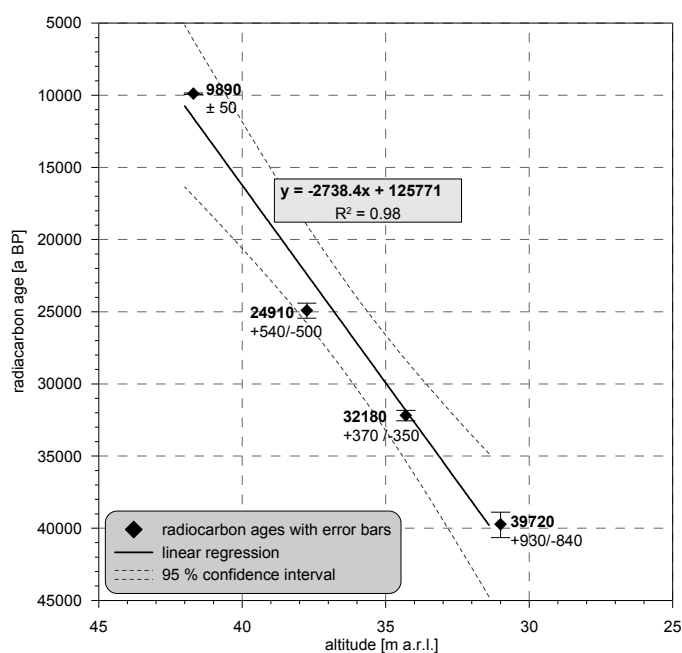


Fig. 5-2: Altitude-age relationship with a linear regression line of the Ice Complex profile DY-01. Both axes are labelled descending.

5.3 Sediment facies discussion

According to REINECK and SINGH (1980) a sediment facies is the sum of all primary characteristics of a sediment unit (e.g. surface markings, bedforms, bedding). In this chapter the term ‘sediment facies’ is used to describe different transportation and sedimentation conditions.

5.3.1 Lake deposits

DY-02

The separation into two parts (lake deposits, peat layer) is supported by several parameters. The cryostructure in the lower part is diagonal and horizontal reticular (Fig. 5-3). These cryostructures and an epigenetic ice wedge are diagnostic for epigenetic freezing of the sediment (FRENCH 2007; MACKAY 1974). The cryostructure at the upper peaty part is layered. These ice layers are ice enrichments near the permafrost table (DOSTOVALOV and KUDRYAVTSEV 1967) indicating stable surface conditions and stable active layer depth as well as syngenetic freezing.

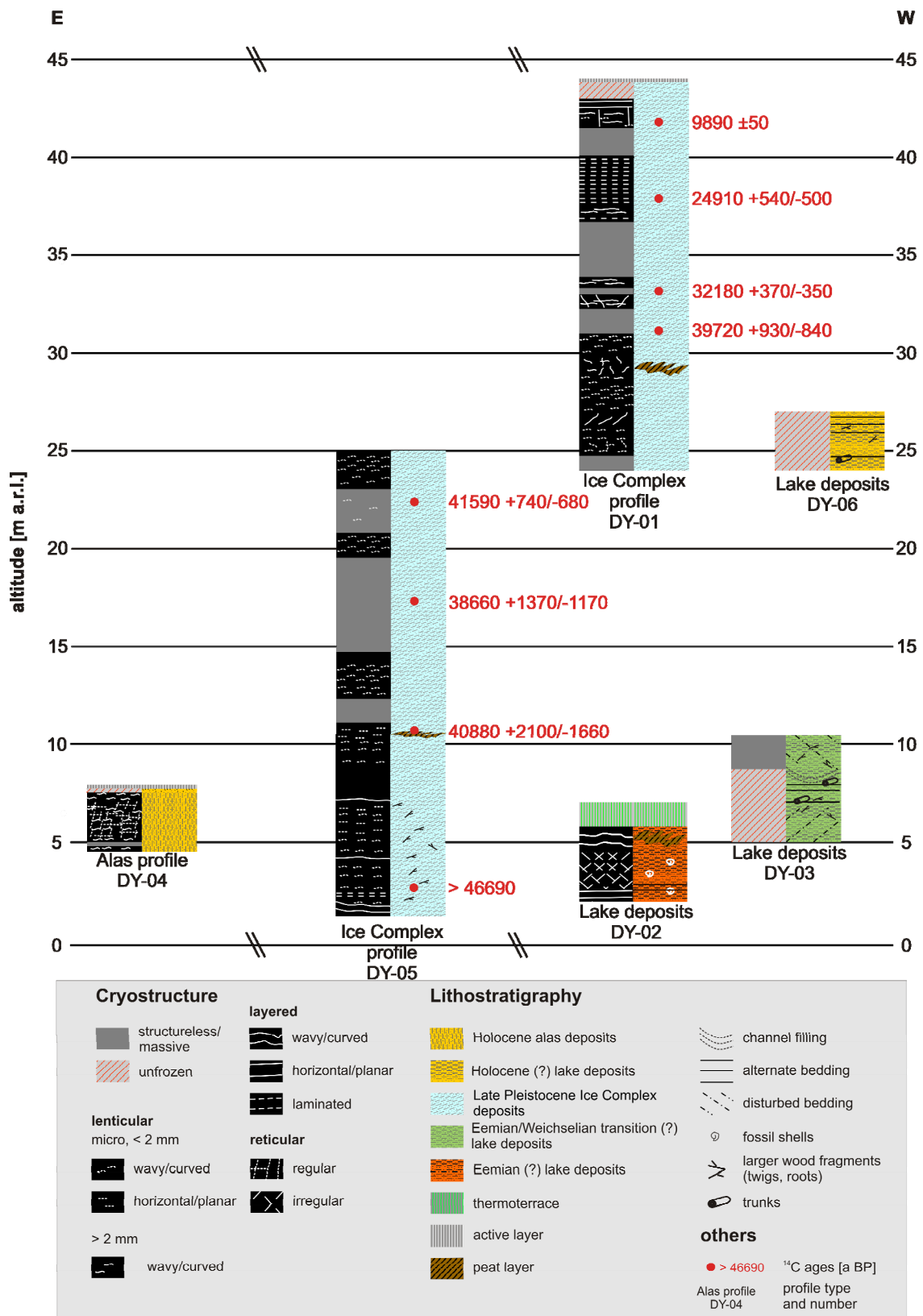


Fig. 5-3: Generalised cryostructures (left column of each profile) and lithostratigraphical schemes (right column) of the studied profiles from east to west. The results of radiocarbon age determinations are added. Because of not mentioned distances between the different profiles (Fig. 4-1) breaking marks are inserted. The symbols for cryostructure are based on MURTON and FRENCH (1994), in FRENCH (2007, p. 166).

Furthermore, the change in sediment facies towards the top within the DY-02 lake deposits is reflected by a decreasing magnetic susceptibility and finer grain size. Moreover, the TOC/TN ratio increases at the boundary zone between lake sequence and peat soil layer. An inverse pattern is shown in the $\delta^{13}\text{C}$ ratio decreasing from -25 to -32 ‰. This indicates periods of increased organic matter accumulation and its limited decomposition at the peat soil layer. Most likely, this peat soil was developed after a siltation of a lake with a change to anaerobic conditions related to water-supersaturated soils. These preconditions are essential for the accumulation of peat beds. An accompanying succession is shown in Fig. 5-4 following MEYERS (1994). The organic carbon source for the lower part is classified as lacustrine algae. In contrast, the two peaty uppermost samples have an increased TOC/TN and more negative $\delta^{13}\text{C}$, which is rather C_3 land plant detritus than algae detritus.

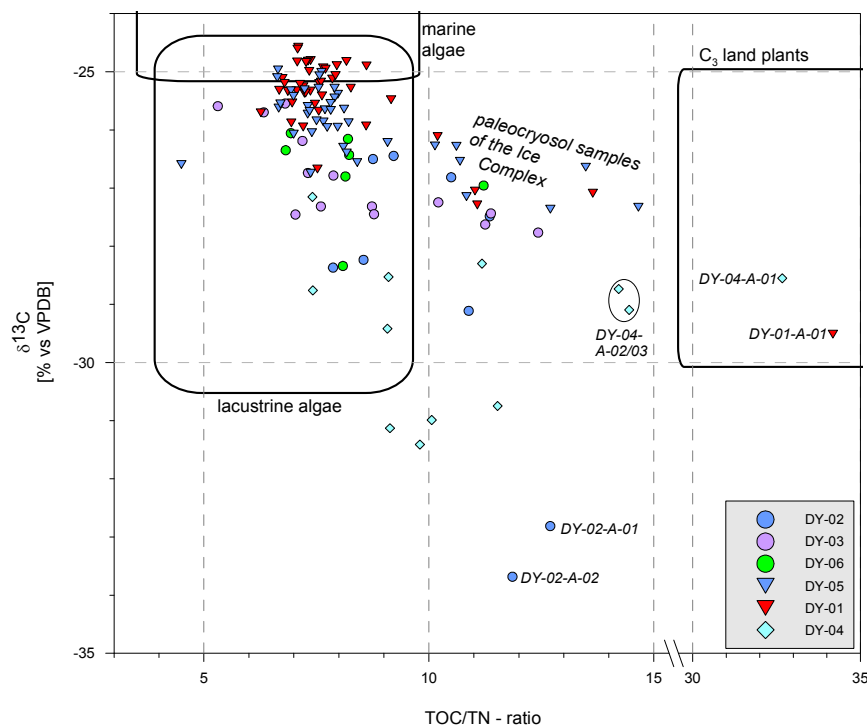


Fig. 5-4: Generalised stable carbon isotope ratios and TOC/TN- ratios of marine and lacustrine algae as well as C_3 plant organic matter; according to MEYERS (1994).

A shift in grain size distribution at DY-02 reveals a change in the energy level related to transportation and deposition of the sediment. The 'gap' at the middle silt fraction at the four lowermost samples indicates different deposition and transportation conditions. This distribution is comparable to parts of other lake profiles, where small and weak developed ripples indicate shallow slow flowing water. In comparison to stagnant waters, the floating sediment freight would be kept in suspension. In contrast to this, the grain size distribution of the upper samples suggests a stagnant water body or wetlands, where the dwell of water is long enough to settle down the suspended sediment freight.

In summary, DY-02 changed from a lake environment, which was silted or dried-out, to an ice wedge polygonal landscape. The polygons were developed on the former lake deposits and a boggy polygonal landscape with peat accumulation was established.

DY-03

The lower part of DY-03 was unfrozen and only the upper third of the profile showed a massive cryostructure with some diagonal ice veins. This can be interpreted as a fast epigenetic freezing of a talik beneath a former lake. Moreover, due to the bedded sediment structure and vivianite inclusions, DY-03 is identified as lake deposits. Ripples were present at the lower part of DY-03 (7.1 m a.r.l.). This gives evidence for shallow and little streaming water, which kept the middle silt fraction in suspension and thus caused the well-differentiated grains size peaks. A special feature is the sequence between 7.75 and 8.8 m a.r.l., because the clay content increases to ~30 vol %, whereas the sand fraction (<8 vol %) and magnetic susceptibility (~26 SI) remain low. In addition, other deviant grain size distributions occur at DY-03. Here, the middle silt fraction increases. This is interpreted as a period of stagnant waters or wetlands. This interpretation is supported by an increased organic content and peaty cryoturbations. Wet and anaerobic conditions constrain the mineralisation of plants, which results in the highest TOC/TN ratio (12.4) of this profile at 8.4 m a.r.l. Following WALTHERT et al. (2004), this TOC/TN ratio is classified as moderate mineralisation. Directly above the stagnant water sequence the sand fraction sets a peak (54 vol %) and a sharp increase in magnetic susceptibility to >100 SI take place. This gives evidence that at this point the environmental conditions switched back to little streaming water.

In summary, the deposition medium of DY-03 changes from shallow and little streaming water (up to 7.4 m a.r.l.) to stagnant water bodies and boggy influences (up to 8.8 m a.r.l.) and back to little streaming conditions. This deposition 'fingerprint' can be related to alluvial conditions and the stable $\delta^{13}\text{C}$ values show a constant source for the organic matter at this profile (Fig. 5-4).

DY-06

This profile was unfrozen and thus no cryostructures were present (Fig. 5-3). The increased magnetic susceptibility at 26.5 m a.r.l. is located in an alternated bedding sequence (Fig. 5-3) and the sampled layer is affected by a different mineral composition. This is possibly caused by an increased aeolian deposition, which is supported by a remarkable high peak in the coarse silt/fine silt border, the 'typical' grain size of aeolian transportation. Generally, like at DY-03 the grain sizes and prevailed ripples indicate shallow slowly flowing waters, which avoided the floating middle silt fraction sediment to settle. The flowing speed became slightly stronger at the two uppermost samples. This interpretation is supported by the bigger 'gap' in the floating middle silt fraction and coarser mean grain sizes. Within the $\delta^{13}\text{C}$ -TOC/TN diagram (Fig. 5-4) the values are concentrated into the field of lacustrine algae.

5.3.2 Ice Complex

The sediments of the Ice Complex profiles contained lenticular and layered cryostructures with numerous large to small ice lenses. Some parts were classified as massive (Fig. 5-3). Lenticular and layered cryostructures are the typical features of sediments, which are formed by syngenetic freezing of permafrost

deposits. The occurrence of ice bands in the lower parts of DY-05 and the laminated cryostructures of DY-01 (Fig. 5-3) indicate that surface conditions and active layer depths were stable during the formation period. During freeze-thaw cycles, ice was accumulated at the permafrost table and formed layered cryostructures. Generally, the Ice Complex profiles are mostly ice saturated. Moreover, ice supersaturations covary with high TOC contents and are an evidence of paleocryosol sequences. The average gravimetric ice content is 55 to 60 wt %. Assuming that ice wedges can account for 50 % at Ice Complex sequences (SCHIRRMEISTER et al. 2002b; ZIMOV et al. 2006a), the total absolute ground ice content can make up about three quarters of the total sequence (SCHIRRMEISTER et al. 2008b). This shows the sensitivity of Ice Complex deposits against warming temperatures and surface subsidence after thawing. The occurrences of syngenetic ice wedges at both Ice Complex profiles indicate syncryogenic incorporation of sediment into the permafrost with on-going sedimentation.

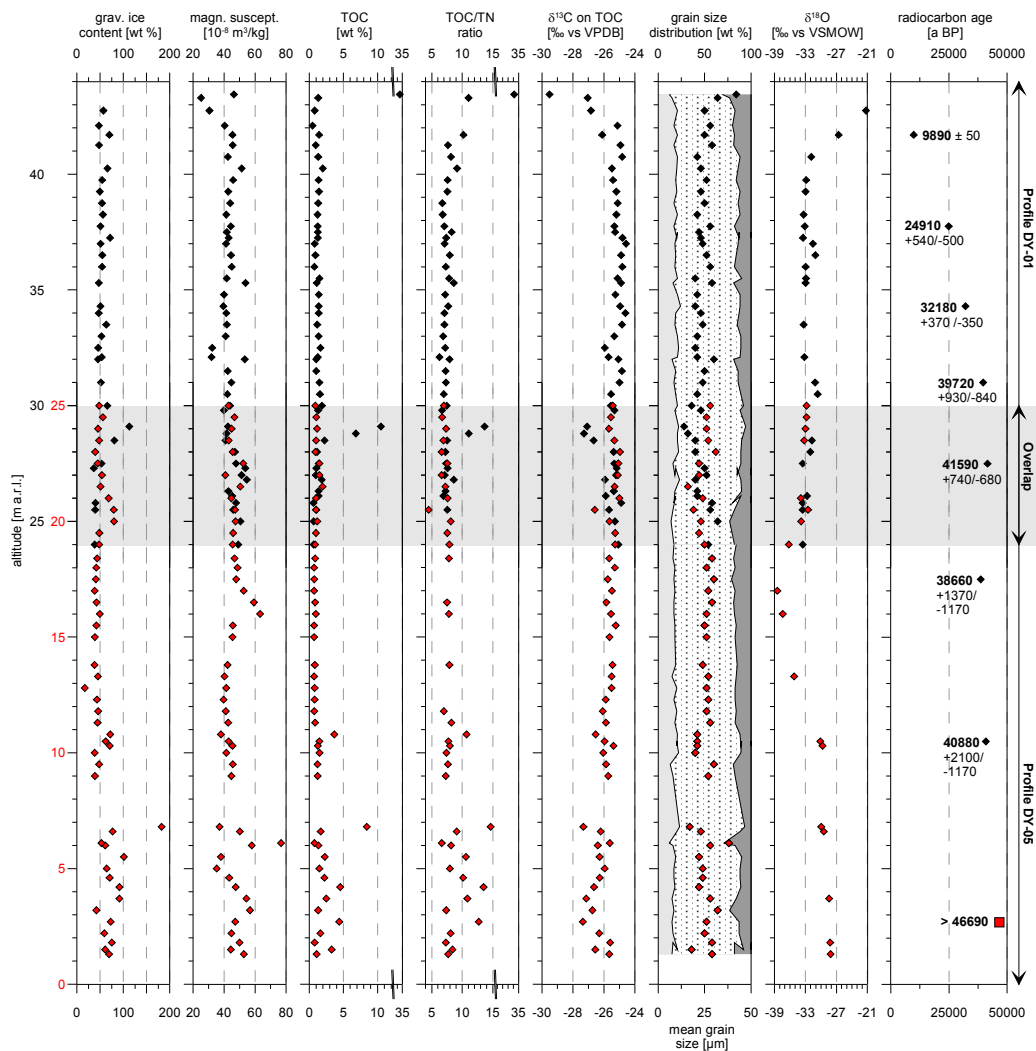


Fig. 5-5: Compilation of the Ice Complex profiles DY-05 and DY-01. The red diamonds are the values of DY-05, the black ones of DY-01. The red labelled altitude is related to DY-05. The overlap is empirically estimated by similarities in the measured parameters.

The sediments of the Ice Complex at Duvanny Yar are remarkably homogeneous and dominated by light grey to light brown silty sediments and filament roots, which occur at the whole altitude of the Ice Complex deposits. In order to get a better overview and to emphasise the genetic connection of DY-05 and DY-01,

both profiles are graphically correlated (Fig. 5-5). The basis for this correlation is a similar magnetic susceptibility in the overlap zone and conformities in other parameters.

With exception from paleocryosol (1.3 to 6.8 m a.r.l. at DY-05, 29 m a.r.l. at DY-01) or Holocene formed parts (> 42 m a.r.l. at DY-01), the values for the magnetic susceptibility are between 30 and 60 SI. Different magnetic susceptibilities occur only at one sample within the paleosol sequence (6.1 m a.r.l.) and at the upper Holocene samples of the Ice Complex deposits. The paleocryosol sample at 6.1 m a.r.l. shows a peak value of 77 SI. As this coincides with the grain size peak in this sample, it must have a different mineral composition. It could be possible, that the deposit energy level was different. A scenario could be seasonal or temporal inundation of a floodplain with stronger streaming conditions or an increased aeolian activity resulting in an enrichment of the fine sand fraction. However, the internal variations of about 32 to 63 SI in the major parts of the Ice Complex (all samples outside paleocryosol or Holocene parts) reveal no further significant changes in the mineral composition. Thus, the sediment source or the fraction of different sources is assumed to be constant. The low susceptibilities in the uppermost samples are caused by the occurrence of peat inclusions, which lower the magnetic susceptibility.

The TOC content in the major parts of the Ice Complex is relatively high, showing values between 0.5 and 2.0 wt %. The paleocryosols (1.3 to 6.8 m a.r.l. at DY-05, 10.8 m a.r.l. at DY-05 and 28.8 to 29.1 m a.r.l. at DY-01) are characterised by peat inclusions and numerous single plant remains, ranging from well-preserved grass roots to twigs and leaves (Fig. 5-3). Here, the TOC reaches max. 10.5 wt %. The mean organic carbon value for the whole profile was 1.5 ± 1.5 wt % (without the uppermost sample) and the $\delta^{13}\text{C}$ values range between -27.4 and -24.6 ‰. Integrating these parameters with the TOC/TN ratios, it is indicated that fresh water and subaerial terrestrial environments are the dominant organic matter source during Ice Complex formation (Fig. 5-4). All Ice Complex samples outside the lacustrine algae rectangle in Fig. 5-4 are part of the different paleocryosol sequences and reflect differences in the prevailing plant association. The high TOC/TN ratios of 10 to 15 indicate a moderate degree of organic matter mineralisation (Table 3-3). Moreover, the organic matter of the paleocryosol parts is influenced by C_3 land plant associations (Fig. 5-4).

In a first interpretation, the lowermost sequence at DY-05 (1.3 to 6.8 m a.r.l.) and the paleocryosol at 10.8 m a.r.l. match well into the Middle Weichselian interstadial periods. This conclusion can be drawn based on the stratigraphical position, the (infinite) age determination and parameters like high TOC contents, high TOC/TN ratios and low $\delta^{13}\text{C}$ values. These are typical indications for interstadial periods with increased bioproductivity and a moderate organic matter mineralisation under anaerobic conditions (e.g. SCHIRRMEISTER et al. in review; WETTERICH et al. 2009). On the contrary, the major part of the Ice Complex above 9 m a.r.l. indicates stadial periods like less variable, generally lower TOC contents and low TOC/TN ratios. Consequently, stable environments with reduced bioproductivity were present (SCHIRRMEISTER et al. in review). However, this explanation has to be approached with caution, because the heterogeneity in the formation area as represented by polygonal nets and lakes could produce signifi-

cant variations. Organic matter formed at the well aerated polygon wall would have produced different signals as in an anaerobe lake (KUTZBACH et al. 2004). As the uppermost sample is taken from the Holocene litter horizon, it reflects the dominance of terrestrial C₃ plants in the organic matter (Fig. 5-4).

The grain size composition within the entire sequence is uniform. All sediments are very poorly sorted (3.0 to 4.2) and the percentages of the grain size fractions do not show any significant differences. The clay and sand content are both < 25 vol % and the silt fractions dominates (~50 to 70 vol %). The mean grain size values of major parts in both Ice Complex profiles range uniformly between 16 to 32 µm. Within the paleocryosol sequence a sand peak (29 vol %) and a maximum grain size mean value (38 µm) occurs at 6.1 m a.r.l.. The sand fraction reaches a minimum in paleocryosol samples of DY-01 (28.5 to 29.1 m a.r.l.). Generally the paleocryosols are characterised by more alternating mean grain sizes. This could be a consequence of faster environmental changes, increased bioproductivity and thaw processes during warmer periods. The maximum mean grain size occurs at the uppermost samples in DY-01 (42 and 32 µm). The grain size of this sample is coarser, because the sediment has been subjected to freeze-thaw cycle and its *in-situ* frost weathering for the shortest period of time. Moreover, vegetation like moss is an excellent sediment trap for coarser grain size fractions during aeolian processes (SEPPÄLÄ 2004). The high degree of homogeneity in grain sizes is also reflected in the distribution curves. All samples show a distinct two major peak distribution with a smaller peak in the fine silt fraction (between 3 and 4 µm, fine silt) and a greater peak in the coarse silt fraction (at ~40 to 60 µm). A more or less well distinct third peak in the fine sand fraction is found for nearly all samples, too. Three characteristics can be seen in these grain size distributions. Firstly, a sand maximum with a wider curve width at the coarse silt peak, as shown by the sand maximum sample at 6.1 m a.r.l., could be caused by a higher energetic level during the deposition period. This could be caused by an increased streaming velocity during a flooding period or an additional aeolian input. Secondly, a well distinct third small peak in the fine sand fraction (at ~160 µm), as shown by the samples at 16, 22 and 23 m a.r.l. at DY-05, can be explained by an increased fraction of the saltation and rolling sediment load in the transport medium (REINECK and SINGH 1980). Thirdly, a relative enrichment at the middle silt fraction, as shown by the paleocryosol samples of DY-01 at 28.8 to 29.1 m a.r.l., can be an indication for ponding, not flowing water. The enrichment of silt at this paleocryosol sequence could be enhanced by former frost weathering during the exposed period of this paleosurface. Nevertheless, during a ponding period the suspended middle silt fraction has a sufficient settling velocity for its deposition (cp. Hjulström's diagram in HJULSTRÖM 1939). Additionally, the increased organic content is interpreted as a result of ponding water and boggy conditions, where the rate of organic matter mineralisation was lowered, too.

Origin of the Ice Complex deposits at Duvanny Yar

The Ice Complex development is a source of debate as mentioned in the introductory chapter (summarised concepts in Table 2-1). The differentiation between the preferred developmental concepts of alluvial floodplain deposits or loess deposits is difficult as suggested in Table 5-1.

Table 5-1: Grain size parameters of sediments of chosen environments (FÜCHTBAUER et al. 1988), shortened.

<i>Fluvial environment</i>	River bed and point bars
	- sorting mostly > 1.2 - skewness < 1, seldom > 1
	Floodplain
	- sorting mostly > 2 - skewness always < 1 (fine grained tail in grain size distribution)
<i>Aeolian environment</i>	Loess
	- poorly sorted
	- skewness mostly < 1 (much fin grained fraction)
	- median diameter generally < 100 µm, 70-95 % of grain sizes < 60 µm (SEPPÄLÄ 2004)

A short definition of loess is given by PETTIJOHN (1975): “Loess is unconsolidated porous silt, commonly buff in colour, characterised by its lack of stratification. It is generally highly calcareous and effervesces in weak acid. Loess is essentially silt.” According to PÉCSI (1990), calcium carbonate should not be used as a diagnostic criterion to define loess. Furthermore, aeolian silt without calcite is called loess-like sediment (SEPPÄLÄ 2004). As caused by grinding processes, loess is rather common in glacial environments and is drifted from outwash plains by wind. Therefore PYE (1995) defined a subcategory of loess named ‘periglacial loess’, which “occurs at mid-continental shield areas beyond the limits of ice sheets”. However, also subaquatic fluvial and lacustrine silts can be loess-like, as well as some alluvial and colluvial deposits (KONISHCHEV 1987).

All Ice Complex sediments are very poorly sorted according to the grain size parameters after Trask et al. (1932) (3.0 to 4.2, mean 3.7) and the skewness is between 0.2 and 0.9 (mean 0.5). The mean grain size is between 14 to 38 µm (mean 24). Following Table 5-1, both developmental concepts are possible, flood plain and loess deposits. As an example for the ‘periglacial loess’ Pye (1995) showed grain size distributions with a well-defined unimodal character in the coarse silt/fine sand fractions. Therefore, the polymodal (bi- to trimodal) grain size distribution pattern of Ice Complex at the Duvanny Yar disproves a pure aeolian hypothesis. Especially the first peak (at 3 to 4 µm, Fig. 4-17 A and Fig. 4-27 A) cannot be explainable by pure aeolian processes. Walger (1962) argues, that polymodality can be caused by a sampling error, because material from different small layers are sampled in one single sample. Moreover, Walger (1962) states that each of the three basic transport and deposition mechanisms suspension, saltation and rolling is contained in every single grain size distribution. Due to the absence of visible layered structures and considering Walger’s (1962) hypotheses, the interactive peak fitting was accomplished. For this reason the grain size distribution was separated into five Gaussian distributions, which contain the homogeneous grain size distribution of the Ice Complex deposits. Four Gaussian curves, the ~4 Φ with the ~5 Φ peak and the ~8 Φ with the ~10 Φ, are not independent from each other. As a consequence, the grain size distribution of the Ice Complex deposits could be seen as 3 peak system. According to WALGER (1962), each peak could be dominated by one of the three deposition mechanisms. If this hypothesis is applicable to Ice Complex deposits is questionable. A more reliable aspect of the grain size distribution fitting is the variation of position and area of the single peaks. These slight variations are likely to be caused by changes in the transportation and deposition processes. However, the variations remain in a relatively narrow range and no significant outliers are present. The composition

within the entire sequence is uniform, which reflects stable transport and accumulation processes or stable proportions of different processes during the whole Ice Complex formation period.

Another process of the production of fine grained sediments is the *in-situ* frost weathering of the material. A homogeneous grain size distribution could be caused by a stable and continuous cryogenic or syndepositional weathering. Intense freeze-thaw cycles and wet conditions around polygonal ponds and seasonal snowfields support the formation of fine-grained material by *in-situ* frost weathering. BERG (1964) suggested that this could be a dominant factor during the loess formation. BERG's hypotheses did not become accepted, but *in-situ* frost weathering can have a significant influence on permafrost sediments (SCHWAMBORN et al. 2008).

Due to the very poorly sorted sediments, the polymodal grain size distribution, the lack of carbonate, the absence of glaciers and ice sheets (HUBBERTEN et al. 2004; SVENDSEN et al. 2004; VELICHKO et al. 1997) with their grinding processes (SEPPÄLÄ 2004) it is concluded, that the Ice Complex at Duvanny Yar is not primarily of aeolian origin. This contradicts the current concept of pure "Arctic loess" (e.g. PÉWÉ et al. 1983; TORMIRDIARIO and CHYORNEN 1987). It is assumed that the Ice Complex sediments at Duvanny Yar are floodplain sediments. Due to the present vicinity of the Kolyma River, it is likely that sediments were deposited by seasonal flooding by the Kolyma River. So the floodplain was affected by suspension freight, which settles down in e.g. polygon basins progressively. Nevertheless, it is very unlikely that large rivers like the Kolyma with its floods and wide floodplains did not produce any suitable deposits for aeolian transport. Thus, potentially during low water periods of the Kolyma, fine deposits could dry on the lowlands and afterwards the wind could transport this material and could be responsible for the aeolian components in the distribution curves (SEPPÄLÄ 2004). Moreover, nival processes (KUNITSKY et al. 2002) and *in-situ* cryogenic and syndepositional weathering (BERG 1964; SCHWAMBORN et al. 2008) could have played an important role, too. It is also possible that seasonal differentiated deposition occurs. This combination of processes can explain both, the aeolian grain fraction and the low sorting of the studied Ice Complex deposits.

Comparisons with other Ice Complex deposits

Due to the above mentioned complexity of the environment, it is very difficult to appoint a single process for the formation of the Ice Complex. In comparison to other Ice Complex sediments, Duvanny Yar has the lowest gravimetric ice content. The TOC content and the mean grain sizes range in the lower third (Fig. 5-6). The remarkable difference in grain size from Lena Delta sites could be caused by the length of the sediment transportation. At the Lena Delta the probable sediment source region is close to the deposition area (SCHIRRMEISTER et al. 2003). As grain sizes decrease in the direction of transport (REINECK and SINGH 1980) the unknown sediment source area of Duvanny Yar is presumably farther away compared to the sediment source of the Lena Delta.

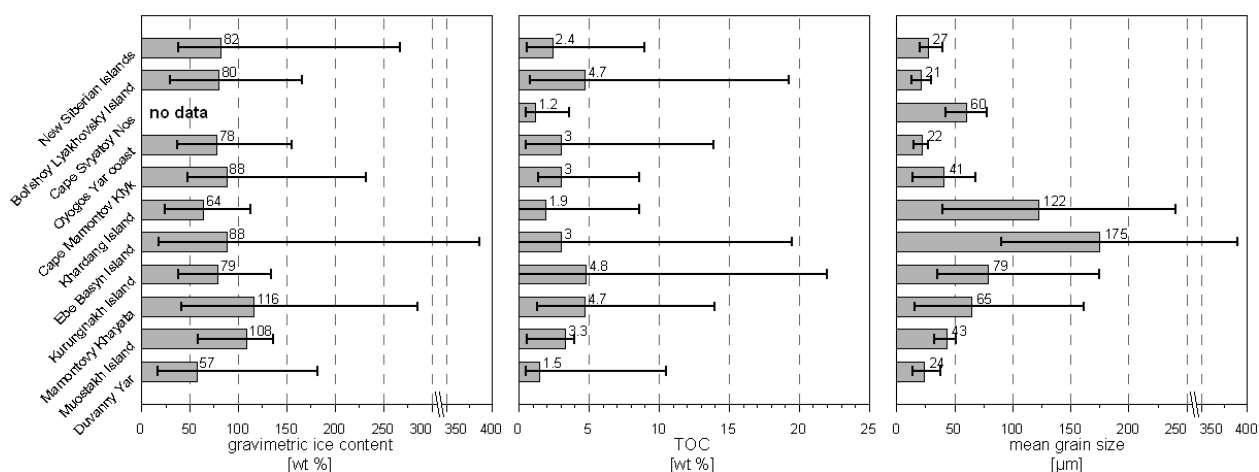


Fig. 5-6: Variations of gravimetric ice content, TOC and mean grain size of different Ice Complex studies. The arithmetic means are illustrated by the values; the range is shown by the bars. This study is illustrated below, the other values are taken from SCHIRRMESTER et al. (2003, 2008a, b, 2009, in review). A map of the mentioned sections is published in SCHIRRMESTER et al. (2008b)

5.3.3 Alas

Alas deposits within a thermokarst depression are of specific and different thermo-erosional characteristics. Thus, banded, lenticular and reticular cryostructures in the lower sample (Fig. 5-3) show a mixture of syn- and epigenetic freezing. This could be caused by an episode of thawing and subsidence followed by epigenetic freezing. The massive frozen part is evidence for epigenetic freezing. The following alternations between reticular and lenticular cryostructures are also an indication for thawing and epigenetic freezing. In the upper part horizontal ice bands and lenticular cryostructures indicate stable and syngenetic freezing conditions.

The magnetic susceptibility values range between 38 and 63 SI without any significant trend. Due to peat inclusions the second and third highest samples at 7.5 and 7.7 m a.r.l. have minimal magnetic susceptibilities. The TOC content shows an increasing trend from the bottom to the top, ranging from 2 to 40 wt % at the uppermost sample. This extremely high content is normal for a litter horizon in the active layer. The samples below have a recent root penetration and so they are increased in TOC as well. The TOC/TN ratio shows a similar pattern like the TOC content. Following WALTHERT et al. (2004), the mineralisation of the organic matter is low to moderate. Due to the increasing and less decomposed organic matter content, the gravimetric ice contents increase with height as well. The $\delta^{13}\text{C}$ values of -31.4 to -27.2 ‰ (mean isotopic composition -29.4 ‰) form the most negative cluster for Duvanny Yar. Integrated with increased TOC/TN ratios, the alternating $\delta^{13}\text{C}$ values show fresh water and subaerial terrestrial environments as well as changes to C_3 land plant associations. At the uppermost vegetation cover sample the C_3 plant association dominance is well defined (Fig. 5-4). In an alas basin the variation in $\delta^{13}\text{C}$ can be explained by wet and dry stadiums (Fig. 2-8) and the resulting succession of different plant associations. All alas samples are very poorly sorted (2.6 to 4.6). The grain sizes of sediment samples range between 20 to 33 vol % for clay, 64 to 76 vol % for silt and 3 to 12 vol % for sand. However, the percentages of different grain size fractions show

two distinct features. Firstly, there is no sand fraction at 4.7 m a.r.l. and the sample directly below is enriched in the coarse silt and fine sand (18 vol %) fraction. This phenomenon can be explained by a progressive splitting of the grain size fractions as a result of a different settling velocity during water ponding deposition conditions. The second distinct grain size feature occurs at the uppermost sample within the Holocene litter horizon. Here, the maximum in the sand fraction (24 vol %) can be explained by moss vegetation functioning as a sediment trap similar to the uppermost sample in the Ice Complex profile.

In terms of grain size distributions the alas profile is less homogeneous compared to other profiles at Duvanny Yar. The grain size distribution curves range from unimodal (4.7 m a.r.l.) over different groups of bimodal curves (5.3 and 5.7, 6.9 and 7.2 m a.r.l.) to trimodal curves (6.1, 6.5, 7.7 m a.r.l.) and the multimodal distribution curve at the uppermost sample. This variety of distributions can be explained by the fact, that some grain size curves with similar characteristics to Ice Complex sediments could be more or less unaltered remnants of these, whereas other samples could be altered by degradation processes and became similar to lake deposits. The Ice Complex-like deposits have a middle silt depletion, whereas the lake-like deposits show a not well defined distinction between the first two main peaks. Thus, it becomes evident that thermokarst processes resulted in the inversion of the relief, masking the initial geomorphic conditions (KONISHCHEV 1987).

5.4 Organic carbon content calculation

The calculation of the organic carbon content is limited to the Ice Complex deposits and the alas profile, because only for these sufficient measurements of the ice content are available.

The major part of the Ice Complex deposits is homogeneous. The values scatter little around the mean value of $\sim 14 \text{ kg TOC} \cdot \text{m}^{-3}$ for the organic carbon content. These little differences are caused by differences in the absolute ice content. As expected, the lower paleocryosol sequence at the Ice Complex (1.3 up to 6.8 m a.r.l. at DY-05) is characterised by an alternating bulk density and generally high alternating organic carbon contents (between 6 and 37 $\text{kg TOC} \cdot \text{m}^{-3}$, mean value of 19 $\text{kg TOC} \cdot \text{m}^{-3}$). Between 28.5 and 29.1 m a.r.l. (at DY-01) the paleocryosol samples shows similar characteristics. Its peat inclusions and the high ice content caused a minimum in bulk density, but a peak in the organic carbon (63 $\text{kg TOC} \cdot \text{m}^{-3}$). Due to Holocene vegetation, the uppermost Ice Complex sample is increased in organic carbon content (292 $\text{kg TOC} \cdot \text{m}^{-3}$).

The decreasing trend in bulk density from bottom to top found at the alas deposits is caused by decreasing mineral densities and increasing ice contents. The alas deposits show the highest values of organic carbon content (54 $\text{kg TOC} \cdot \text{m}^{-3}$). This is most likely caused by the age of the geomorphologic feature alas. It is a degradation of the Ice Complex deposits and is the youngest geomorphologic feature at Duvanny Yar. Thus, the decomposition of organic matter is not progressed as far as at the Ice Complex deposits. More-

over, Holocene mixing during surface subsidence could have brought less mineralised organic matter in deeper parts of the profile.

Comparison of the organic carbon content with other Ice Complex studies

Due to the occurrence of paleocryosol sequences, the organic carbon content of the Ice Complex shows a wide range between 5 and 68 kg TOC · m⁻³ related to the bulk density. Nevertheless, the Ice Complex deposits has a large amount of organic carbon with a mean of $\sim 14 \pm 9$ kg TOC · m⁻³ and form a massive carbon reservoir. Applying broad upscaling, ZIMOV et al. (2006b) estimated the organic carbon reservoir in frozen Ice Complex to be ~ 500 Gt. The assumed parameters for this calculation were a distribution of Ice Complex over 1 million km² (following Fig. 2-9), an average Ice Complex thickness of 25 m, an average TOC content of 2.6 wt %, a bulk density of 1.65 t · m⁻³ and an ice wedge content of 50%. If one applies the average values of 1 t · m⁻³ for bulk density and 1.9 wt % for TOC content, which are measured in this study and apart from that uses the same set of parameters, a carbon reservoir of ~ 240 Gt can be calculated. However, these large scale extrapolations must be handled with care, because of great uncertainties of e.g. Yedoma hill remnants distribution or Ice Complex depth.

5.5 Climatic information from ground ice

5.5.1 Ice wedges

Ice wedges in periglacial landscapes are one of the most promising archives for paleoclimate reconstructions. The repeated frost cracking and melt water freezing induces vertically-foliated ice wedges. Syngenetic ice wedges are direct indicators of a past existence of permafrost with mean annual air temperatures not exceeding -6 °C (VASIL'CHUK and VASIL'CHUK 1997).

The ice wedge in the Eemian lake deposits DY-02 was both, epi- and syngenetically formed and most likely of Weichselian age. Its mean isotopic composition is -28.6 ‰ for $\delta^{18}\text{O}$ and -225.4 ‰ $\delta^2\text{H}$. The heaviest values could have been affected by exchange processes with the surrounding texture ice, because their values are very different from the main cluster and were located at the edge of the ice wedge. The low isotope values in relation to recent fresh water (summer precipitation as fog and rain: $\delta^{18}\text{O}$: -15.9 ‰; $\delta^2\text{H}$: -123.3 ‰) indicate a significant colder temperatures during the ice wedge formation. However, it has to be taken into account that the precipitation samples were taken in summer (August 2008), whilst the source for wedge ice is winter precipitation, which has a lower isotope ratio due to lower temperatures (seasonal effect). Therefore, isotope measurements of winter precipitation are necessary to compare isotopic values for ice wedges and precipitation accurately. At the Dmitry Laptev Strait on Bol'shoy Lyakhovsky Island (~ 825 km distance to the study site) MEYER et al. (2002b) measured winter precipitation in snow patches. The mean isotopic values were -26.3 ‰ for $\delta^{18}\text{O}$ and -199 ‰ for $\delta^2\text{H}$. VASIL'CHUK and VASIL'CHUK (2008b) described a range from -27 to -24 ‰ for $\delta^{18}\text{O}$ in recent ice wedges of the Kolyma Lowland, which supports the validity and the transferability of the

winter precipitation data from Bol'shoy Lyakhovsky Island to Duvanny Yar. Compared to this, the ice wedge isotopic ratios of DY-02 show colder temperatures. The difference in $\delta^{18}\text{O}$ values compared to recent winter precipitation on Bol'shoy Lyakhovsky Island is about 2.5 ‰. If drawing on the attempt to relate the $\delta^{18}\text{O}$ range to absolute temperatures made by VASIL'CHUK (1992) and NIKOLAYEV and MIKHALEV (1995), the available ice wedge data indicates a mean winter temperatures temperature of ~ 2 to 3 °C lower than today. The d excess of this ice wedge has a small range between 1.3 and 4.3 ‰. Due to the missing reference for winter precipitation data at Duvanny Yar, it is not possible to draw solid conclusions on the precipitation source of the ice wedge water. However, it is safe to say that the main source of winter precipitation must have been constant during ice vein formation or in the case of two or more different sources that their relative amount must have been constant. Low d excess values in ice wedges were also reported by MEYER et al. (2002a, b) for the Laptev Sea region. Such values could be caused by diverse conditions. However, kinetic fractionation due to sublimation/evaporation effects before and during the melting and percolation of melt water through the snow pack might have contributed to the d excess shift to relatively low values (DEREVIAGIN et al. 2002). Moreover, a moisture source with a lower humidity and/or high sea surface temperature could have caused a low d excess. Generally, moisture originating from the Pacific Ocean has a lower d excess with values of ~ 3 to 7 ‰ compared to Atlantic Ocean moisture (CLARK and FRITZ 1997). As illustrated in Fig. 5-7, a Pacific moisture source scenario during the Late Glacial Maximum is considered to be possible. Additionally to the low d excess, all samples of this ice wedge are linear correlated in the $\delta^2\text{H}$ - $\delta^{18}\text{O}$ diagram (Fig. 4-6) with a slope of 7.2 and an intercept of -20 ($R^2 = 0.996$). Consequently, fractionation during ice wedge freezing is unlikely. Having a neutral pH (7.31) and a low electrical conductivity ($83 \mu\text{S} \cdot \text{cm}^{-1}$), the hydrochemical results reflect no obvious chemical alteration.

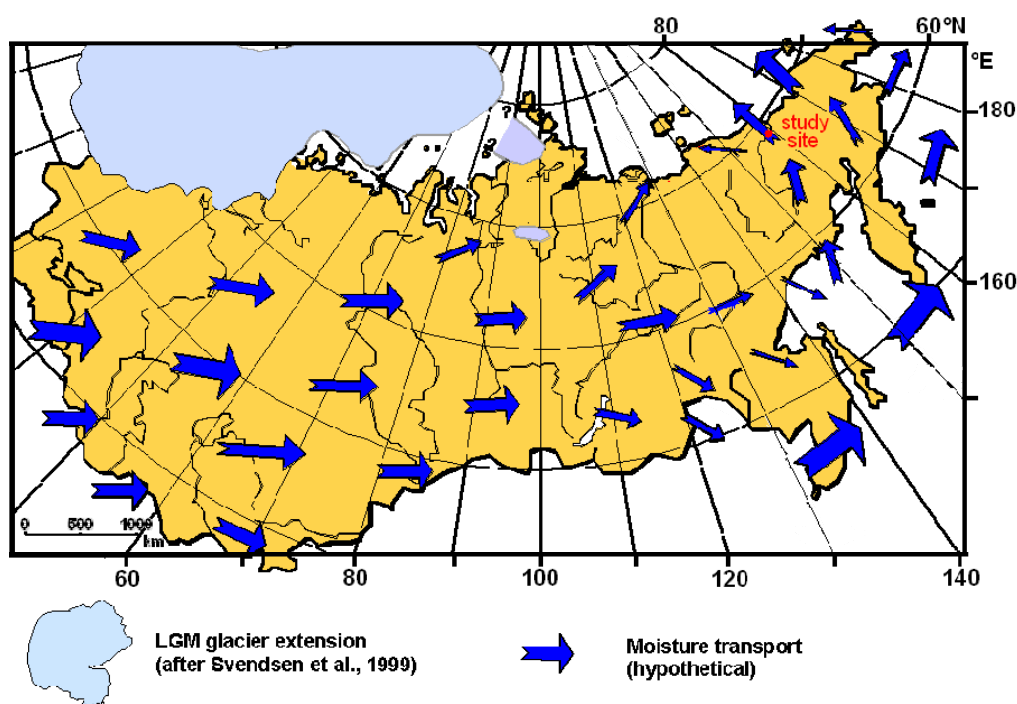


Fig. 5-7: Supposed moisture transport in Eurasia during the Late Glacial Maximum (LGM), drawn by H. MEYER, unpublished, on the basis of KUZNETSOVA (1998).

The lowermost ice wedge of the Ice Complex (DY-05-A-100) shows more negative isotopic values than DY-02. Its mean values are -30.6 ‰ for $\delta^{18}\text{O}$ and 236.9 ‰ for $\delta^2\text{H}$. Therefore, the winter temperatures during the formation of this ice wedge must have been colder than during the formation of the ice wedge in DY-02 and today. At DY-05-A-100 the d excess (mean 7.9 ‰, range 6.1 to 9.9 ‰) is the highest for all ice wedges, which suggests a greater influence of Atlantic moisture on the precipitation origin (Fig. 5-7). The most negative isotopic composition of all ice wedges in this study is measured for the ice wedge DY-05-F-300. Its mean isotopic composition is -33.9 for $\delta^{18}\text{O}$ and 267.2 for $\delta^2\text{H}$. Consequently, the winter precipitation during the formation of DY-05-F-300 must have been the coldest. The wide range in d excess (-0.2 ‰ to 11.4 ‰; standard deviation: 4.4) indicates a complex structure in this ice wedge. Due to the edge position of one outlier (11.4 ‰), an isotopically alteration for this sample cannot be ruled out.

The isotopic composition of the ice wedge DY-01-D-400, which was located in the upper part of the Ice Complex, lies close to the GMWL (mean d excess: 5.5 ‰). Its mean isotopic values are -32.3 ‰ for $\delta^{18}\text{O}$ and -253.2 ‰ for $\delta^2\text{H}$. The heavier composition as compared to the ice wedge at 15 m a.r.l. reflects a warming in the winter temperature. The uppermost and at the same time widest ice wedge sampled from the Ice Complex was DY-01-A-100. It is characterised by a narrow range in isotopic composition with mean values of -31.5 ‰ for $\delta^{18}\text{O}$, -248.5 for $\delta^2\text{H}$ and d excess of 3.3 ‰. The slope is 8.1 and shows a parallel course to the GMWL (Fig. 4-29). As discussed for other samples with low d excess (DY-02, ice wedge DY-05-F-300, both ice wedges in DY-01), it is assumed that a lower d excess value represents a greater contribution of Pacific moisture. According to VASIL'CHUK (1992) and NIKOLAYEV and MIKHALEV (1995), the ice wedges at the Ice Complex were formed when mean winter temperatures were ~ 4 to 8 °C colder than the recent winter temperatures measured at Bol'shoy Lyakhovsky Island (MEYER et al. 2002b) and for recent ice wedges of the Kolyma Lowland (VASIL'CHUK et al. 2008b).

5.5.2 Fissure ice and texture ice

The ice samples of uncertain origin are called fissure ice. The reason for this uncertainty is the limited number of samples for each fissure ice vein and the remarkable high d excess. The sample DY-05-B-200, which was at 5.7 m a.r.l. (0.7 m wide), has a d excess of 14.1 ‰. A similar phenomenon occurs in the upper part of the Ice Complex at several small fissure ice samples, which were 0.03 to 0.80 m wide (DY-01-H-900, H-800 (Fig. 4-28 A), G-700, D-500, D-300 and DY-01-B-200). At these sites the d excess is even higher (15.1 to 30.4 ‰). Due to their small width, the composition of ice veins (1 to 10 mm) and thin sediment veins (1 to 2 mm) it is possible that the fissure ice samples are extremely altered by exchange processes. MEYER et al. (in review) assumed an exchange rate between an ice wedge and surrounding sediments of about 10 to 15 centimetre per $10\,000$ years. Accordingly, the fissure ice samples, considered as narrow ice wedges, would have been completely affected by exchange processes. However, also other factors could have influenced the high d excesses. As discussed above the d excess is influenced by primary

evaporation from the ocean surface. A very low humidity at the location of moisture origin could have produced such a high d excess (Fig. 5-8). Some parts of the moisture could also be of secondary origin, which means that the precipitation is evaporated from terrestrial waters in the region. Moreover, processes within the snow must be taken into account when studying ground ice formation. These processes are sublimation, melting and refreezing of the melt water.

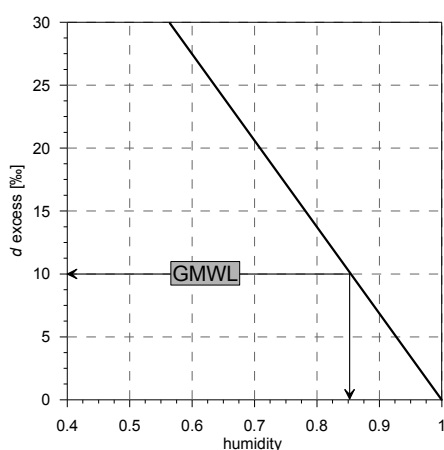


Fig. 5-8: The d excess parameter as a function of humidity during kinetic evaporation from the ocean surface; in CLARK and FRITZ (1997), modified.

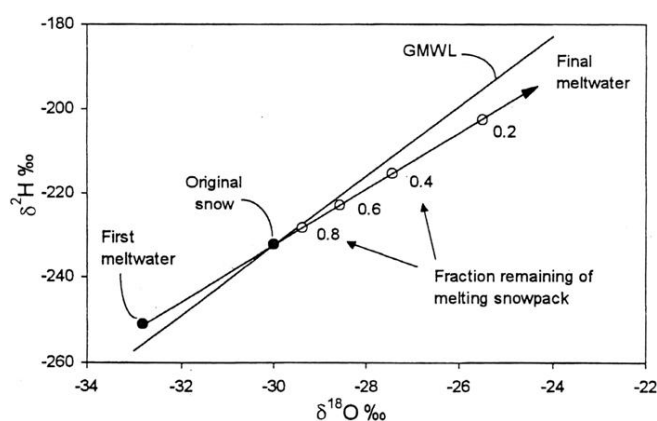


Fig. 5-9: Evolution of melt water draining from base of snowpack, based on complete equilibrium between the water and the snowpack; in CLARK and FRITZ (1997).

The usually thin snow cover at Duvanny Yar at winter is susceptible for sublimation or vapour exchange and therewith for fractionation processes. Fractionation freezing influences the d excess when the freezing velocity is lower than $2 \text{ mm} \cdot \text{h}^{-1}$ (VAIKMÄE 1991). Melt water from different stages of snow melt exhibits different isotope signatures due to progressive isotopic fractionation. Initial melt water shows more negative $\delta^{18}\text{O}$ and higher d excess values than that generated later (Fig. 5-9; CLARK and FRITZ 1997; LAURIOL et al. 1995). Thus, the fissure ice could be strongly affected by initial melt water. As shown in the $\delta^2\text{H}$ - $\delta^{18}\text{O}$ diagrams (Fig. 4-19 A and Fig. 4-29 A), the isotopic signal is similar to the texture ice and the high d excess could indicate not only exchange processes with the surrounding sediment but also the same genetic origin. Furthermore, the hydrochemistry shows a difference between the ice wedges and the fissure ice. At the four ice wedges a mean electrical conductivity of $104 \mu\text{S} \cdot \text{cm}^{-1}$ occurs, whereas the fissure ice has a mean conductivity of $\sim 270 \mu\text{S} \cdot \text{cm}^{-1}$. Especially the two outliers DY-01-G-701 and DY-01-D-500 (650 and $720 \mu\text{S} \cdot \text{cm}^{-1}$, respectively) indicate remarkable high external alterations.

Besides stable isotope signatures of ice wedges, the isotopic composition of texture ice, which is contained in the frozen sediments, can be used as environmental marker. Despite the complexity of influences from water sources, seasonal water mixture and fractionation processes, texture ice can be used to determine environmental and climatic changes (e.g. BURN et al. 1986; SCHWAMBORN et al. 2006; VAIKMÄE 1989). At the DY-02 profile the mean isotopic composition is -16.6 ‰ for $\delta^{18}\text{O}$ and -149.3 ‰ for $\delta^2\text{H}$. This isotopic composition represents the highest values measured at Duvanny Yar and lies within the range of summer precipitation samples which were taken during the expedition. The d excess is remarkably

negative (-25 to -10 ‰). In general, the d excess can be reduced to values lower than 0 ‰ by nonequilibrium fractionations, which appear during subsequent phase changes. At the study site evaporation or slow freezing/melting (Fig. 5-9) are the important fractionation processes. Evaporation, which is likely at warm periods, generally enriches the heavier like the less negative isotopes. This process lowers the d excess significantly. Therefore, the texture ice samples are interpreted as a warm temperature signal. As suggested by the palynological results, this signal is interpreted as Eemian. The linear correlation ($R^2=0.99$) indicate a constant fractionation of the texture ice. An extension of the regression line cuts the GMWL approximately at -24 ‰ for $\delta^{18}\text{O}$ and -180 ‰ for $\delta^2\text{H}$ (Fig. 4-6), which could serve as rough estimate for the original isotopic signal. This isotopic signal is lighter than the recent summer precipitation, but falls within the expected range of isotopic values of winter precipitation measured by MEYER et al. (2002b) for Bol'shoy Lyakhovsky Island.

The isotopic signals from texture ice of the lower Ice Complex shows four different clusters (Fig. 4-19). The three lower clusters lie on an imaginary regression line (1.3 to 21 m a.r.l.), whereas the uppermost cluster is separated. The lowermost cluster (1.3 to 1.8 m a.r.l.) shows the warmest signal. It is possible that these two lowermost samples are affected by intermediate temperatures during the Late Eemian/Weichselian transition. Data for the second lowermost texture ice sample (3.7 to 10.3 m a.r.l.) can be interpreted as a progressive temperature cooling, but it would still represent warm conditions related to the Ice Complex. The following cluster (13.3 to 21 m a.r.l.) is characterised by a high linearity in the $\delta^{18}\text{O}$ - $\delta^2\text{H}$ diagram (R^2 : 0.98, slope 5.5). However, the first impression of this well developed freezing/melting fractionation (Fig. 5-9) is generated by chance, because there is no fractionation-altitude-correlation. This correlation is essential, because the freezing front and its influence on the isotopic composition would correlate with height. In particular, the isotopic values of the texture ice decrease at 13.3 to 17 m a.r.l. to a minimum for Duvanny Yar at -38.45 ($\delta^{18}\text{O}$) and -269.43 ($\delta^2\text{H}$). After that, from 17 to 20.5 m a.r.l., the temperature became warmer and resulted in a plateau at ca. -34 to -32 ‰ ($\delta^{18}\text{O}$). The cluster from 23.5 to 25 m a.r.l. is characterised by an isotopic constancy ($\delta^{18}\text{O}$ between -33.3 ‰ and -32.8 ‰; $\delta^2\text{H}$ between -251.9 ‰ and -245.2 ‰) and a small offset relative to the GMWL (mean d excess 15.1 ‰). A reason for this could be either a lower fractionation during freezing compared to the previous clusters or the effect of a different moisture source. Furthermore, the distinct and stable d excess could also be due to different proportions of winter and summer precipitation. However, the isotopic composition in the major part of the upper Ice Complex ranges between ca. -34 to -32 ‰ ($\delta^{18}\text{O}$) and around -240 ‰ ($\delta^2\text{H}$). Compared to these isotopic signals, a slightly warmer temperature signal could be expected for a sequence between 28 to 31 m a.r.l., which developed ~40000 a BP. This expectation is well supported by the isotopic signal of the sampled ice lens DY-01-F-600 at 28.5 m a.r.l. (Fig. 5-10), which fits well into this texture ice isotopic signal.

The two uppermost texture ice samples of the Ice Complex, which are in or directly below the active layer show heavier values and consequently a warmer temperature signal. The large difference of ~5 ‰ for $\delta^{18}\text{O}$ between these samples occurs within 1 m only. It is caused by Holocene deposition and moisture percola-

tion, fractionalised melting and freezing in the active or transient layer. Despite the fractionation during freezing and melting, the generally high d excess for the texture ice at Ice Complex deposits (mean value ~ 25 ‰) could be influenced by a dry climate at Duvanny Yar during the Ice Complex formation. Therefore, fractionation by secondary evaporation is highly relevant. Nevertheless, according to paleoclimate reconstruction from pollen in VELICHKO et al. (2005), the slight changes in the isotopic composition of the texture ice of the Ice Complex reflects the environmental changes since at least the Middle Weichselian interglacial to the end of the Late Weichselian.

The two uppermost samples of the Ice Complex lead smoothly over into the isotopic signature of the alas ground ice. A similar isotopic composition of the alas ground ice to recent waters gives indication for a genetic connection. The heavy isotope values ($\delta^{18}\text{O}$: -18.5; $\delta^2\text{H}$: -155.62) are a proof for a warmer period. Therefore this isotopic composition is interpreted as a Holocene. The d excess ranges between -10 and -2.2 ‰ and had a mean value of -7.4 ‰. It shows freeze-thaw and evaporation fractionating processes, which are typical for this thermokarst feature. Therefore, the d excess is determined by the evaporation of lake water, which could also be the origin of the texture ice water.

5.5.3 Summarised paleoclimate interpretation

Generally the isotopic values of texture ice, ice wedges and fissure ice reveal a related trend (Fig. 5-10). The isotopic values for texture ice samples are generally very low. A reason could be that all precipitation occurred as snow and/or summer precipitation played no significant role. For this reason, the isotopic signal from the texture ice is interpreted as winter precipitation like the ice wedges.

After the warm Eemian period the winter temperatures cooled-down so that epigenetic ice wedge development in Eemian deposits became possible. Both ice wedges and texture ice have minimal isotopic values at an altitude between ~ 15 to 18 m a.r.l., (Fig. 5-10), which corresponds to a radiocarbon age of ~ 39000 a BP. Therefore, the coldest winter temperatures were reached during this period. Afterwards the temperatures increased and stayed on a similar level until ~ 10000 a BP although they remained colder related to today. There is no evidence for a 'typical' temperature minimum during the Last Glacial Maximum shown in Fig. 5-10. The warming trend between Pleistocene and Holocene is well documented by a sharp increase in $\delta^{18}\text{O}$ and $\delta^2\text{H}$ values in ice wedges. This increase of 13 ‰ for $\delta^{18}\text{O}$ and 75 ‰ for $\delta^2\text{H}$ could be correlated to the warming during the Early Holocene, when the Ice Complex formation at Duvanny Yar ended. This phenomenon is also found at the Laptev Sea coast (MEYER et al. 2002a, b; WETTERICH et al. 2008b). Since the isotopic signatures of the Holocene alas and the Eemian lake deposits are similar, it is suggested that the Eemian times represent a paleoanalogue of the recent warm temperature conditions at Duvanny Yar.

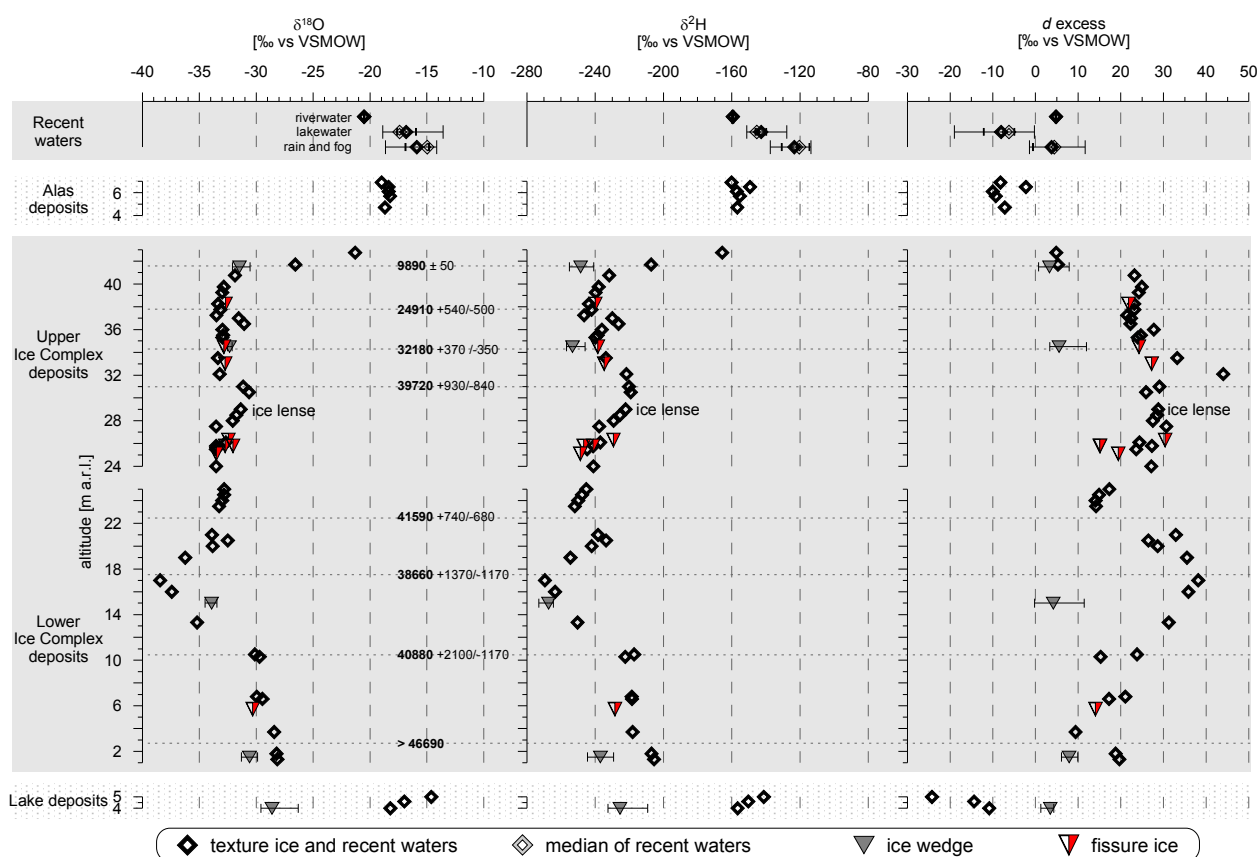


Fig. 5-10: Development of $\delta^{18}\text{O}$, $\delta^2\text{H}$ and d excess of all ground ice samples sorted in a stratigraphic order. For the recent samples and ice wedge samples ranges (outer bars) are plotted. For the recent waters the quartiles Q_1 and Q_3 (small inner bars) are illustrated as well.

5.5.4 Comparisons to other studies

Important controls for polygon diameter and thus ice wedge distance are the mean annual temperature and the amplitude of temperature at the surface. The colder the temperature the smaller is the polygon diameter at the surface (TOMIRDIARO 1982). At Duvanny Yar the polygon diameter at the lower part of the Ice Complex deposits (28 to 30 m below surface level) was ~ 12 m and at the middle part (15 to 17 m below surface level) it was ~ 4 m (VASIL'CHUK et al. 2001). If assumed that the surface level in this and VASIL'CHUK's study is ~ 45 m a.r.l., the coldest temperatures inferred from the polygon diameter are shown at ~ 30 m a.r.l. and the warmest at ~ 15 m a.r.l.. Assuming that the results from VASIL'CHUK et al. (2001) and this study are comparable albeit different measuring times and altitudes, they are contrary, because in this study the lowest temperatures as indicated by the lowest isotopic signal are found between 15 and 18 m a.r.l. (Fig. 5-10).

However, a different sampling strategy has to be taken into account when comparing results from this study with VASIL'CHUK et al. (2001). Despite the peculiar ice wedge growth and a preferable horizontal sampling strategy (e.g. MICHEL 1990), VASIL'CHUK et al. (2001) conducted a vertical sampling strategy for most of the studied ice wedges. The reason for this is that vertical sampling allows a correlation with time and alti-

tude (VASIL'CHUK et al. 1997). Moreover, $\delta^2\text{H}$ measurements and d excess calculations were rarely done by VASIL'CHUK (Fig. 5-11). VASIL'CHUK et al. (2001) measured $\delta^{18}\text{O}$ values ranging from -32.7 to -28.7 ‰ for Ice Complex ice wedges at Duvanny Yar. In comparison to that, the five ice wedges, which were analysed in this study, range from -34.5 to -28.6 ‰ and show lighter $\delta^{18}\text{O}$ values at an altitude of ~15 m a.r.l. (Fig. 5-11). In the upper part of the Ice Complex the isotopic compositions match well. Comparing the d excess measurements of both studies, the d excess is similar. The variations in d excess as described by VASIL'CHUK et al. (2001) did not exceed 3.4 to 8.1 ‰. Therefore, it is evident that the moisture source or its partial composition was constant during Ice Complex formation. Due to a low d excess VASIL'CHUK's data suggests a Pacific moisture source, too (Fig. 5-7).

Recent ice wedges of the Kolyma Lowland varied in terms of $\delta^{18}\text{O}$ between -27 and -24 ‰ (VASIL'CHUK et al. 2008b). Therefore, the mean winter temperatures during the Late Pleistocene Ice Complex formation ($\delta^{18}\text{O}$: -34.5 to -28.6 ‰) were significantly colder compared to recent ice wedges. According to VASIL'CHUK (1992) and NIKOLAYEV and MIKHALEV (1995) the mean winter temperature during Late Pleistocene ice wedges formation was ~4 to 8 °C colder compared to conditions during recent ice wedge development.

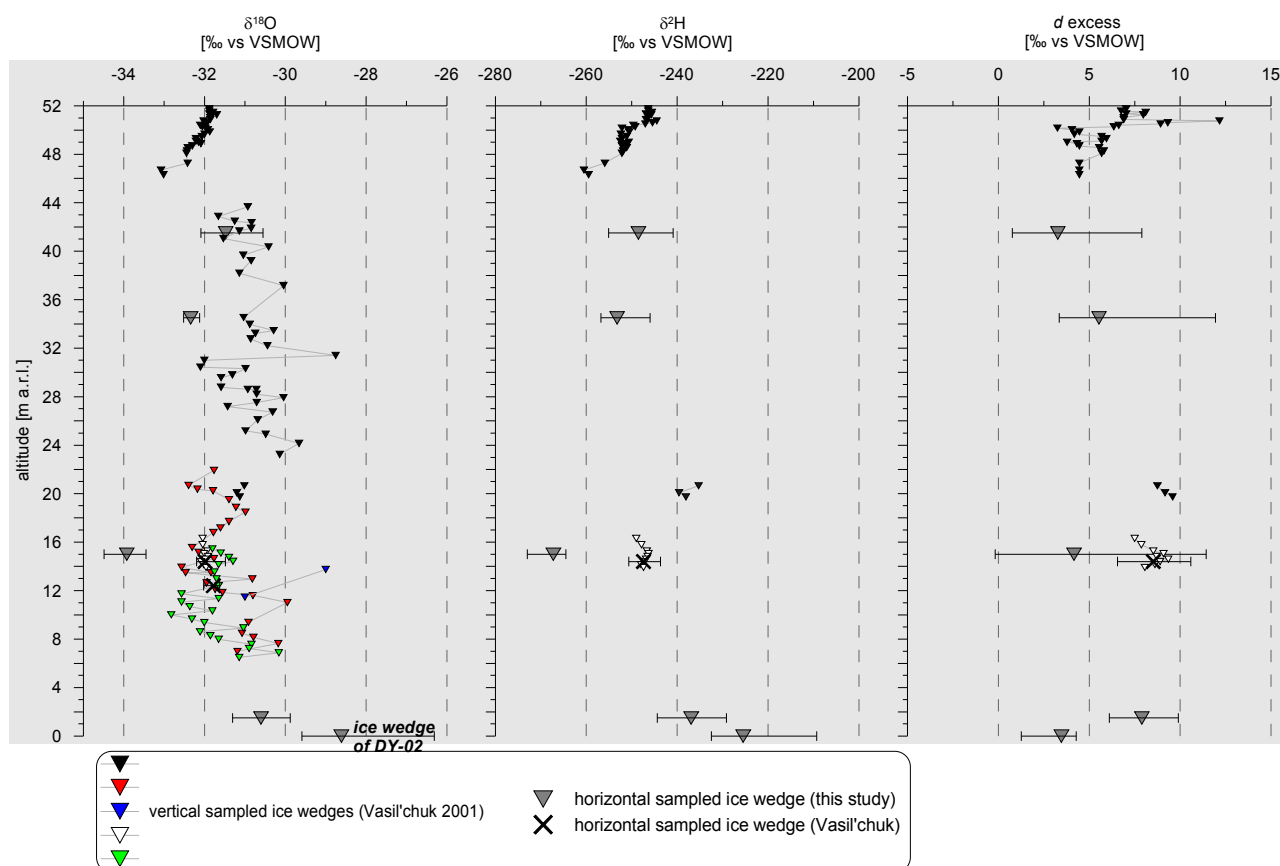


Fig. 5-11: Comparison of the isotopic composition of different ice wedges at Duvanny Yar. The data was digitalised from VASIL'CHUK et al. (2001). The lowermost ice wedge is the Late Pleistocene epigenetic ice wedge in the Eemian Lake deposits.

D.V. MICHIKAELEVA (in VASIL'CHUK 1992) measured the isotopic composition of texture ice. As shown in Fig. 5-12 the data from the different studies are divergent in their isotopic signature at the bottom. This is possibly caused by a different sample location, where deposits are exposed on a different level. So, the temperature minimum indicated by this study at an altitude of 13 to 19 m a.r.l. is not reflected by any other study. The similarities are the occurrence of the heaviest isotope ratios in the part below 12 m a.r.l. (except from the Holocene top above ~40 m a.r.l.). Moreover, the isotope ratios of all studies match well in the upper part (>22 m a.r.l.). Moreover, there is an agreement in isotope compositions in the alas deposits since the mean value for this study is -18.5 ‰ and VASIL'CHUK describes a isotopic range in alas deposits between -23.0 and -19.1 ‰ for the Kolyma Lowland.

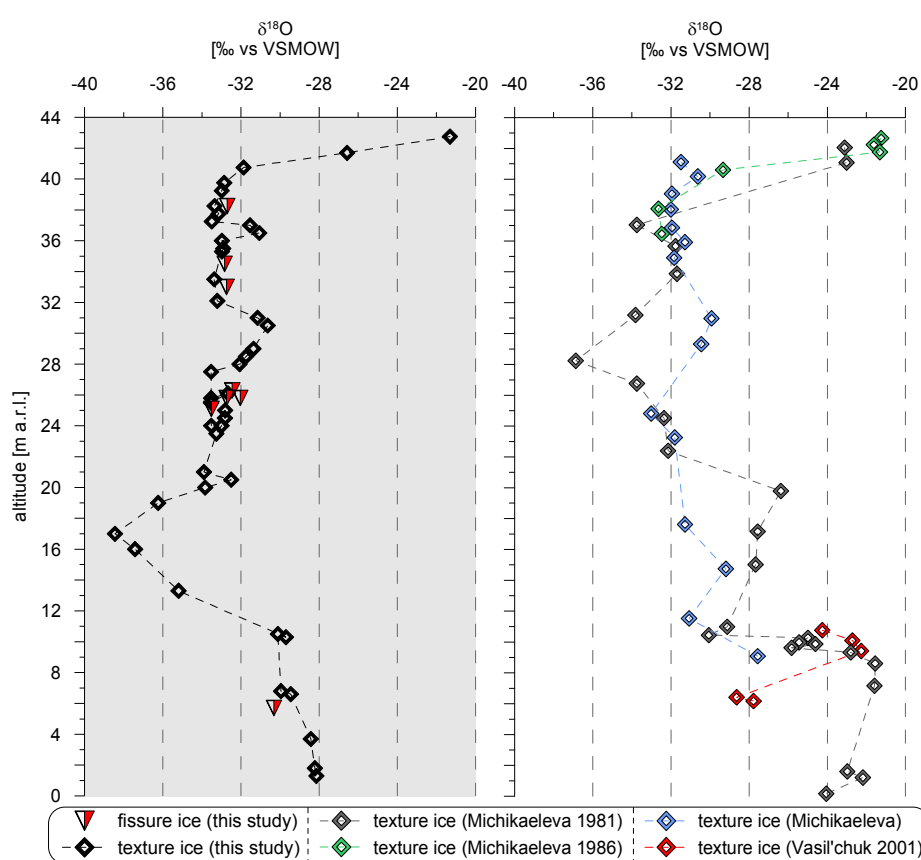


Fig. 5-12: Comparison of the oxygen isotope composition of texture ice at Duvanny Yar. The data from MICHIKAELEVA, sampled between 1981 and 1986, was summarised in VASIL'CHUK (1992). The altitude correlation is questionable, because the exact position of the studies from MICHIKAELEVA and VASIL'CHUK are unknown.

Another ice wedge isotope study was done at Bol'shoy Lyakhovsky Island, which is 825 km off from Duvanny Yar (MEYER et al. 2002b). Unlike sediment parameters, which are mostly controlled by local factors, the isotopic composition of ice wedges is determined by precipitation, which is an integrative regional signal. So this broader scale comparison is valid.

MEYER et al.(2002b) analysed eight ice wedges in Ice Complex deposits from Bol'shoy Lyakhovsky Island. Their mean $\delta^{18}\text{O}$ and $\delta^2\text{H}$ values ranged from -32.5 ‰ to -28.5 ‰ and from -247.9 ‰ to -220.1 ‰, respectively. The mean d excess was between 5 and 10.3 ‰. As shown in e.g. Fig. 5-11 the mean $\delta^{18}\text{O}$ and $\delta^2\text{H}$ values of Duvanny Yar range from -33.9 to -28.6 ‰ and -267.2 to -225.4 ‰, respectively. The d excess is between 3.5 and 7.9 ‰ and slightly lower compared to Bol'shoy Lyakhovsky

Island. The similar ranges between both studies are remarkable. Therefore, it is assumed that there was a similar cold and continental paleoclimate during the deposition of the Ice Complex deposits at both sites. Due to the low d excess, MEYER et al.(2002b) suggested a Pacific influence of the precipitation, which is suggested for Duvanny Yar, too.

If comparing the isotopic data of this study with Greenland ice core records (e.g. DANSGAARD et al. 1993) significant differences become obvious. On the basis of their ice wedge studies at Duvanny Yar, VASIL'CHUK and VASIL'CHUK (2008b) suggested for the $\delta^{18}\text{O}$ oscillations measured at 24 to 44 m a.r.l. (Fig. 5-11) two Dansgaard-Oeschger events as reason for the sudden and pronounced isotope shifts. It could be possible, that two little isotopic peaks of this study, which occur in the isotopic composition of the texture ice at ~30 m a.r.l. (approximately 39720 a BP) and at ~37 m a.r.l. (approximately 25000 a BP) are caused by Dansgaard-Oeschger events, but this interpretation is highly speculative. It is more likely, that the little peak in heavier isotopes is the result from the Middle Weichselian warm interstadial (e.g. SHER et al. 2005).

5.6 Synthesis of the Late Quaternary environmental dynamics at Duvanny Yar

Eemian interglacial

At the Eemian interglacial the winter temperature has been ~2 °C warmer than today and it is described as the paleoanalogue of the recent climate warming (VELICHKO et al. 2005). This warmer climate conditions are supported by the isotopic signature of texture ice measured at this study (Table 5-2). Based on pollen records, GRISHUK (1982) suggested mean annual temperatures of the Indigirka-Kolyma Lowlands of approximately -5 °C. ANDREEV (pers. com.) and VELICHKO and NECHAEV (2005) characterise the vegetation as wooded with *Larix-Betula* (birch) forests of the north taiga type. In particular spruce, larch and pine trees/shrubs were present. The sediment analysis suggests little streaming conditions initially, which were possibly due to flooding events and changed to boggy and stagnant water conditions later.

Eemian/Weichselian transition

In this study the Eemian/Weichselian transition period comprised a lake sediment sequence. The pollen spectra indicate a cooling climate (ANDREEV, pers. com.) and the grain size distribution shows a change from little streaming conditions to stagnant water conditions and back to streaming conditions. Some grain size characteristics are similar to the Weichselian Ice Complex deposits.

Weichselian glaciation

In regard to the reconstruction of Late Quaternary environmental dynamics at the Duvanny Yar site it is of great importance, that the shoreline was located near the shelf margin about 500 km north of the present coastline (ROMANOVSKII et al. 1998) as it was the case during the Last Glacial Maximum, which amplified the continentality of the climate.

A paleocryosol sequence as well as high TOC contents, which imply a high bioproductivity, is suggesting advanced living conditions at Duvanny Yar during the first stage of the Weichselian Ice Complex deposition. However, during the whole period of Ice Complex deposition very low winter temperatures prevailed as indicated by stable isotope values of ice wedges and texture ice. The palynological spectra of the Ice Complex described by SHER et al. (1979) showed a predominance of grass pollen. This spectra reflects a treeless tundra-steppe landscape, which combines both, tundra and steppe characteristics (HOPKINS 1982). This paleoecosystem is termed Mammoth steppe, too. Bones that were found during the expedition in 2008 were fragments of tooth and jaws of *Bison priscus* (steppe bison), *Coelodonta antiquitatis* (woolly rhino), *Equus* sp. (horse), *Mammuthus primigenius* (woolly mammoth) and *Rangifer tarandus* (caribou). The taxonomic composition of this bones is typical of the 'mammoth fauna' in East Siberia (ANDREEV et al. 2009). Moreover, the presence of these mammals are an indication for open landscapes with rich herbaceous covering (SHER et al. 1979). Generally the existence of an Ice Complex is a proof for a dry climate without glaciation and only a thin snow cover during the winter. Moreover, it gives evidence for the persistence of stable, poorly drained, low topographic-gradient accumulation plains (TOMIRDIARO 1982). The large and deep ice wedges indicate harsh winter temperatures. Following VASIL'CHUK (1992) and NIKOLAYEV and MIKHALEV (1995) the isotope composition of ice wedges and texture ice suggest ~ 4 to 8 °C lower winter temperatures compared to recent winter temperatures. As implied by the polymodal but remarkable homogenous grain size distribution, the different and long-term transport processes (alluvial, aeolian, *in-situ* frost weathering, nival processes) seem to play a crucial role in the accumulation of the Ice Complex. These processes were constant over the entire Ice Complex formation period, which ended ~ 10000 a BP.

Holocene

The Pleistocene/Holocene transition was characterised by a rise in temperatures across Northeastern Siberia (ANDREEV et al. 2009; SCHIRRMESTER et al. 2002a, b; WETTERICH et al. 2009). Due to the warming trend during the early Holocene, the landscapes were reorganised by the degradation of ice-rich permafrost sequences, in particular thermokarst and thermo-erosional processes. The isotope signal reflects this dramatic change with a sharp increase towards heavy isotopes in the texture ice. High organic matter content and peaty soil formation indicate an increased bioproductivity. SHER et al. (1979) describes an increasing thermo-erosion and alas development since 9200 ± 150 a BP. This age determination matches well with the youngest date at the Ice Complex. The grain size distributions document the genetic connection of alas with both lake and Ice Complex deposits. This illustrates hydrological reorganisation features like lake formation. Moreover, the landscape developed towards the modern polygonal tundra. With respect to climatic conditions, the measured isotope compositions of texture ice in alas deposits confirm the Holocene as a period of relatively small temperature oscillations, which is also observed from Greenland ice cores. (e.g. DANSGAARD et al. 1993).

Table 5-2: Synthesis of stratigraphy, facies interpretation and sedimentological, cryolithological and stable water isotope features.

Period (Unit/facies)	Sedimentological and cryolithological features	Stable water isotopes	Environmental conditions
Holocene (<i>alas and lake deposits</i>)	<ul style="list-style-type: none"> • banded, lenticular and reticular cryostructures → mixture of syn- and epigenetic freezing; • peat inclusions; • wet and dry stadiums 	texture ice $\delta^{18}\text{O}$: 18.9 to -18.2 ‰ $\delta^2\text{H}$: -160.1 to -149.2 ‰ mean <i>d</i> excess: -7.4 ‰	<ul style="list-style-type: none"> • relatively warm climate; • increasing thermokarst development • thaw lake formation; • modern polygonal tundra conditions
Weichselian (<i>Ice Complex</i>)	<ul style="list-style-type: none"> • lenticular and layered cryostructures → syngenetic freezing; • ice-rich (gravimetric ice content 17 to 182 wt %); • paleocryosol sequences; • homogeneous sediments especially in grain size; • floodplain sediments influenced by other processes like wind retransport 	ice wedges $\delta^{18}\text{O}$: -33.9 to -28.6 ‰ $\delta^2\text{H}$: -267.2 to -225.4 ‰ mean <i>d</i> excess: 4.9 ‰ texture ice $\delta^{18}\text{O}$: -38.5 to -28.1 ‰ $\delta^2\text{H}$: -269.4 to -205.5 ‰ mean <i>d</i> excess: -24.1 ‰	<ul style="list-style-type: none"> • stable cold and dry climate, harsh winters; • ice wedge growth • low sea level → amplified continentality; • mean winter temperature ~4 to 8 °C lower than today; • mammoth-steppe, large herbivores
Eemian/ Weichselian transition (<i>lake deposits</i>)	<ul style="list-style-type: none"> • massive cryostructure → epigenetic freezing; • stagnant waters to little streaming water 		<ul style="list-style-type: none"> • climate cooling; • lakes and boggy wetlands
Eemian (<i>lake deposits</i>)	<ul style="list-style-type: none"> • reticular to layered cryostructure → change from epi- to syngenetic freezing; • increasing organic matter accumulation; • slow flowing water and siltation 	texture ice $\delta^{18}\text{O}$: -18.2 to -14.6 ‰ $\delta^2\text{H}$: -156.5 to -141.2 ‰ mean <i>d</i> excess: -16.5 ‰	<ul style="list-style-type: none"> • ~1 to 2 °C warmer than today; • woody vegetation

6 Conclusions and outlook

The aim of this study was to investigate the environmental dynamics at the Duvanny Yar section during the Late Quaternary. It was attempted to answer questions regarding the history of sediment deposition and the assessment of the climatic history as well as to make small and large scale comparisons with already available paleoclimate data (chapter 1.2).

The **history of sediment deposition in the Late Quaternary** was characterised by changing facies. During the Eemian and Eemian/Weichselian transition times, lake, little streaming and boggy wetland conditions prevailed. The paleogeography was similar to recent times and woody vegetation was dominant. During the Weichselian glaciation the Ice Complex was likely to be deposited by a constant proportion of alluvial, aeolian and *in-situ* frost weathering processes. Moreover, the formation of polygonal ice wedge systems and continuous sequences of ice-rich deposits was closely related to the persistence of stable, poorly drained and flat accumulation plains of the Kolyma floodplain. The accumulation of Ice Complex sequences was promoted by the absence of large glaciers and ice sheets. These stable transportation, deposition and environmental conditions become evident by remarkable homogeneous sediments. Consequently a significant internal lithostratigraphy of the Ice Complex deposits was not pronounced. Some paleocryosol samples indicated periods of increased bioproductivity. At the end of the Late Quaternary towards the Holocene sedimentation regimes, the periglacial paleolandscape of Duvanny Yar changed from an alluvial and aeolian influenced to a thermokarst affected landscape. Thus the landscape evolution at Duvanny Yar became determined by degradation of permafrost and surface subsidence. The resulting alas depressions were characterised by a variability of processes of sediment deposition, which is expressed in less homogeneous grain size distributions. However, the genetic connection to the Ice Complex and the influence of lake deposits was still apparent.

The **climatic history since Late Quaternary times** was assessed on the basis of the isotopic compositions of ice wedge, fissure ice and texture ice. The ice wedge, fissure ice and texture ice isotope values reveal an according trend. Generally, texture ice showed a very light isotopic composition. Therefore, it is likely that the main or single water source for texture ice was winter precipitation. Consequently conclusions on climatic trends could only be drawn on winter temperatures. In Eemian times the winter temperature was 1 to 2 °C warmer than today. Afterwards, during Weichselian times the winter temperature cooled down to a highly continental and harsh winter climate. The minimum of winter temperature was reached around ~39000 a BP. The stable climatic conditions during the Weichselian cold climate were reflected in the homogeneous sedimentation pattern which leads to highly homogeneous sediments. During the Holocene the winter temperatures increased to recent levels.

Small-scale comparisons were made to other studies at Duvanny Yar (e.g. VASIL'CHUK et al. 2001). The winter temperature inferred from isotopic compositions from these studies show slight differences. However, due to different expedition times and different measurement techniques this should

not be overrated. Furthermore, also larger- scale comparisons between the isotopic signature of the Ice Complex and isotopic results from the Dmitry Laptev Strait confirm the predominance of similar climatic conditions in both regions. In comparison to other Ice Complex studies, a young age (9890 ± 50 a BP) was determined for the end of the Ice Complex formation. **Large-scale comparisons** with Greenland ice cores showed that the local paleoclimate signal did not correspond with a temperature minimum during the Last Glacial Maximum in western Eurasia and the occurrence of short temperature oscillations like Dansgaard-Oeschger events are uncertain. Generally, the Late Quaternary reconstruction of Duvanny Yar fitted into the climatic context of Northeast Siberia and the Northern Hemisphere.

Although it is already possible to draw a fairly good picture on the paleoenvironment in Northern Siberia, further investigations like pollen analyses would give more detailed information about summer temperatures and would improve our understanding of the paleoenvironment at Duvanny Yar. Therefore, a selection of the sediment samples from this study will be analysed for *Rhizopoda* species. Akin to palynological studies, *Rhizopoda* can be used as an indicator for hydrological and temperature regimes (e.g. BOBROV et al. 2003). Furthermore age determinations will verify periods of important paleoenvironmental changes. Therefore Optically Stimulated Luminescence (OSL) dating of sediments and $^{36}\text{Cl}/^{10}\text{Be}$ dating of ice wedges are in progress and additional radiocarbon dating is planned. A statistical approach for more detailed grain size analyses like end-member modelling (e.g. WELTJE 1997) could help to separate specific single sedimentation processes which participate in Ice Complex formation. Moreover, further analyses on the carbon content, as they were initiated by carbon content calculations in this study, could describe the fate of organic matter in past times in more detail. This would be highly relevant because organic matter can be converted into greenhouse gases and a more detailed characterisation and quantification of organic matter would help to predict future changes against the background of a warming Arctic.

References

- ACIA (2004). Impacts of a Warming Arctic - Arctic Climate Impact Assessment: 144 pp.
- Ad-hoc-Arbeitsgruppe-Boden (2004). Bodenkundliche Kartieranleitung. Hannover, Schweizerbart, 422 pp. (in German).
- Ahlenius, H. (2007). Permafrost extent in the Northern Hemisphere. In: Global Outlook for Ice and Snow - Chapter 7. Romanovsky, V. E., Gruber, S., Instanes, A., Jin, H., Marchenko, S. S., Smith, S. L., Trombotto, D. and Walter, K. M., United Nations Environment Programme: p. 183.
- Ahnert, F. (2003). Einführung in die Geomorphologie. Stuttgart, Ulmer, 477 pp. (in German).
- Anderson, P.M. and Lozhkin, V.A. (2001). The Stage 3 interstadial complex (Karginskii/middle Wisconsinan interval) of Beringia: variations in paleoenvironments and implications for paleoclimatic interpretations, *Quaternary Science Reviews* 20(1-3): 93-125.
- Andreev, A.A., Grosse, G., Schirrmeister, L., Kuznetsova, T.V., Kuzmina, S.A., Bobrov, A.A., Tarasov, P.E., Novenko, E.Y., Meyer, H., Derevyagin, A.Y., Kienast, F., Bryantseva, A. and Kunitsky, V.V. (2009). Weichselian and Holocene palaeoenvironmental history of the Bol'shoy Lyakhovsky Island, New Siberian Archipelago, Arctic Siberia, *Boreas* 38(1): 72-110.
- Arkhangelov, A.A., Popov, V.V. and L'yanos-Mas, A.V. (1979). About permfrost-facial structure of the Yedoma horizon of Dyvanny Yar, Kolyma Lowland. In: Problems of cryolithology, Moscow University Press. 8: 145-156. (in Russian).
- Astakhov, V. (2001). The stratigraphic framework for the Upper Pleistocene of the glaciated Russian Arctic: changing paradigms, *Global and Planetary Change* 31(1-4): 283-295.
- Berg, L.S. (1964). Loess as a product of weathering and soil formation, *Israel Program for Scientific Translations*, 207.
- Biske, S.F. (1957). Quaternary deposits of the Kolyma Lowlands. In: Materials for geology and resources of Northeast USSR, Magadan publishing house. 11. (in Russian).
- Bobrov, A.A., Siegert, C., Andreev, A.A. and Schirrmeister, L. (2003). Testaceans (Protozoa: Testacea) in Quaternary Permafrost Sediments of Bykovsky Peninsula, Arctic Yakutia, *Biology Bulletin* 30(2): 191-206.
- Boike, J., Hubberten, H.-W., Lantuit, H., Overduin, P.P., Schirrmeister, L., Wagner, D. and Huch, M. (2009). Permafrost und der globale Klimawandel, *Polarforschung* 78(2): 129-132. (in German).
- Brandova, Y.P. (1957). Quaternary deposits of the Kolyma Lowlands. In: Materials for geology and resources of Northeast USSR, Magadan publishing house. (in Russian).
- Burn, C.R., Michel, F.A. and Smith, M.W. (1986). Stratigraphic, isotopic, and mineralogical evidence for an early Holocene thaw unconformity at Mayo, Yukon Territory, *Canadian Journal of Earth Sciences* 23(6): 794-803.
- Butler, R.F. (1992). Paleomagnetism. Cambridge, Blackwell Scientific Publishing, 319 pp.
- Clark, I.D. and Fritz, P. (1997). Environmental isotopes in hydrogeology, CRC, 328 pp.
- Craig, H. (1953). The geochemistry of the stable carbon isotopes, *Geochimica et Cosmochimica Acta* 3: 53 - 92.
- Craig, H. (1961). Isotopic variations in meteoric waters, *Science* 133(3465): 1702.
- Craig, H. and Gordon, L.I. (1965). Deuterium and oxygen 18 variations in the ocean and the marine atmosphere. In: *Stable Isotopes in Oceanographic Studies and Paleotemperatures*. Tongiorgi, E.: 9-130.
- Dansgaard, W. (1964). Stable isotopes in precipitation, *Tellus* 16(4): 436-468.
- Dansgaard, W., Johnsen, S.J., Clausen, H.B., Dahl-Jensen, D., Gundestrup, N.S., Hammer, C.U., Hvidberg, C.S., Steffensen, J.P., Sveinbjörnsdóttir, A.E. and Jouzel, J. (1993). Evidence for general instability of past climate from a 250-kyr ice-core record, *Nature* 364(6434): 218-220.
- Dearing, J. (1999). Environmental Magnetic Susceptibility - Using the Bartington MS2 System.
- Degens, E.T. (1968). Geochemie der Sedimente. Stuttgart, Enke, 282 pp. (in German).

- Degens, E.T. (1969). Biogeochemistry of stable carbon isotopes. In: Organic geochemistry: methods and results. Eglinton, G. and Murphy, M. T. J., Springer: 304-329.
- Dereviagin, A.Y., Meyer, H., Hubberten, H.W. and Simonov, E.F. (2002). New Data on the Isotopic Composition and Evolution of Modern Ice Wedges in the Laptev Sea Region, *Polarforschung* 70: 27-35.
- Dostovalov, B.N. and Kudryavtsev, V.A. (1967). General geocryology (Obshchee mersotovedenie), Moscow University publishing house. (in Russian).
- Dutta, K., Schuur, E.A.G., Neff, J.C. and Zimov, S.A. (2006). Potential carbon release from permafrost soils of Northeastern Siberia, *Global Change Biology* 12(12): 2336-2351.
- Fradkina, A.F., Grienenko, O.V., Laukhin, S.A., Nechaev, V.P., Andreev, A.A. and Klimanov, V.A. (2005). Northesatern Asia. In: Cenozoic Climatic and Environmental Changes in Russia. Wright Jr., H. E., Blyakharchuk, A. A., Velichko, A. A. and Borisova, O., The Geological Society of America - Special Paper 382.
- French, H.M. (2007). The periglacial environment, Wiley, 458 pp.
- Füchtbauer, H., Heling, D., Müller, G., Richter, D., Schmincke, H.-U., Schneider, H., Valetton, I., Walther, H. and Wolf, M. (1988). Sediment und Sedimentgestein. Stuttgart, E. Schweizerbart'sche Verlagsbuchhandlung, 1141 pp. (in German).
- Furtak, H. and Langguth, H.R. (1967). Zur hydrochemischen Kennzeichnung von Grundwässern und Grundwassertypen mittels Kennzahlen. Mem. IAH-Congress. Hannover. 7: 89-96. (in German).
- Gat, J.R. (1996). Oxygen and hydrogen isotopes in the hydrologic cycle, *Annual Review of Earth and Planetary Sciences* 24(1): 225-262.
- Giterman, R.E., Sher, A.V. and Matthews, J.V. (1982). Comparison of the Development of Tundra-Steppe Environments in West and East Beringia: Pollen and Macrofossil Evidence from Key Sections. In: Paleocology of Beringia. Hopkins, D. M., Matthews, J. V., Schweger, C. E. and Young, S. B., Academic Press.
- Godwin, H. (1962). Half-life of radiocarbon, *Nature* 195(984).
- Gravis, G.F. (1969). Slope deposits in Yakutia. Moscow, Nauka. (in Russian).
- Grishuk, M.P. (1982). Paleoclimate inferred by palynological data. In: Geographical Investigations of the Quaternary. Rychagov, G. I., Anayev, G. S. and Kaplin, P. A. Moscow, Moscow University Press: 45-57. (in Russian).
- Grootes, P.M., Nadeau, M.J. and Rieck, A. (2004). 14C-AMS at the Leibniz-Labor: radiometric dating and isotope research, *Nuclear Instruments and Methods in Physics Research* 223: 55-61.
- Grosswald, M.G. (1998). Late-Weichselian ice sheets in Arctic and Pacific Siberia, *Quaternary International* 45: 3-18.
- Gubin, S.V. (1999). Late Pleistocene soil formations in loess-ice deposits of northeast Eurasia. Institute of Physicochemical and Biological Problems of Soil Science, Russian Academy of Sciences. Pushchino. abstract PhD thesis. (in Russian).
- Handbook_Dionex (2000). Handbook Dionex DX-320, Dionex Corp.
- Harris, S.A., French, H.M., Heginbottom, J.A., Johnston, G.H., Ladayi, B., Sego, D.C. and van Everdingen, R.O. (1988). Glossary of permafrost and related ground ice terms. Ottawa 156 pp.
- Heinrichs, H. and Herrmann, A.G. (1990). Praktikum der analytischen Geochemie. Berlin, Heidelberg, Springer, 669 pp. (in German).
- Hjulström, F. (1939). Transportation of detritus by moving water. In: Recent marine sediments. Trask, P. D., American Association of Petroleum Geologists. 59: 5-31.
- Hoefs, J. (1997). Stable Isotope geochemistry. Berlin, Heidelberg, Springer-Verlag, 201 pp.
- Höltling, B. and Coldewey, W.G. (2009). Hydrologie - Einführung in dieAllgemeine und Angewandte Hydrogeologie. Heidelberg, Spektrum, 386 pp. (in German).
- Hopkins, D.M. (1982). Aspects of the paleogeography of Beringia during the Late Pleistocene. In: Paleocology of Beringia. Hopkins, D. M., Matthews, J. V., Schweger, C. E. and Young, S. B., Academic Press: 3-28.

- Horita, J., Ueda, A., Mizukami, K. and Takatori, I. (1989). Automatic D and ^{18}O analyses of multi-water samples using H_2 - and CO_2 - water equilibration methods with a common equilibration set-up, *Applied Radiation and Isotopes* 40(9): 801-805.
- Hubberten, H.W., Andreev, A., Astakhov, V.I., Demidov, I., Dowdeswell, J.A., Henriksen, M., Hjort, C., Houmark-Nielsen, M., Jakobsson, M., Kuzmina, S., Larsen, E., Lunkka, J.P., Lysa, A., Mangerud, J., Möller, P., Saarnisto, M., Schirmer, L., Sher, A.V., Siegert, C., Siegert, M.J. and Svendsen, J.I. (2004). The periglacial climate and environment in northern Eurasia during the Last Glaciation, *Quaternary Science Reviews* 23(11-13): 1333-1357.
- Huh, Y., Panteleyev, G., Babich, D., Zaitsev, A. and Edmond, J.M. (1998). The fluvial geochemistry of the rivers of Eastern Siberia: II. Tributaries of the Lena, Omoloy, Yana, Indigirka, Kolyma, and Anadyr draining the collisional/accretionary zone of the Verkhoyansk and Cherskiy ranges, *Geochimica et Cosmochimica Acta* 62: 2053-2075.
- IPCC (2007). *Climate change 2007: the physical science basis*, Intergovernmental Panel on Climate Change, 996 pp.
- IUSS-Working-Group-WRB (2007). *World Reference Base for Soil Resources 2006, first update 2007*. World Soil Resources Reports. Rome, IUSS/ISRIC/FAO.
- Jakobsen, B.H., Siegert, C. and Ostroumov, V. (1996). Effect of Permafrost and Palaeo-Environmental History on Soil Formation in the lower Kolyma Lowland, Siberia, *Danish Journal of Geography* 96: 40-50.
- Jouzel, J. (2003). Water Stable Isotopes: Atmospheric Composition and Applications in Polar Ice Core Studies. In: *Treatise on Geochemistry - The Atmosphere*. Keeling, R. F., Holland, H. and Turekian, K. K., Elsevier. 4: 213-243.
- Jouzel, J. and Merlivat, L. (1984). Deuterium and oxygen 18 in precipitation: modeling of the isotopic effects during snow formation, *Journal of Geophysical Research* 89(D7).
- Kanevskiy, M. (2003). Cryogenic structure of mountain slope deposits, northeast Russia. 8th International Conference on Permafrost, Zurich, Switzerland.
- Kaplina, T. and Lozhkin, A. (1979). Age of alass deposits of the Maritime Lowland of Yakutia, *Izvestiya Akademii Nauk, Sojus Sowjetskich Sozialistitscheskich Respublik (SSSR), Seriya Geologicheskaya* 2: 69-76. (in Russian).
- Kaplina, T.N., Giterman, R.E., Lakhtina, O.V., Abrashov, B.A., Kiselyov, S.V. and Sher, A.V. (1978). Duvanny Yar - a key section of Upper Pleistocene deposits of the Kolyma lowland, *Bulletin of Quaternary Research Commission* 48: 49-65. (in Russian).
- Karte, J. (1979). *Räumliche Abgrenzung und regionale Differenzierung des Periglaziärs*. Geowissenschaften. Bochum, Ruhr Universität. PhD- thesis. (in German).
- Kehew, A. (2001). *Applied chemical hydrology*, Prentice Hall, 368 pp.
- Kendall, C. and Doctor, D.H. (2003). Stable Isotope Applications in Hydrologic Studies. In: *Treatise on Geochemistry - Surface and Ground Waters, Weathering, and Soils*. Drever, J. I., Elsevier. 5.
- Kienast, F., Schirmer, L., Siegert, C. and Tarasov, P. (2005). Palaeobotanical evidence for warm summers in the East Siberian Arctic during the last cold stage, *Quaternary Research* 63(3): 283-300.
- Kind, N.V. (1975). Glaciations in the Verkhoyansk Mountains and their place in the radiocarbon geochronology of the Siberian Late Anthropogene, *Biuletyn Peryglacjalny* 2: 41-54.
- Konishchev, V.N. (1983). Cryolithological evidences of the heterogeneous structure of "Ice Complex" deposits in the Dyvanny yar section. In: *Problems of cryolithology*, Moscow University Press. 8: 56-64. (in Russian).
- Konishchev, V.N. (1987). Origin of loess-like silt in Northern Yakutia, USSR, *GeoJournal* 15(2): 135-139.
- Koppe, W. (2003). Infoblatt Permafrost Retrieved 2009, from http://www.klett.de/sixcms/list.php?page=infothek_artikel&extra=TERRA-Online%20/%20Realschule&artikel_id=104654&inhalt=kss_klett01.c.154637.de. (in German).
- Kunitsky, V.V., Schirmer, L., Grosse, G. and Kienast, F. (2002). Snow patches in nival landscapes and their role for the Ice Complex formation in the Laptev Sea coastal lowlands, *Polarforschung* 70: 53-67.

- Kutzbach, L., Wagner, D. and Pfeiffer, E.M. (2004). Effect of microrelief and vegetation on methane emission from wet polygonal tundra, Lena Delta, Northern Siberia, *Biogeochemistry* 69(3): 341-362.
- Kuznetsova, L.P. (1998). Atmospheric moisture content and transfer over the territory of the former USSR. The Second International Workshop on Energy and Water Cycle in Siberia and GAME (GEWEX Asian Monsoon Experiment), November 26-28, 1997, Moscow, Russia.
- Lachenbruch, A.H. (1963). Contraction theory of ice-wedge polygons: A qualitative discussion. Permafrost international conference, Lafayette, National Academy of Sciences-National Research Council.
- Lauriol, B., Duchesne, C. and Clark, I.D. (1995). Systématique du Remplissage en Eau des Fentes de Gel: Les Résultats d'une Étude Oxygène-18 et Deutérium, *Permafrost and Periglacial Processes* 6(1): 47-55. (in French).
- Libby, W.F. (1955). *Radiocarbon Dating*. Chicago, University of Chicago Press.
- Libby, W.F. (1961). *Radiocarbon Dating*, *Science* 133(3453): 621-629.
- MacKay, J.R. (1972). The world of underground ice, *Annals of the Association of American Geographers* 62(1): 1-22.
- MacKay, J.R. (1974). Reticulate ice veins in permafrost, northern Canada, *Canadian Geotechnical Journal* 11(2): 230-237.
- MacKay, J.R. (1990). Some observations on the growth and deformation of epigenetic, syngenetic and anti-syngenetic ice wedges, *Permafrost and Periglacial Processes* 1(1): 15-29.
- MacKay, J.R. (2000). Thermally induced movements in ice-wedge polygons, western Arctic coast: a long-term study, *Géographie physique et Quaternaire* 54(1): 41-68.
- McGuire, A.D., Anderson, L.G., Christensen, T.R., Dallimore, S., Guo, L., Hayes, D.J., Heimann, M., Lorenson, T.D., Macdonald, R.W. and Roulet, N. (2009). Sensitivity of the carbon cycle in the Arctic to climate change, *Ecological Monographs* 79(4): 523-555.
- Meyer, H., Dereviagin, A., Siegert, C. and Hubberten, H.W. (2002a). Paleoclimate studies on Bykovsky Peninsula, North Siberia—hydrogen and oxygen isotopes in ground ice, *Polarforschung* 70(1/2): 37–51.
- Meyer, H., Dereviagin, A., Siegert, C., Schirrmeister, L. and Hubberten, H.W. (2002b). Palaeoclimate Reconstruction on Big Lyakhovsky Island, North Siberia--Hydrogen and Oxygen Isotopes in Ice Wedges, *Permafrost and Periglacial Processes* 13(2): 91-105.
- Meyer, H., Schirrmeister, L., Andreev, A., Wagner, D., Hubberten, H.-W., Yoshikawa, K., Bobrov, A., Wetterich, S., Opel, T., Kandiano, E. and Brown, J. (in review). Late Glacial and Holocene isotopic and environmental history of northern coastal Alaska - results from a buried ice-wedge system at Barrow, *Quaternary Science Reviews*.
- Meyer, H., Schönicke, L., Wand, U., Hubberten, H.W. and Friedrichsen, H. (2000). Isotope studies of hydrogen and oxygen in ground ice-experiences with the equilibration technique, *Isotopes in Environmental and Health Studies* 36(2): 133-149.
- Meyers, P.A. (1994). Preservation of elemental and isotopic source identification of sedimentary organic matter, *Chemical Geology* 114(3-4): 289-302.
- Meyers, P.A. (2003). Applications of organic geochemistry to paleolimnological reconstructions: a summary of examples from the Laurentian Great Lakes, *Organic Geochemistry* 34(2): 261-289.
- Michel, F.A. (1990). Isotopic composition of ice-wedge ice in northwestern Canada. *Proceedings of the Fifth Canadian Permafrost Conference*, Québec City.
- Murton, J.B. and French, H.M. (1994). Cryostructures in permafrost, Tuktoyaktuk coastlands, western arctic Canada, *Canadian Journal of Earth Sciences* 31(4): 737-747.
- Nagaoka, D. (1994). Properties of Ice Complex deposits in eastern Siberia. 2nd Symposium on the Joint Siberian Permafrost Studies between Japan and Russia, Tsukuba, Japan.
- Nelson, R.E., Carter, L.D. and Robinson, S.W. (1988). Anomalous radiocarbon ages from a Holocene detrital organic lens in Alaska and their implications for radiocarbon dating and paleoenvironmental reconstructions in the arctic, *Quaternary Research* 29(1): 66-71.

- Nier, A.O. (1950). A Redetermination of the Relative Abundances of the Isotopes of Carbon, Nitrogen, Oxygen, Argon, and Potassium, *Physical Review* 77(6): 789.
- Nikolayev, V.I. and Mikhalev, D.V. (1995). An oxygen-isotope paleothermometer from ice in Siberian permafrost, *Quaternary Research* 43(1): 14-21.
- Nölte, J. (2001). *ICP Emissions-spektrometrie für Praktiker*, Wiley, 271 pp. (in German).
- O'Haver, T. (2009). *Interactive Peak Fitter*, Department of Chemistry and Biochemistry, University of Maryland Retrieved 2009/10/12, from <http://terpconnect.umd.edu/~toh/spectrum/InteractivePeakFitter.htm>.
- Oechel, W.C., Hastings, S.J., Vourlitis, G., Jenkins, M., Riechers, G. and Grulke, N. (1993). Recent change of Arctic tundra ecosystems from a net carbon dioxide sink to a source, *Nature* 361(6412): 520-523.
- Olsson, I.U. (1991). Accuracy and precision in sediment chronology, *Hydrobiologia* 214(1): 25-34.
- Parfenov, L.M. (1991). Tectonics of the Verkhoyansk-Kolyma Mesozoides in the context of plate tectonics, *Tectonophysics* 199(2-4): 319-342.
- Park, R. and Epstein, S. (1960). Carbon isotope fractionation during photosynthesis, *Geochimica et Cosmochimica Acta* 21: Medium: X; Size: Pages: 110-26.
- Pécsi, M. (1990). Loess is not just accumulation of airborne dust, *Quaternary International* 7/8: 1–21.
- Pettijohn, F.J. (1975). *Sedimentary Rocks*. New York, Harper and Row, 628 pp.
- Péwé, T.L. and Journaux, A. (1983). Origin and character of loesslike silt in unglaciated south-central Yakutia, Siberia, USSR, *Geological Survey Professional Paper* 1262.
- Pye, K. (1995). The nature, origin and accumulation of loess, *Quaternary Science Reviews* 14(7-8): 653-667.
- Reimer, P.J., Baillie, M.G.L., Bard, E., Bayliss, A., Beck, J.W., Bertrand, C.J.H., Blackwell, P.G., Buck, C.E., Burr, G.S., Cutler, K.B., Damon, P.E., Edwards, R.L., Fairbanks, R.G., Friedrich, M., Guilderson, T.P., Hogg, A.G., Hughen, K.A., Kromer, B., McCormac, G., Manning, S., Ramsey, C.B., Reimer, R.W., Remmele, S., Southon, J.R., Stuiver, M., Talamo, S., Taylor, F.W., Plicht, J.v.d. and Weyhenmeyer, C.E. (2004). IntCal04 atmospheric radiocarbon age calibration, 0-26 cal kyr BP, *Radiocarbon* 46: 1029-1058.
- Reineck, H.E. and Singh, I.B. (1980). *Depositional Sedimentary Environments*. Berlin, Heidelberg, New York, Springer, 549 pp.
- Rivas-Martínez, S. and Rivas-Sáenz, S. (1996-2009). *Worldwide Bioclimatic Classification System*, Retrieved 2009/10/15, from <http://www.globalbioclimatics.org/station/ru-kolym.htm>.
- Romanovskii, N.N. (1977). Formirovaniye poligonal'nozhil'nykh struktur (Formation of polygonal-wedge structures), *Nauka*, 215 pp. (in Russian).
- Romanovskii, N.N. (1993). *Fundamentals of cryogenesis of lithosphere*. Moscow, Moscow University Press, 336 pp. (in Russian).
- Romanovskii, N.N., Gavrilov, A.V., Kholodov, A.L., Pustovoit, G.P., Niessen, F., Kassens, H. and Hubberten, H.W. (1998). Map of predicted offshore permafrost distribution on the Laptev Sea Shelf. *Permafrost - Seventh International Conference*, Yellowknife, Canada, Colloection Nordicana.
- Romanovsky, V.E., Gruber, S., Instanes, A., Jin, H., Marchenko, S.S., Smith, S.L., Trombotto, D. and Walter, K.M. (2007). *Frozen Ground* (Chapter 7). In: *Global Outlook for Ice and Snow*, UNEP: 183–200.
- Rozenbaum, G.E. (1981). Special features of lithogenesis of the alluvial planes in the Eastern Subarctic as related to the problem of the Ice (Yedoma) Complex. In: *Problems of Cryolithology*. Moscow, MSU Press. 9: 87–100. (in Russian).
- Scheffer, F. and Schachtschabel, P. (2002). *Lehrbuch der Bodenkunde*. Heidelberg, Berlin, Spektrum, 593 pp. (in German).
- Schidlowski, M., Hayes, J.M. and Kaplan, I.R. (1983). Isotopic inferences of ancient biochemistries- Carbon, sulfur, hydrogen, and nitrogen. In: *Earth's earliest biosphere: its origin and evolution*. Schopf, J. W., Walter, M. R. and Schopf, J. W., Princeton.
- Schirrmeister, L., Grosse, G., Kunitsky, V.V., Magens, M., Meyer, H., Derivyagin, A.Y., Kuznetsova, T., Andreev, A.A., Babiy, O., Kienast, F., Grigoriev, M., Overduin, P.P. and Preusser, F. (2008a). Periglacial land-

- scape evolution and environmental changes of Arctic lowland areas for the last 60 000 years (western Laptev Sea coast, Cape Mamontov Klyk), *Polar Research* 27: pp. 249-272.
- Schirrneister, L., Grosse, G., Schwamborn, G., Andreev, A.A., Meyer, H., Kunitsky, V.V., Kuznetsova, T.V., Dorozhkina, M.V., Pavlova, E.Y. and Bobrov, A.A. (2003). Late Quaternary history of the accumulation plain north of the Chekanovsky Ridge (Lena Delta, Russia): a multidisciplinary approach, *Polar Geography* 27(4): 277-319.
- Schirrneister, L., Kunitsky, V.V., Grosse, G., Kuznetsova, T.V., Derevyagin, A.Y., Wetterich, S. and Siegert, C. (2008b). The Yedoma Suite of the Northeastern Siberian Shelf Region: Characteristics and Concept of Formation. 9th International Conference on Permafrost, University of Alaska Fairbanks.
- Schirrneister, L., Kunitsky, V.V., Grosse, G., Wetterich, S., Meyer, H., Schwamborn, G., Babiy, O., Derevyagin, A.Y. and Siegert, C. (in review). Characteristics and origin of Late Pleistocene fine-grained ice-rich cover deposits (Ice Complex) in the East Siberian Arctic lowlands, *Quaternary International*.
- Schirrneister, L., Siegert, C., Kunitzky, V.V., Grootes, P.M. and Erlenkeuser, H. (2002a). Late Quaternary ice-rich permafrost sequences as a paleoenvironmental archive for the Laptev Sea Region in northern Siberia, *International journal of earth sciences* 91(1): 154-167.
- Schirrneister, L., Siegert, C., Kuznetsova, T., Kuzmina, S., Andreev, A., Kienast, F., Meyer, H. and Bobrov, A. (2002b). Paleoenvironmental and paleoclimatic records from permafrost deposits in the Arctic region of Northern Siberia, *Quaternary International* 89(1): 97-118.
- Schirrneister, L., Wetterich, S., Grosse, G., Siegert, C., Overduin, P.P. and Hubberten, H.W. (2009). Organic Carbon in Ice Complex deposits - characteristics and origin of the Yedoma Suite in East Siberian Arctic lowlands. 8th International Carbon Dioxide Conference. Jena, Germany.
- Schirrneister, L., Wetterich, S. and Kholodov, A.L. (in press). The joint Russian-German Expedition BERINGIA/KOLYMA 2008. In: Reports on Polar and Marine Research: 43 pp.
- Schwamborn, G., Förster, A., Diekmann, B., Schirrneister, L. and Fedorov, G. (2008). Mid- to Late-Quaternary Cryogenic Weathering Conditions at Elgygytgyn Crater, Northeastern Russia: Inference from Mineralogical and Microtextural Properties of the Sediment Record. 9th International Conference on Permafrost, University of Alaska Fairbanks.
- Schwamborn, G., Meyer, H., Fedorov, G., Schirrneister, L. and Hubberten, H.W. (2006). Ground ice and slope sediments archiving late Quaternary paleoenvironment and paleoclimate signals at the margins of El'gygytgyn Impact Crater, NE Siberia, *Quaternary Research* 66(2): 259-272.
- Seppälä, M. (2004). Wind as a geomorphic agent in cold climates, Cambridge University Press, 358 pp.
- Shepard, F.P. (1954). Nomenclature based on sand-silt-clay ratios, *Journal Sedimentary Petrology* 24(3): 151-158.
- Sher, A.V. (1971). Mammals and Stratigraphy of the Pleistocene of the Extreme Northeast of the USSR and North America, Nauka. (in Russian).
- Sher, A.V. (1995). Is there any real evidence for a huge shelf ice sheet in East Siberia?, *Quaternary International* 28: 39-40.
- Sher, A.V., Kaplina, T.N., Giterman, R.E., Lozhkin, A.V., Arkhangelov, A.A., Kiselyov, S.V., Kouznetsov, Y.V., Virina, E.I. and Zazhigin, V.S. (1979). Late Cenozoic of the Kolyma Lowland. 14th Pacific Science Congress, Khabarovsk, Academy of Science, USSR.
- Sher, A.V., Kuzmina, S.A., Kuznetsova, T.V. and Sulerzhitsky, L.D. (2005). New insights into the Weichselian environment and climate of the East Siberian Arctic, derived from fossil insects, plants, and mammals, *Quaternary Science Reviews* 24(5-6): 533-569.
- Shur, Y., Hinkel, K.M. and Nelson, F.E. (2005). The transient layer: implications for geocryology and climate-change science, *Permafrost and Periglacial Processes* 16(1): 5-17.
- Soffel, H.C. (1991). Paläomagnetismus und Achäomagnetismus. Heidelberg, Springer, 276 pp. (in German).
- Sokolov, S.D., Bondarenko, G.Y., Morozov, O.L., Shekhovtsov, V.A., Glotov, S.P., Ganelin, A.V., Kravchenko, B. and Berezhnoy, I.R. (2002). South Anyui suture, northeast Arctic Russia: facts and problems. In: Tectonic Evolution of the Bering Shelf-Chukchi Sea-Arctic Margin and Adjacent Landmasses. Miller, E., Grantz, A. and Klemperer, S., Geological Society of America -Special Paper 360: 209-224.

- Soloviev, P.A. (1973). Thermokarst phenomena and landforms due to frost heaving in Central Yakutia, *Biuletyn Peryglacjalny* 23: 135-155.
- Sommerkorn, M. and Hamilton, N. (2008). Arctic Climate Impact Science - an update since ACIA, WWF, 123 pp.
- Sommerkorn, M. and Hassol, S.J. (2009). Arctic Climate Feedbacks: Global Implications, WWF, 97 pp.
- Stuiver, M. and Polach, H.A. (1977). Discussion: reporting of ^{14}C data, *Radiocarbon* 19(3): 355-363.
- Svendsen, J.I., Alexanderson, H., Astakhov, V.I., Demidov, I., Dowdeswell, J.A., Funder, S., Gataullin, V., Henriksen, M., Hjort, C., Houmark-Nielsen, M., Hubberten, H.W., Ingólfsson, Ó., Jakobsson, M., Kjær, K.H., Larsen, E., Lokrantz, H., Lunkka, J.P., Lyså, A., Mangerud, J., Mantiouchkov, A., Murray, A., Möller, P., Niessen, F., Nikolskaya, O., Polyak, L., Saarnisto, M., Siegert, C., Siegert, M.J., Spielhagen, R.F. and Stein, R. (2004). Late Quaternary ice sheet history of northern Eurasia, *Quaternary Science Reviews* 23(11-13): 1229-1271.
- Tomirdiario, S.V. (1982). Evolution of Lowland Landscapes in Northeastern Asia during Late Quaternary Time. In: *Paleoecology of Beringia*. Hopkins, D. M., Matthews, J. V., Schweger, C. E. and Young, S. B., Academic Press: 29.
- Tormirdiario, S.V. and Chyomen, B.I. (1987). Cryogenic eolian deposits of Eastern Arctic and Subarctic, *Nauka*. (in Russian).
- Trask, P.D., Hammar, H.E., Wu, Z. and Wu, C. (1932). Origin and environment of source sediments of petroleum. Houston, Gulf Publishing Company.
- Tucker, M. (1996). *Methoden der Sedimentologie*. Stuttgart, Enke, 366 pp. (in German).
- Vaikmäe, R. (1989). Oxygen isotopes in permafrost and ground ice—A new tool for paleo-climatic investigations. 5th Working Meeting 'Isotopes in Nature', Leibzig.
- Vaikmäe, R. (1991). Oxygen-18 in permafrost ice. International Symposium of the Use of Isotope Techniques in Water Resources Development, Vienna.
- van Everdingen, R.O. (1998). Multi-language glossary of permafrost and related ground-ice terms. revised May 2005, Boulder, CO: National Snow and Ice Data Center/World Data Center for Glaciology, 233 pp.
- Vasil'chuk, A.C. and Vasil'chuk, Y.K. (2008a). Appearance of Heinrich events on pollen plots of Late Pleistocene ice wedges. Ninth International Conference on Permafrost, Fairbanks.
- Vasil'chuk, Y.K. (2005). Heterochroneity and Heterogeneity of the Duvanny Yar Edoma, *Doklady Earth Science* 402(4): 568-573.
- Vasil'chuk, Y.K., Kim, J.C. and Vasil'chuk, A.C. (2004). AMS ^{14}C dating and stable isotope plots of Late Pleistocene ice-wedge ice, *Nuclear Instruments and Methods in Physics Research B* 223: 650-654.
- Vasil'chuk, Y.K. and Vasil'chuk, A.C. (1997). Radiocarbon Dating and Oxygen Isotope Variations in Late Pleistocene Syngenetic Ice Wedges, Northern Siberia, *Permafrost and Periglacial Processes* 8(3): 335-345.
- Vasil'chuk, Y.K. and Vasil'chuk, A.C. (2008b). Dansgaard-Oeschger events on Isotope Plots of Siberian Ice Wedges. Ninth International Conference on Permafrost, Fairbanks.
- Vasil'chuk, Y.K., Vasil'chuk, A.C., Rank, D., Kutschera, W. and Kim, J.C. (2001). Radiocarbon dating of ^{18}O -D plots in Late Pleistocene ice-wedges of the Duvanny Yar (Lower Kolyma River, Northern Yakutia), *Radiocarbon* 43: 541-553.
- Vasil'chuk, Y.K., Kim, J.C. and Vasil'chuk, A.K. (2002). Radiocarbon AMS Dating of Isotopic Diagrams of Late Pleistocene Reformed Ice Wedges, *Doklady Earth Science* 383 A: 282-287.
- Vasil'chuk, Y.K. (1992). Oxygen Isotope Composition of Ground Ice. Application to Paleogeocryological Reconstructions. Moscow, Geological Faculty of Moscow State University, Russian Academy of Sciences. (in Russian).
- Vasil'chuk, Y.K., Vaikmae, R.A., Punning, J.-M.K. and M.O. Leibman (1988). Oxygen-isotope distribution, palynology and hydrochemistry wedge ice in organic-mineral complex of Duvanny Yar type section, *Transactions (Doklady) of the USSR Academy of Sciences, Earth Science Section* 292(5): 69-72. (in Russian).

- Velichko, A.A., Kononov, Y.M. and Faustova, M.A. (1997). The last glaciation of earth: Size and volume of ice-sheets, *Quaternary International* 41-42: 43-51.
- Velichko, A.A. and Nechaev, V.P. (2005). Cenozoic climatic and environmental changes in Russia, *Geological Society of America*, 226 pp.
- Viana, M., Jouannin, P., Pontier, C. and Chulia, D. (2002). About pycnometric density measurements, *Talanta* 57(3): 583-593.
- von Lozinski, W. (1909). Über die mechanische Verwitterung der Sandsteine im gemäßigten Klima, *Bulletin international de l'Académie des Sciences de Cracovie. Classe des Sciences mathématiques et Naturelles* 1: 1-25.
- Wagner, G.A. (1995). Altersbestimmung von jungen Gesteinen und Artefakten. Stuttgart, Enke. (in German).
- Walger, E. (1962). Die Korngrößenverteilung von Einzellagen sandiger Sedimente und ihre genetische Bedeutung, *Geologische Rundschau* 51(2): 494-507. (in German).
- Walter, K.M., Zimov, S.A., Chanton, J.P., Verbyla, D. and Chapin, F.S. (2006). Methane bubbling from Siberian thaw lakes as a positive feedback to climate warming, *Nature* 443(7107): 71-75.
- Walthert, L., Zimmermann, S., Lüscher, P. and Luster, J. (2004). *Waldböden der Schweiz - Grundlagen und Region Jura*, Ott Verlag, 768. (in German).
- Washburn, A.L. (1979). *Geocryology: a survey of periglacial processes and environments*, Edward Arnold, 406 pp.
- Washburn, A.L. (1981). Periglaziale Forschung in Revue, *Geologische Rundschau* 70(2): 664-690. (in German).
- Weise, O.R. (1983). *Das Periglazial*. Berlin, Stuttgart, Gebrüder Borntraeger, p. 199. (in German).
- Weiß, J. (2001). *Ionenchromatographie*, Wiley. (in German).
- Weltje, G.J. (1997). End-member modeling of compositional data: numerical-statistical algorithms for solving the explicit mixing problem, *Mathematical Geology* 29(4): 503-549.
- Wetterich, S., Herzschuh, U., Meyer, H., Pestryakova, L., Plessen, B., Lopez, C.M.L. and Schirrmeister, L. (2008a). Evaporation effects as reflected in freshwaters and ostracod calcite from modern environments in Central and Northeast Yakutia (East Siberia, Russia), *Hydrobiologia* 614(1): 171-195.
- Wetterich, S., Kuzmina, S., Andreev, A.A., Kienast, F., Meyer, H., Schirrmeister, L., Kuznetsova, T. and Sierralta, M. (2008b). Palaeoenvironmental dynamics inferred from late Quaternary permafrost deposits on Kurungnakh Island, Lena Delta, northeast Siberia, Russia, *Quaternary Science Reviews* 27(15-16): 1523-1540.
- Wetterich, S., Schirrmeister, L., Andreev, A.A., Pudenz, M., Plessen, B., Meyer, H. and Kunitsky, V.V. (2009). Eemian and Late Glacial/Holocene palaeoenvironmental records from permafrost sequences at the Dmitry Laptev Strait (NE Siberia, Russia), *Palaeogeography, Palaeoclimatology, Palaeoecology*.
- Yershov, E.D. and Williams, P.J. (2004). *General Geocryology*, Cambridge University Press, 580 pp.
- Zhang, T. (1999). Statistics and characteristics of permafrost and ground-ice distribution in the Northern Hemisphere, *Polar Geography* 23: 132-154.
- Zimov, S.A., Davydov, S.P., Zimova, G.M., Davydova, A.I., Schuur, E.A.G., Dutta, K. and Chapin, F.S. (2006a). Permafrost carbon: Stock and decomposability of a globally significant carbon pool, *Geophysical Research Letters* 33(20): L20502.
- Zimov, S.A., Schuur, E.A.G. and Chapin, F.S. (2006b). Climate change: Permafrost and the global carbon budget, *Science* 312(5780): 1612-1613.

Appendix

This chapter serves as data base for all the analytical results on sediments, radiocarbon dates, ground ice or recent water samples and hydrochemistry. It is divided into the following:

Appendix 1 (page 97)

- Overview over sedimentological results for single sediment samples

Appendix 2 (page 102)

- Radiocarbon age determinations for organic matter from sediment samples and ice wedge samples

Appendix 3 (page 103)

- Results for stable isotope analyses ($d^{18}\text{O}$, $d^2\text{H}$ and d excess, together with standard deviation) on ground ice samples and recent water samples

Appendix 4 (page 106)

- Results for hydrochemical analyses of selected samples

Sample	altitude	magnetic susceptibility	gravimetric ice content	absolute ice content	Clay	Silt	Sand	Median	Mean	Sorting	TOC	TIC	TN	TOC/TN	δ 13C	bulk density	TOC
	m a.r.l.	SI [10 ⁻⁸ m ³ · kg ⁻¹]	[wt %]	[%]	[vol. %]	[vol. %]	[vol. %]	[µm]	[µm]		[wt %]	[wt %]	[wt %]		[‰ vs. VPDB]	[g · cm ⁻³]	[kg · m ⁻³]
DY-01-A-01	43.45	46			12	57	31	32	42	3.6	34.5	0.0	1.0	34.2	-29.5	0.8	292.4
DY-01-A-02	43.30	25			15	62	23	27	32	3.5	1.3	0.2	0.1	11.0	-27.1	1.0	13.5
DY-01-A-03	42.75	31	57	36	21	62	17	13	25	4.2	0.8	0.1	0.0	N.A.	-26.8	1.0	7.8
DY-01-A-04	42.10	40	47	32	17	63	20	20	28	3.7	0.5	0.2	0.0	N.A.	-25.1	1.1	5.2
DY-01-A-05	41.70	45	70	41	21	61	18	14	25	4.2	1.4	0.2	0.1	10.2	-26.1	0.9	12.4
DY-01-B-06	41.25	46	48	32	17	64	19	27	29	3.7	0.9	0.3	0.1	7.7	-24.9	1.1	10.3
DY-01-B-07	40.75	42			21	67	12	12	21	3.9	1.3	0.3	0.2	8.2	-24.8	1.0	13.6
DY-01-B-08	40.25	51	66	40	20	66	14	15	23	3.8	2.0	0.5	0.2	9.2	-25.5	0.9	17.4
DY-01-B-09	39.75	46	54	35	19	65	16	20	26	3.8	1.4	0.4	0.2	7.6	-25.4	1.0	13.8
DY-01-B-10	39.25	43	49	33	20	68	12	16	23	3.7	1.4	0.4	0.2	7.6	-25.2	1.1	15.3
DY-01-B-11	38.75	44	54	35	17	69	14	20	25	3.5	1.3	0.6	0.2	6.7	-25.1	1.0	13.2
DY-01-B-12	38.25	41	56	36	21	67	12	13	21	3.8	1.2	0.5	0.2	6.8	-25.2	1.0	11.9
DY-01-B-13	37.75	44	51	34	17	65	18	25	28	3.7	1.2	0.4	0.2	7.1	-25.3	1.1	13.1
DY-01-B-14	37.25	43	72	42	20	67	13	15	23	3.9	1.3	0.5	0.2	7.4	-24.8	0.9	10.9
DY-01-C-15	37.50	42			21	66	13	14	22	3.9	1.3	0.5	0.2	8.3	-25.3	1.0	13.2
DY-01-C-16	37.00	41	51	34	18	68	14	18	24	3.7	0.8	0.4	0.1	7.1	-24.6	1.1	8.3
DY-01-C-17	36.50	44	55	35	19	65	16	22	26	3.9	0.9	0.3	0.1	8.0	-24.9	1.0	9.2
DY-01-C-18	36.00	45	54	35	18	64	18	24	28	4.0	0.7	0.3	0.1	7.3	-24.8	1.0	7.7
DY-01-C-19	35.50	42			21	69	10	12	20	3.7	1.5	0.5	0.2	7.9	-25.1	1.0	15.6
DY-01-D-20	35.30	54	47	32	16	65	19	30	29	3.8	1.1	0.3	0.1	8.6	-24.9	1.1	12.2
DY-01-D-21	34.80	40			21	67	12	14	21	3.8	1.4	0.5	0.2	7.2	-25.3	1.0	14.5
DY-01-D-22	34.30	40	51	34	24	64	12	11	20	4.2	1.4	0.4	0.2	7.7	-25.0	1.1	14.6
DY-01-D-23	34.00	41	47	32	19	68	13	16	23	3.6	1.4	0.5	0.2	7.1	-24.6	1.1	15.2
DY-01-D-24	33.50	42	63	39	18	67	15	16	24	3.7	1.2	0.4	0.2	7.1	-24.8	0.9	10.8
DY-01-D-25	33.00	41	53	35	21	68	11	13	21	3.8	1.4	0.6	0.2	6.9	-25.3	1.0	14.0
DY-01-D-26	32.50	32	46	31	22	67	11	12	20	3.9	1.6	0.6	0.2	7.2	-26.0	1.1	18.0
DY-01-D-27	32.10	32	54	35	21	67	12	13	21	3.8	1.3	0.6	0.2	6.3	-25.7	1.0	12.9
DY-01-E-28	32.00	53	46	31	15	66	19	32	30	3.4	1.0	0.3	0.1	7.9	-25.1	1.1	11.5
DY-01-E-29	31.50	42			19	67	14	20	25	3.8	1.0	0.4	0.1	7.3	-24.8	1.1	10.6
DY-01-E-30	31.00	45	52	34	17	69	14	18	24	3.5	1.5	0.5	0.2	7.3	-25.0	1.1	15.5
DY-01-E-31	30.50	42			19	70	11	15	21	3.4	1.6	0.7	0.2	7.0	-25.5	1.0	16.3

Sample	altitude	magnetic susceptibility	gravimetric ice content	absolute ice content	Clay	Silt	Sand	Median	Mean	Sorting	TOC	TIC	TN	TOC/TN	δ 13C	bulk density	TOC
	m a.r.l.	SI [10 ⁻⁸ m ³ · kg ⁻¹]	[wt %]	[%]	[vol. %]	[vol. %]	[vol. %]	[µm]	[µm]		[wt %]	[wt %]	[wt %]		[‰ vs. VPDB]	[g · cm ⁻³]	[kg · m ⁻³]
DY-01-E-32	30.00	44	66	40	21	71	8	12	18	3.5	1.8	0.6	0.2	7.5	-25.6	0.9	16.7
DY-01-F-33	29.80	40			18	70	12	19	23	3.5	1.3	0.6	0.2	6.7	-25.3	1.0	13.4
DY-01-F-34	29.10	43	113	53	22	72	6	9	14	3.2	10.5	1.0	0.8	13.6	-27.1	0.6	62.7
DY-01-F-35	28.80	42			21	71	8	10	16	3.4	6.8	2.0	0.6	11.1	-27.3	1.0	68.2
DY-01-F-36	28.50	41	81	45	21	69	10	13	20	3.7	2.2	1.0	0.3	7.5	-26.7	0.8	17.6
DY-01-F-37	28.00	47			22	67	11	11	20	3.9	1.1	0.4	0.2	7.2	-25.4	1.0	12.0
DY-01-F-38	27.50	48	53	35	16	73	11	18	22	3.2	1.4	0.5	0.2	7.4	-25.3	1.0	14.3
DY-01-F-39	27.00	51			18	67	15	24	26	3.6	0.9	0.4	0.1	7.1	-25.2	1.1	9.8
DY-01-G-40	27.30	54	37	27	19	66	15	20	25	3.9	1.0	0.4	0.1	7.6	-25.2	1.3	13.3
DY-01-G-41	26.80	55			23	66	11	11	20	4.0	1.8	0.4	0.2	8.6	-25.9	1.0	18.9
DY-01-G-42	26.30	43			18	72	10	16	21	3.3	1.3	0.4	0.2	7.3	-25.4	1.0	14.0
DY-01-G-43	25.80	48	40	29	17	63	20	24	29	3.8	0.6	0.5	0.0	N.A.	-24.9	1.2	7.5
DY-01-H-44	26.10	45			19	70	11	14	21	3.5	1.4	0.5	0.2	6.9	-25.9	1.0	14.2
DY-01-H-45	25.50	46	40	28	16	66	18	25	28	3.6	1.0	0.4	0.1	7.6	-25.7	1.2	12.5
DY-01-H-46	25.00	51			14	63	23	30	32	3.5	0.6	0.3	0.0	N.A.	-25.3	1.1	6.8
DY-01-H-47	24.00	49	38	28	17	65	18	21	27	3.8	0.6	0.3	0.0	N.A.	-25.1	1.3	8.0
DY-02-A-01	5.00	31	247	71	20	74	6	10	13	2.9	16.4	0.0	1.3	12.7	-32.8	0.3	51.3
DY-02-A-02	4.60	34			22	73	5	8	11	2.8	17.9	0.0	1.5	11.9	-33.7	0.9	166.0
DY-02-A-03	4.20	48	63	39	25	69	6	7	11	3.1	4.4	0.1	0.4	10.9	-29.1	0.9	40.1
DY-02-A-04	4.00	59			22	73	5	7	10	2.7	3.6	0.5	0.3	11.4	-27.5	1.0	37.6
DY-02-A-05	3.70	39			24	72	4	7	10	2.9	1.4	0.2	0.2	7.9	-28.4	1.1	15.0
DY-02-A-06	3.40	44			28	69	3	5	NA	NA	1.4	0.3	0.2	8.5	-28.2	1.1	15.1
DY-02-A-07	3.10	45	43	30	21	71	8	14	17	3.5	1.4	0.2	0.1	10.5	-26.8	1.2	16.1
DY-02-A-08	2.80	43			15	61	24	32	33	3.6	1.0	0.3	0.1	9.2	-26.4	1.1	10.8
DY-02-A-09	2.50	45			21	69	10	15	21	3.8	1.4	0.3	0.2	8.8	-26.5	1.0	14.9
DY-02-A-10	2.10	52	30	23	16	48	36	40	41	4.4	0.4	0.2	0.0	N.A.	-25.5	1.4	6.0
DY-03-A-01	5.00	50			17	62	21	20	29	3.9	0.8	0.5	0.1	6.8	-25.5	1.1	8.3
DY-03-A-02	5.50	50			16	62	22	24	31	3.7	0.8	0.5	0.1	6.3	-25.7	1.0	8.6
DY-03-A-03	6.00	52			17	62	21	23	30	3.8	0.7	0.5	0.1	5.3	-25.6	1.0	7.5
DY-03-A-04	6.30	51			19	61	20	18	28	4.2	1.0	0.5	0.1	7.3	-26.7	1.0	9.5

Sample	altitude	magnetic susceptibility	gravimetric ice content	absolute ice content	Clay	Silt	Sand	Median	Mean	Sorting	TOC	TIC	TN	TOC/TN	δ 13C	bulk density	TOC
	m a.r.l.	SI [10 ⁻⁸ m ³ · kg ⁻¹]	[wt %]	[%]	[vol. %]	[vol. %]	[vol. %]	[µm]	[µm]		[wt %]	[wt %]	[wt %]		[‰ vs. VPDB]	[g · cm ⁻³]	[kg · m ⁻³]
DY-03-A-05	6.50	44			18	65	17	24	27	3.9	0.8	0.3	0.1	7.2	-26.2	1.0	8.0
DY-03-A-06	6.70	43			17	61	22	24	31	4.0	1.7	0.4	0.2	11.4	-27.4	1.0	18.0
DY-03-A-07	7.10	47			17	58	25	30	33	4.2	1.3	0.3	0.1	10.2	-27.2	1.1	13.5
DY-03-A-08	7.60	46			17	62	21	25	30	3.9	1.9	0.4	0.2	11.3	-27.6	1.0	19.3
DY-03-A-09	7.90	43			17	72	11	19	22	3.3	1.1	0.3	0.1	7.9	-26.8	1.0	11.5
DY-03-A-10	7.40	44			16	62	22	31	31	3.7	0.7	0.5	0.0	N.A.	-25.9	1.1	7.0
DY-03-A-11	7.75	39			20	73	7	13	17	3.3	1.3	0.3	0.1	8.7	-27.3	1.0	13.7
DY-03-A-12	8.10	42			22	74	4	10	13	3.1	1.0	0.3	0.1	7.0	-27.5	1.1	10.4
DY-03-A-13	8.40	26			27	70	3	6	NA	NA	5.4	0.5	0.4	12.4	-27.8	1.0	54.7
DY-03-A-14	8.80	27	29	23	25	70	5	7	11	3.2	2.0	0.6	0.3	7.6	-27.3	1.4	28.4
DY-03-A-15	9.30	51			17	75	8	21	22	3.2	1.5	0.4	0.2	8.8	-27.5	1.0	15.3
DY-03-A-16	9.80	117	27	21	14	32	54	71	62	4.8	0.4	0.2	0.0	N.A.	-26.6	1.5	5.9
DY-03-A-17	10.30	73			16	57	27	33	35	4.0	0.6	0.3	0.0	N.A.	-26.6	1.1	5.8
DY-04-A-01	7.85	61			19	57	24	8	31	4.6	40.3	0.0	1.2	32.7	-28.6	0.8	326.8
DY-04-A-02	7.70	32	136	58	22	72	6	8	12	3.0	13.1	0.4	0.9	14.5	-29.1	0.5	67.5
DY-04-A-03	7.50	30	227	69	20	68	12	11	18	3.4	13.0	0.4	0.9	14.2	-28.7	0.3	44.3
DY-04-A-04	7.20	51	107	52	29	65	6	5	NA	NA	4.4	0.1	0.4	10.1	-31.0	0.6	28.0
DY-04-A-05	6.90	63	154	61	33	64	3	4	NA	NA	3.7	0.2	0.4	9.8	-31.4	0.5	18.0
DY-04-A-06	6.50	45	77	43	23	71	6	8	12	3.0	2.4	0.3	0.3	9.1	-28.5	0.8	19.3
DY-04-A-07	6.10	59	126	56	24	68	8	7	12	3.2	6.9	0.2	0.6	11.5	-30.7	0.6	38.3
DY-04-A-08	5.70	48	41	29	23	66	11	11	20	4.1	2.1	0.3	0.2	9.1	-29.4	1.2	24.8
DY-04-A-09	5.30	52	63	39	21	72	7	12	20	3.8	1.0	0.5	0.1	7.4	-27.2	0.9	9.1
DY-04-A-10	5.00	49	40	28	21	76	3	10	13	2.9	3.0	0.3	0.3	9.1	-31.1	1.2	35.9
DY-04-A-11	4.70	38	50	33	33	67	0	4	NA	NA	1.9	0.1	0.3	7.4	-28.8	1.1	20.2
DY-04-A-12	4.40	51	71	42	20	62	18	22	27	4.2	1.9	0.4	0.2	11.2	-28.3	0.9	16.6
DY-05-A-01	1.30	53	69	41	15	67	18	29	29	3.4	1.1	0.4	0.1	7.7	-25.7	0.9	9.3
DY-05-A-02	1.80	50	75	43	16	66	18	31	29	3.6	0.8	0.3	0.1	7.3	-25.6	0.8	6.4
DY-05-B-03	1.50	44	61	38	21	71	8	12	18	3.6	3.3	1.4	0.4	8.4	-26.6	0.9	30.5
DY-05-B-04	2.20	45	59	37	16	71	13	24	25	3.2	1.6	0.8	0.2	8.1	-26.3	1.0	15.8
DY-05-B-05	2.70	47	73	42	15	72	13	25	26	3.2	4.4	0.6	0.3	12.7	-27.4	0.8	36.6

Sample	altitude	magnetic susceptibility	gravimetric ice content	absolute ice content	Clay	Silt	Sand	Median	Mean	Sorting	TOC	TIC	TN	TOC/TN	δ 13C	bulk density	TOC
	m a.r.l.	SI [10 ⁻⁸ m ³ · kg ⁻¹]	[wt %]	[%]	[vol. %]	[vol. %]	[vol. %]	[µm]	[µm]		[wt %]	[wt %]	[wt %]		[‰ vs. VPDB]	[g · cm ⁻³]	[kg · m ⁻³]
DY-05-B-06	3.20	57	42	30	17	60	23	32	32	4.0	1.3	0.7	0.2	7.4	-26.7	1.2	15.3
DY-05-B-07	3.70	54	91	48	15	69	16	29	28	3.0	2.5	0.7	0.2	10.8	-27.1	0.7	17.9
DY-05-B-08	4.20	48	92	48	18	71	11	18	22	3.5	4.5	0.6	0.3	13.5	-26.6	0.7	32.0
DY-05-B-09	4.60	43	71	41	17	71	12	21	24	3.4	2.2	0.5	0.2	10.1	-26.3	0.9	19.1
DY-05-B-10	5.00	35	64	39	17	71	12	23	24	3.2	1.5	0.7	0.2	8.0	-26.0	0.9	13.4
DY-05-B-11	5.50	38	101	50	19	71	10	17	22	3.6	2.3	0.6	0.2	10.6	-26.3	0.7	15.1
DY-05-B-12	6.00	58	61	38	16	67	17	27	28	3.5	1.3	0.7	0.2	8.2	-26.4	1.0	12.6
DY-05-C-13	6.10	77	53	34	12	59	29	38	38	3.2	0.8	0.3	0.1	6.7	-25.6	1.0	7.9
DY-05-C-14	6.60	50	77	43	20	68	12	15	23	4.0	1.7	0.5	0.2	9.1	-26.2	0.8	13.5
DY-05-C-15	6.80	37	182	65	23	70	7	9	17	3.7	8.4	0.9	0.6	14.7	-27.3	0.4	34.7
DY-05-D-16	9.00	45	39	28	16	67	17	26	27	3.6	1.2	0.4	0.2	7.3	-25.7	1.2	15.1
DY-05-D-17	9.50	46	48	32	13	68	19	30	30	3.0	1.2	0.3	0.2	7.7	-25.9	1.1	13.1
DY-05-D-18	10.00	41	38	28	22	67	11	11	20	4.0	1.5	0.5	0.2	7.4	-26.0	1.2	18.6
DY-05-D-19	10.50	43	62	38	20	70	10	13	21	3.7	1.5	0.6	0.2	7.7	-26.0	0.9	13.9
DY-05-E-20	10.30	45	71	41	20	69	11	14	21	3.8	1.3	0.6	0.2	8.0	-25.4	0.9	10.9
DY-05-E-21	10.80	38	72	42	21	67	12	11	21	3.9	3.7	1.1	0.3	10.7	-26.5	0.8	30.8
DY-05-E-22	11.30	43	45	31	18	65	17	29	28	4.0	0.8	0.2	0.1	8.2	-25.9	1.2	9.6
DY-05-E-23	11.80	41	46	31	20	64	16	20	26	4.1	0.7	0.3	0.1	7.0	-26.1	1.1	8.1
DY-05-E-24	12.30	40	43	30	17	66	17	24	27	3.8	0.8	0.2	0.0	N.A.	-25.9	1.2	9.0
DY-05-E-25	12.80	41	17	15	20	63	17	17	26	4.1	0.8	0.2	0.0	N.A.	-25.5	1.8	13.8
DY-05-E-26	13.30	40	45	31	15	69	16	25	27	3.3	0.7	0.2	0.0	N.A.	-25.5	1.1	7.8
DY-05-E-27	13.80	42	38	27	19	66	15	16	24	3.8	0.8	0.2	0.1	7.9	-25.5	1.3	10.3
DY-05-E-28	15.00	45	39	28	18	65	17	18	26	3.9	0.7	0.3	0.0	N.A.	-25.6	1.2	8.5
DY-05-F-29	15.50	46	42	30	18	66	16	18	25	3.8	0.7	0.3	0.0	N.A.	-25.2	1.2	8.1
DY-05-F-30	16.00	63	50	33	17	65	18	17	26	3.7	1.0	0.4	0.1	7.8	-25.5	1.1	10.3
DY-05-F-31	16.50	59	42	30	17	64	19	27	29	3.8	0.8	0.3	0.1	7.5	-25.8	1.2	9.9
DY-05-F-32	17.00	53	38	28	18	65	17	23	27	3.9	0.7	0.2	0.0	N.A.	-25.5	1.3	8.6
DY-05-F-33	17.50	48	41	29	17	62	21	26	30	3.9	0.7	0.3	0.0	N.A.	-25.8	1.2	8.6
DY-05-F-34	18.00	49	42	29	18	65	17	18	26	3.8	0.7	0.3	0.0	N.A.	-25.3	1.2	8.3
DY-05-F-35	18.40	47	44	30	16	65	19	26	29	3.6	0.8	0.3	0.1	7.8	-25.7	1.2	9.9

Sample	altitude	magnetic susceptibility	gravimetric ice content	absolute ice content	Clay	Silt	Sand	Median	Mean	Sorting	TOC	TIC	TN	TOC/TN	$\delta^{13}\text{C}$	bulk density	TOC
	m a.r.l.	SI [$10^{-8} \text{ m}^3 \cdot \text{kg}^{-1}$]	[wt %]	[%]	[vol. %]	[vol. %]	[vol. %]	[μm]	[μm]		[wt %]	[wt %]	[wt %]		[‰ vs. VPDB]	[$\text{g} \cdot \text{cm}^{-3}$]	[$\text{kg} \cdot \text{m}^{-3}$]
DY-05-F-36	19.00	45	48	32	17	67	16	19	25	3.7	0.8	0.2	0.1	7.9	-25.3	1.1	9.4
DY-05-F-37	19.50	46	48	33	20	68	12	14	22	3.9	1.0	0.4	0.1	7.5	-25.3	1.1	10.7
DY-05-F-38	20.00	47	80	44	19	69	12	18	23	3.8	1.2	0.4	0.1	8.1	-25.6	0.8	9.2
DY-05-F-39	20.50	47	79	44	21	69	10	11	19	3.7	1.0	1.2	0.2	4.5	-26.6	0.8	7.8
DY-05-G-40	21.00	45	68	41	18	68	14	18	24	3.7	1.0	0.4	0.1	7.6	-25.0	0.9	8.7
DY-05-G-41	21.50	50	51	34	23	71	6	9	16	3.6	1.9	0.7	0.3	7.2	-25.3	1.1	20.5
DY-05-G-42	22.00	41	54	35	19	67	14	14	22	3.6	1.5	0.7	0.2	6.6	-25.1	1.0	15.0
DY-05-G-43	22.50	52	45	31	22	67	11	13	22	4.0	1.5	0.5	0.2	7.6	-25.1	1.1	16.8
DY-05-G-44	23.00	45	40	28	16	61	23	21	31	3.9	0.9	0.6	0.1	6.6	-25.0	1.2	10.9
DY-05-H-45	23.50	43	48	32	18	66	16	23	27	3.9	1.0	0.4	0.1	6.9	-25.3	1.1	11.1
DY-05-H-46	24.00	45	46	31	17	69	14	26	26	3.7	1.1	0.3	0.2	7.3	-25.7	1.1	13.0
DY-05-H-47	24.50	47	56	36	19	66	15	24	26	4.0	1.0	0.4	0.2	6.7	-25.6	1.0	10.3
DY-05-H-48	25.00	43	48	32	17	66	17	27	28	3.8	0.9	0.3	0.1	7.0	-25.4	1.1	9.7
DY-06-A-01	27.00	59			13	45	42	48	49	4.1	0.9	0.2	0.1	8.2	-26.2	1.1	9.0
DY-06-A-02	26.50	89			17	49	34	37	40	4.6	0.6	0.2	0.0	N.A.	-26.2	1.0	6.0
DY-06-A-03	26.00	46			17	57	26	27	34	4.3	1.1	0.3	0.1	8.2	-26.4	1.0	11.0
DY-06-A-04	25.40	45			21	67	12	10	19	3.7	1.4	0.4	0.2	8.1	-28.3	1.0	14.3
DY-06-A-05	25.00	43			14	59	27	32	36	3.7	0.7	0.3	0.1	6.8	-26.4	1.1	7.7
DY-06-A-5a	25.00	49			17	55	28	26	37	4.3	2.1	0.4	0.2	11.2	-27.0	1.0	21.7
DY-06-A-06	24.50	49			16	61	23	28	32	3.7	1.0	0.3	0.1	8.1	-26.8	1.1	10.9
DY-06-A-07	24.00	53			15	58	27	28	36	4.1	0.8	0.4	0.1	6.9	-26.1	1.1	8.1

Lab. N°	Sample	Description	Altitude [m a.r.l.]	¹⁴C age [a BP]	calibrated years; two sigma range [a BC]
KIA39774	DY-01-A-05	plant remains	41.7	9890 ± 50	9649 - 9607
KIA38378	DY-01-B-13	plant remains	37.75	24910 + 540 / -500	
KIA39775	DY-01-D-22	plant remains	34.3	32180 + 370 / -350	
KIA38380	DY-01-E-30	plant remains	31.0	39720 + 930 / -840	
KIA39776	DY-05-G-43	plant remains	22.5	41590 + 740 / -680	
KIA38383	DY-05-F-33	plant remains	17.5	38660 + 1370 / -1170	
KIA38382	DY-05-D-19	plant remains	10.5	40880 + 2100 / -1660	
KIA38381	DY-05-B-05	plant remains	2.7	> 46690	

Ground ice sample	Remarks	Width m	Altitude m a.r.l.	N	$\delta^{18}\text{O}$					$\delta^2\text{H}$					<i>d</i> excess					slope	intercept	R ²
					min	mean	median	max	s.d.	min	mean	median	max	s.d.	min	mean	median	max	s.d.			
DY-01-A-100	ice wedge	4	41.5	9	32.1	31.5	31.7	30.6	0.5	255.1	-248.5	-249.2	-240.9	4.7	0.8	3.3	3.1	7.9	2.1	8.1	5.5	0.81
DY-01-A-101						31.7					-252.6					0.8						
DY-01-A-102						31.6					-250.7					2.3						
DY-01-A-103						30.6					-241.8					3.1						
DY-01-A-104						30.6					-240.9					3.6						
DY-01-A-105						31.8					-253.1					1.1						
DY-01-A-106						32.1					-255.1					1.7						
DY-01-A-107						31.2					-245.3					4.7						
DY-01-A-108						32.0					-247.9					7.9						
DY-01-A-109						31.7					-249.2					4.4						
DY-01-B-201	fissure ice	0.03	38.3	1		32.7					-239.9					21.8						
DY-01-D-301	fissure ice	0.05	34.5	1		32.8					-238.5					24.2						
DY-01-D-400	ice wedge	0.8	34.5	5	32.5	32.3	32.4	32.1	0.2	256.8	-253.2	-254.9	-245.9	3.9	3.4	5.5	4	11.9	3.2	16.7	285.7	0.42
DY-01-D-401						32.2					-245.9					11.9						
DY-01-D-402						32.1					-252.9					4.0						
DY-01-D-403						32.5					-255.6					4.3						
DY-01-D-404						32.5					-256.8					3.4						
DY-01-D-405						32.4					-254.9					4.0						
DY-01-D-501	fissure ice	0.07	33	1		32.7					-234.6					27.2						
DY-01-F-601	ice lense		28.5	1		31.4					-222.1					28.8						
DY-01-G-701	fissure ice	0.07	26.3	1		32.5					-229.2					30.4						
DY-01-G-702	fissure ice	0.5	25.8	1		32.7					-246.7					15.1						
DY-01-H-801	fissure ice	0.2	25.8	1		32					-241.2					15.1						
DY-01-H-901	fissure ice	0.2	25.1	1		33.5					-248.7					19.4						
DY-05-F-300	ice wedge	0.7	15	4	34.5	33.9	33.9	33.5	0.4	273.0	-267.2	-265.7	-264.5	3.4	-0.2	4.2	2.7	11.4	4.4	1.1	-230.1	0.02
DY-05-F-301						33.7					-266.5					2.8						
DY-05-F-302						34.1					-273.0					-0.2						
DY-05-F-303						33.5					-265.0					2.6						
DY-05-F-304						34.5					-264.5					11.4						
DY-05-B-201	fissure ice	0.7	5.7	1		30.3					-228.5					14.1						
DY-05-A-100	ice wedge	0.35	1.4	4	31.3	30.6	30.6	29.9	0.7	244.3	-236.9	-237.1	-229.1	6.8	6.1	7.9	7.8	9.9	1.6	10.4	82.5	0.99
DY-05-A-101						29.9					-229.1					9.9						
DY-05-A-102						31.2					-243.0					6.6						
DY-05-A-103						31.3					-244.3					6.1						
DY-05-A-104						30.0					-231.2					9.0						
DY-02-A-100	ice wedge	1.5	4	10	29.6	28.6	29	26.3	1	232.5	-225.4	-228.3	-209.2	6.9	1.3	3.5	3.7	4.3	0.9	7.2	-20	0.99
DY-02-A-101						29.0					-228.8					3.2						
DY-02-A-102						29.2					-230.2					3.3						
DY-02-A-103						29.6					-232.5					4.3						
DY-02-A-104						29.3					-230.4					4.2						
DY-02-A-105						29.1					-228.3					4.1						
DY-02-A-106						29.0					-228.3					3.5						
DY-02-A-107						29.0					-227.5					4.1						
DY-02-A-108						28.4					-222.9					4.0						
DY-02-A-109						27.4					-216.4					2.7						
DY-02-A-110						26.3					-209.2					1.3						

sample name	water type	altitude	pH	cond.	Al	Ba	Ca	Fe	K	Mg	Mn	Na	P	Si	Sr	F	Cl	Sulphate	Br	Nitrate	Phosphate	HCO ₃ ⁻	NICB
		m a.r.l.		μS·cm ⁻¹	μg·l ⁻¹	μg·l ⁻¹	mg·l ⁻¹	μg·l ⁻¹	mg·l ⁻¹	mg·l ⁻¹	μg·l ⁻¹	mg·l ⁻¹	mg·l ⁻¹	mg·l ⁻¹	μg·l ⁻¹	mg·l ⁻¹	%						
DY-01-A-100	Pleistocene ice wedge	41.5	7.53	156	145.0	<20	12.5	163.0	2.1	5.9	319.0	8.3	<0.1	0.5	50.5	0.2	7.7	4.5	0.05	0.17	<0.10	75.8	-2.2
DY-01-B-200	Fissure ice	38.25	8.18	165	132.0	<20	9.8	138.0	0.9	9.6	167.0	6.1	<0.1	0.4	43.9	0.2	9.5	3.6	0.06	<0.15	<0.10	70.6	4.3
DY-01-D-400	Pleistocene ice wedge	34.5	8.02	97	215.0	<20	6.8	287.0	1.1	4.8	157.0	2.9	<0.1	0.4	31.6	<0.05	4.4	3.7	<0.05	<0.15	<0.10	41.6	0.3
DY-01-D-500	Fissure ice	33.0	7.12	718			55.7		5.5	45.3		28.1					87.5	37.4				217.8	14.3
DY-01-G -701	Fissure ice	26.3	7.20	653			44.7		2.1	30.3		42.9					91.0	19.5				199.6	6.1
DY-01-G -702	Fissure ice	25.8	7.67	172	49.5	72.8	12.4	63.0	1.2	9.1	267.0	5.0	<0.1	0.3	66.8	<0.05	20.0	8.7	0.08	<0.15	<0.10	45.3	8.1
DY-01-H -800	Fissure ice	25.8	7.47	113	90.3	24.1	8.8	103.0	1.4	5.3	317.0	2.7	<0.1	0.4	40.0	<0.05	5.2	4.1	<0.05	<0.15	<0.10	47.6	1.7
DY-01-H -900	Fissure ice	25.1	7.52	80	111.0	35.9	5.5	151.0	0.8	3.0	147.0	3.0	<0.1	0.3	31.7	<0.05	6.0	2.8	<0.05	<0.15	<0.10	27.8	-0.9
DY-05-F-300	Pleistocene ice wedge	15.0	7.42	103	59.1	20.3	6.7	76.9	1.1	3.7	165.0	4.9	<0.1	0.3	38.0	<0.05	7.6	8.1	<0.05	0.28	<0.10	28.5	2.7
DY-05-B-200	Fissure ice	5.7	7.40	178	84.1	99.1	12.7	147.0	1.7	10.0	394.0	5.5	<0.1	0.4	52.5	<0.05	6.7	2.9	0.10	0.16	<0.10	86.8	3.8
DY-05-A-100	Pleistocene ice wedge	1.4	6.54	61	93.6	<20	4.3	210.0	2.5	2.9	154.0	1.4	<0.1	0.2	<20	<0.05	2.4	1.0	<0.05	0.37	<0.10	23.6	17.7
DY-02-A-100	Pleistocene ice wedge	4.0	7.31	83	68.3	<20	4.9	223.0	3.2	3.5	116.0	2.2	<0.1	0.3	29.4	<0.05	3.7	2.6	<0.05	0.69	<0.10	15.6	50.7
Kolyma080806	river water	-	7.80	87	33.9	<20	10.5	137.0	0.5	2.4	77.3	1.8	<0.1	2.6	57.3	0.1	0.6	10.8	<0.05	<0.15	<0.10	32.3	5.1
Kolyma080820	river water	-	7.70	112	30.2	<20	13.1	101.0	0.6	3.3	53.8	2.2	<0.1	2.5	73.4	0.1	1.0	15.4	<0.05	0.20	<0.10	42.2	-0.5
Kol-01a	thermokarst lake	-	5.9	26	121.0	<20	2.3	3520.0	0.3	1.4	40.9	0.6	<0.1	1.2	<20	<0.05	0.7	0.7	<0.05	<0.15	<0.10	8.2	43.7
Kol-01b	thermokarst lake	-	6.9	26	111.0	<20	2.4	3350.0	0.4	1.4	46.7	0.6	<0.1	1.3	<20	<0.05	0.8	0.7	<0.05	<0.15	<0.10	8.4	44.0
Kol-01c	thermokarst lake	-	6	26	120.0	<20	2.4	3670.0	0.4	1.4	46.7	0.6	<0.1	1.3	<20	<0.05	0.8	0.6	<0.05	<0.15	<0.10	9.3	38.4
Kol-01d	thermokarst lake	-	6.5	27	119.0	<20	2.5	3720.0	0.4	1.5	77.5	0.6	<0.1	1.3	<20	<0.05	0.8	0.7	<0.05	0.15	<0.10	8.5	43.5
Kol-02	thermokarst lake	-	6.3	66	56.0	<20	5.0	2670.0	0.6	3.5	60.5	3.1	<0.1	1.0	28.0	0.1	3.0	0.1	<0.05	<0.15	<0.10	29.3	19.2
Kol-03	thermokarst lake	-	6.5	49	30.7	<20	4.4	2610.0	<0.2	2.7	103.0	1.6	<0.1	1.0	20.7	0.1	1.2	1.5	<0.05	<0.15	<0.10	19.1	29.5
Kol-04	thermokarst lake	-	7.3	51	<20	<20	4.6	220.0	0.5	2.8	<20	1.3	<0.1	0.1	22.0	0.1	1.1	<0.10	<0.05	<0.15	<0.10	25.2	17.4
Kol-05	Polygon pond	-	6.8	137	25.9	<20	12.4	1190.0	0.5	6.5	206.0	6.3	<0.1	0.4	54.3	0.1	4.5	2.2	<0.05	<0.15	<0.10	67.4	12.0
Kol-06	Polygon pond	-	7.3	318	<20	<20	33.7	554.0	2.4	17.6	560.0	6.6	<0.1	1.9	149.0	0.1	9.1	<0.10	0.12	<0.15	<0.10	186.4	4.9
Kol-07	Polygon pond	-	6.4	153	57.0	<20	17.7	6000.0	0.8	6.3	6490.0	1.4	<0.1	1.5	117.0	0.1	0.2	<0.10	<0.05	<0.15	<0.10	92.9	-3.3

Danksagung

Zuallererst möchte ich mich bei **Dr. Lutz Schirrmeister** und **Dr. Sebastian Wetterich** bedanken, die mir die Arbeit am Alfred-Wegener-Institut in Potsdam möglich machten. Ihre Betreuung war sowohl durch fachliche als auch nicht- fachliche Ratschläge und Hilfestellung hervorragend und beide haben mein Interesse für die Arktisforschung nachhaltig geweckt.

Herzlicher Dank auch an **Prof. Dr. Hans-Wolfgang Hubberten** für die Betreuung und Begutachtung dieser Arbeit seitens der Universität Potsdam.

Weiterer Dank gilt den Mitarbeitern des AWI in Potsdam, insbesondere **Ute** für die nette Einführung und Betreuung der Laborarbeiten sowie **Antje** für das freundliche Teilen ihres Büros. Ebenfalls herzlichsten Dank allen Praktikanten, Diplomanden und Doktoranden des AWI, die hier namentlich zu nennen einfach zu lang wäre. Sie haben mich familiär aufgenommen und mich nicht nur durch ständige Hilfs- und Diskussionsbereitschaft unterstützt, sondern auch die Zeit während der Mittags- und anderer Pausen sehr unterhaltsam gestaltet. Ganz besonderen Dank hier an **Stephan**, auch für das Korrekturlesen dieser Arbeit.

Für die schöne Zeit neben der Diplomarbeit und des Studiums möchte ich stellvertretend für alle meine Freunde **Heide, Josef** und **Jannes** danken.

Herzlichster Dank geht an meine Eltern **Regina & Martin** und meine ganze Familie für die moralische und finanzielle Unterstützung, sowie die Motivation und den Rückhalt jegliche Lebenssituation erfolgreich zu meistern.

Den Mut und die Anregungen für mein Studium und noch vieles mehr verdanke ich meinem Bruder **Jan**, dem ich ebenfalls für das intensive Korrekturlesen dieser Arbeit danken möchte.

Zuletzt mein allergrößter Dank an meine Freundin **Judith** für die tolle und liebevolle Unterstützung.

Schließlich möchte ich mich auch bei allen hier nicht genannten Freunden und Bekannten bedanken, die mich unterstützt und zum Erfolg dieser Arbeit beigetragen haben.

Selbstständigkeitserklärung

Hiermit versichere ich, dass ich die vorliegende Arbeit selbstständig verfasst und keine anderen als die angegebenen Quellen und Hilfsmittel verwendet habe. Alle von Autoren wörtlich übernommenen Stellen, wie auch sich an die Gedanken anderer Autoren eng anlehrende Ausführungen meiner Arbeit, sind unter Angabe der Quelle kenntlich gemacht.

Potsdam, 03.02.2010

Jens Strauß